

# Dynamic Simulation of the Maglev Guideway Design

by

Ren Shibo

Submitted to the Faculty of Civil Engineering and Geosciences  
in Partial Fulfillment of the Requirements for the Degree of

Master of Science in Civil Engineering  
at the  
Delft University of Technology

April 2008

Graduation committee:

---

Prof.dr.ir. J.C. Walraven, Chairman,  
Delft University of Technology

Dr.ing. A. Romeijn, Daily supervisor,  
Delft University of Technology

Dr.ir. P.C.J. Hoogenboom,  
Delft University of Technology

Ir. C.Q. Klap,  
Ballast Nedam, IC+E

Ir. R. van der Meijs,  
Planstudie OV SAAL, Ministry of Transportation

Ir. L.J.M. Houben, Coordinator,  
Delft University of Technology



# Table of contents

<b>Preface</b>	<b>vii</b>
<b>Summary</b>	<b>ix</b>
<b>1 Introduction</b>	<b>1</b>
<b>2 Maglev System</b>	<b>5</b>
2.1 Transrapid concept	6
2.2 Transrapid Vehicle	6
2.3 Maglev Guideway	7
<b>3 Guideway Development, 1981-2006</b>	<b>9</b>
3.1 General	10
3.2 Hamburg-Prelude	10
3.3 TVE 1981-1983, C1 & S1	11
3.4 TVE 1984-1986, C2 & S2	12
3.5 TVE 1990, C3 & S3	14
3.6 TVE 1995-1999, C4, S4 & H1	14
3.7 TVE 2001-2006, C5, C6 & H2	16
<b>4 The State of the Art in Guideway Design</b>	<b>17</b>
4.1 General	18
4.2 Shanghai Project	18
4.2.1 Substructure	18
4.2.2 Bearing	19
4.2.3 Superstructure	20
4.3 Munich Project – Munich Girder	23
4.3.1 Superstructure	24
4.3.2 Bearing and Substructure	25
4.3.3 Summary	26
4.4 Munich project - MSB Track 2010	27
4.4.1 The guideway beam	27
4.4.2 The bearing	28
4.4.3 The guideway slab	28
4.4.4 Summary	29
<b>5 Actions on Guideway</b>	<b>31</b>
5.1 General	32
5.2 Permanent Action	32
5.3 Variable Action	33
5.3.1 Vehicle weight and live load, Q1 & Q2	33

5.3.2 Dynamic Action, Q1 & Q2	34
5.3.3 Non-uniformly distributed load in x-direction, Q3	37
5.3.4 Non-uniformly distributed load in y-direction, Q4	38
5.3.5 Lateral force due to guidance dynamic response, Q5	38
5.3.6 Restraint action due to horizontal radius, Q6	38
5.3.7 Aerodynamic action Q7	39
5.3.8 Headwind Action Q8	39
5.3.9 Crosswind Action Q9	41
5.3.10 Temperature Action Q10	42
<b>6 Vehicle/Guideway Interaction Analysis</b>	<b>43</b>
6.1 General	44
6.2 Guideway Model	46
6.3 Vehicle Model and Suspension system	49
6.4 Dynamic Interaction Model I-1	52
6.4.1 Validation of the model	54
6.4.2 Dynamic response	55
6.4.3 Influence of damping	56
6.5 Dynamic Interaction Model I-2	58
6.5.1 Validation of the model	61
6.5.2 Dynamic response and influence of damping	62
6.6 Dynamic Interaction Model I-3	65
6.6.1 Validation of the model	69
6.6.2 Dynamic response and influence of damping	70
6.7 Dynamic Interaction Model II-1	72
6.7.1 Validation of the model	75
6.7.2 Dynamic response	76
6.8 Dynamic Interaction Model II-2	79
6.8.1 Validation of the model	91
6.8.2 Dynamic response of guideway	92
6.8.3 Dynamic response of carriage body	94
6.8.4 Dynamic response of levitation frame	96
6.9 Summary	98
6.9.1 Guideway displacement	98
6.9.2 Dynamic factor in Design Guideline	101
6.9.3 Acceleration of carriage body and levitation frames	101
<b>7 Guideway Surface Roughness</b>	<b>103</b>
7.1 General	104
7.2 White Noise and IIR Filter	105
7.3 Roughness Model I ( $A=1.5 \times 10^{-7}$ )	106
7.3.1 Linked with the Vehicle/Guideway Model	108
7.3.2 Dynamic response of guideway and vehicle	110
7.4 Roughness Model II ( $A=1.5 \times 10^{-6}$ )	111
<b>8 Finite Element Model</b>	<b>117</b>

8.1 General	118
8.2 Modeling	118
8.3 FE Model 1	121
8.4 FE Model 2	123
8.5 FE Model 3	124
8.6 Two-section Vehicle Model	126
<b>9 Conclusions and Recommendations</b>	<b>129</b>
9.1 Conclusions	130
9.2 Recommendations	131
<b>References</b>	<b>133</b>
<b>Appendices</b>	<b>135</b>



# Preface

This report documents the Master thesis project which I undertook to complete my study in Structural Engineering at Faculty of Civil Engineering and Geosciences, Delft University of Technology. The subject of this thesis is to study the dynamic characteristics of the maglev guideway and to develop a numerical method for simulating of the coupled maglev system.

The graduation committee consisted of the following members:

Prof.dr.ir. J.C. Walraven, Delft University of Technology

Dr.ing. A. Romeijn, Delft University of Technology

Dr.ir. P.C.J. Hoogenboom, Delft University of Technology

Ir. C.Q. Klap, Ballast Nedam, IC+E

Ir. R. van der Meijs, Planstudie OV SAAL, Ministry of Transportation

Ir. L.J.M. Houben, Delft University of Technology

I would like to thank my graduation committee members for their support and advice, and especially Dr.ing. A. Romeijn who made this project available to me so that I could solve the fascinating problem.

I owe my thanks to Qian Zhiwei and Megan Neill for the knowledge sharing during the study in Delft and making it an unforgettable period; to Tadao Ando, into whose orbit I have never been pulled but whose forces influence me indirectly.

Finally I would like to express my sincere gratitude to my family for their unceasing encouragement and support.

Ren Shibo  
Delft, April 2008



## Summary

A high speed maglev train is an innovative transportation technology that uses a magnetic levitation and propulsion system. A high-speed link has been proposed between Schiphol airport and the city of Lelystad. Guideway design is an important aspect of this project since the cost of the infrastructure is expected to be roughly 60-80% of the initial capital costs. The tolerable deviations of such structural elements under external actions are extraordinarily small. To control the magnitude of the guideway displacement and vibration, it is important to be able to accurately predict guideway response to the action of high-speed maglev vehicles.

The vehicle and guideway constitute a coupled system, which leads to precisely defined stiffness requirements for the guideway. It is necessary to develop a reliable simulation technique for the dynamic interaction system so as to evaluate a wide range of guideway designs for various operating conditions. The main subject of this thesis is to study the dynamic characteristics of the maglev guideway and to develop a robust numerical method for simulating of the coupled maglev system.

In the first part an overview is given of the guideway development at the Test Facility in Emsland since 1981 and the state of the art guideway design of the Shanghai Project and the Munich Project. The complex external actions on maglev guideways are summarized according to the German design documents.

Following that, the possibilities of modeling vehicle/guideway interaction system which is affected by the high-speed loadings are investigated. An approach toward the dynamic response of the coupled system is developed in Matlab/Simulink. Five numerical models at different levels of accuracy are created. Based on these models, a series of simulations are performed to study the dynamic characteristic of the maglev system. A surface roughness model is also developed in Simulink to evaluate the influence of guideway irregularity.

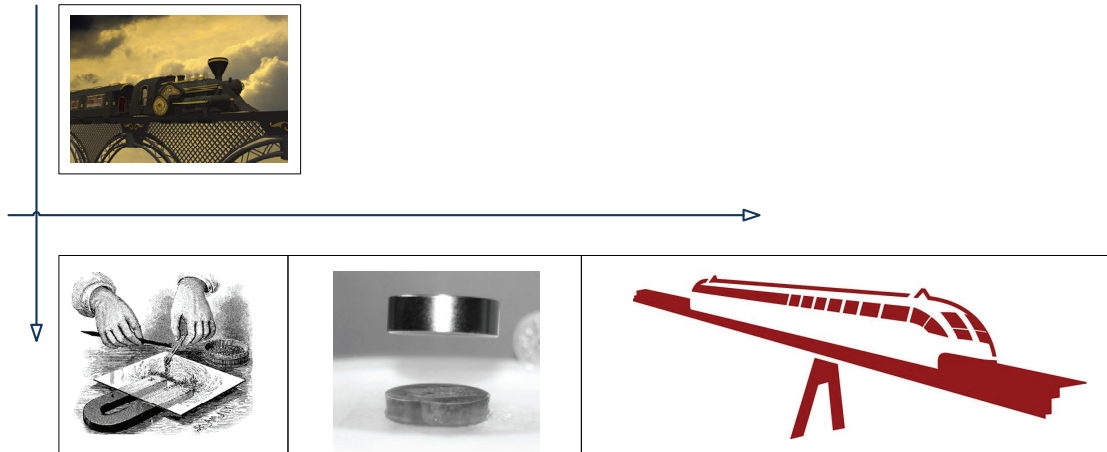
Finite element models corresponding to the first three numerical models are created in Midas/Civil. The intension behind the creation of such an FE model is twofold. On one hand the finite element approach will be used to validate the numerical models developed in Simulink. On the other, the accuracy of Midas when analyzing dynamic characteristics of guideway under high-speed vehicle can be also validated.



# 1

---

## Introduction



The idea of using magnetic action to run a high-speed railroad has been around since 1934, when a German scientist named Hermann Kemper received a patent on this technology. Such trains would be extremely fast and float quietly over the electromagnetic cushion instead of steel wheels (C.P. Wallace, 2002). Although a brilliant idea, the problem has been that it is simply too expensive to implement over a long distance.

The German government began industrial development of the Transrapid in the 1970s. The Transrapid system is designed for speeds ranging from 300 to 500 km/h, using no-contact levitation, guidance and propulsion system technologies. After a short public presentation of the Transrapid 05 in Hamburg at the International Traffic Fair in 1979, a 31 km test track was built in Emsland in the middle of 1980s. Suitability studies have been carried out on the Transrapid Test Facility in Emsland (TVE) since 1984. The first commercial high-speed maglev line was constructed in Shanghai between 2001 and 2004 with the German technology.

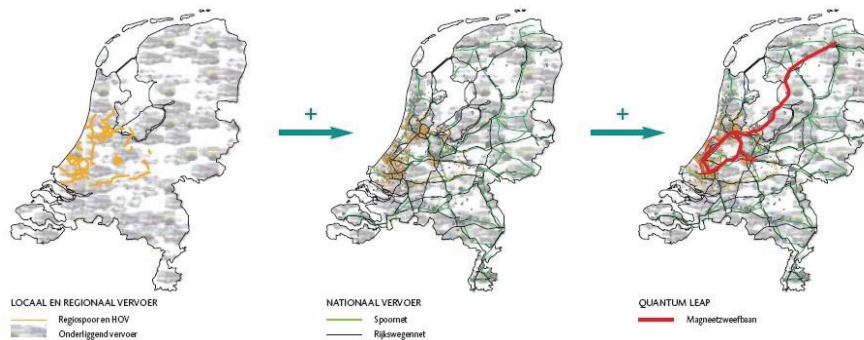


**Figure 1.1 Dutch Maglev Project, [www.magneetwefbaan.nl](http://www.magneetwefbaan.nl)**

There have been considerations in the Netherlands on the application of Transrapid technology for a number of years, particularly with a view to linking the country's major cities. An industrial consortium led by Siemens (Siemens, ABN Amro, Ballast Nedam, BAM and Fluor) and the

## 1 Introduction

Dutch government are currently working on the Randstad Rapid project. The line will connect all the major cities in the Randstad and Groningen to improve the internal public transport accessibility and stimulate the lagging northern economy.

With a maximum speed of 450 km/h, the travel time for the 190 km distance between Schiphol and Groningen will be greatly shortened from 2.45 hours to 1 hour. One of the first important sections to be realized will be the Schiphol-Amsterdam-Almere-Lelystad (SAAL) link.



**Figure 1.2 Dutch Maglev Project, adapted from Google Maps, maps.google.com**

Guideway design is an important aspect of the maglev system. The cost of the infrastructure is expected to be roughly 60-80% of the initial capital (Uher, 1989). Thus, guideway design is a critical area of the cost saving. When the velocity of a maglev vehicle increases to 300-500 km/h, or a guideway is made lighter and more flexible to reduce costs, the dynamic interactions between vehicles and guideway become an important problem. It will play a dominant role in establishing vehicle suspension requirements and specifications for guideway stiffness, span length, and etc. (Y. Cai, 1993)

The main objective of this thesis is to discuss the problem associated with guideway design and modeling vehicle/guideway interactions. A numerical approach toward simulating complex coupling system is developed to simulate the dynamic coupled system.

The first part will summarize the development of maglev guideway at the Test Facility in Emsland during last twenty-five years. The pros and cons of past experience are of crucial importance for an optimized structural design. Three types of guideways that have been, or will be used in the Shanghai Project and Munich Project are then studied, which are believed to represent the state of the arts in maglev guideway design at current stage. Following that, the complex loading cases on guideways will be summarized according to the German documents *Magnetschnellbahn Ausführungsgrundlage-Fahrweg*.

Five numerical models at different levels of accuracy for vehicle/guideway interaction analysis will be developed by using the software Matlab/Simulink. Based on these, a series of numerical

simulations are performed to study the dynamic characteristics of the maglev system. A surface roughness model is developed in Simulink as well to simulate the guideway irregularity and evaluate its influence on guideway displacement and vehicle acceleration.

Finite element models are also created using the software Midas/Civil to study the dynamic response of the guideway. The intension behind the creation of such an FE model is to validate the numerical models that have been developed in Simulink. On the other, the accuracy of Midas when studying the guideway dynamic characteristics under high-speed vehicle can be also validated. The problems associated with modeling maglev guideway in Midas will be discussed.

# 2

---

## Maglev System

## 2.1 Transrapid concept

The Transrapid system has an electromagnetic suspension system, which uses separate sets of conventional iron-core magnets to generate vehicle lift and guidance by means of magnetic attraction. Both the levitation and guidance systems have their own control systems to regulate the air gap between magnet and guideway rail. The control systems maintain the air gap at approximately 10 mm from the guideway. Propulsion is provided by a synchronous long-stator linear motor using the levitation magnets to interact with propulsion windings mounted in the stator packs on the guideway. By reversing the magnetic field, the train can accelerate and brake without contact.

The vehicle wraps around a T-shaped guideway as shown in Figure 2.1. The guidance rails are mounted on the outside edges and the levitation and propulsion stator packs are mounted underneath the guideway.

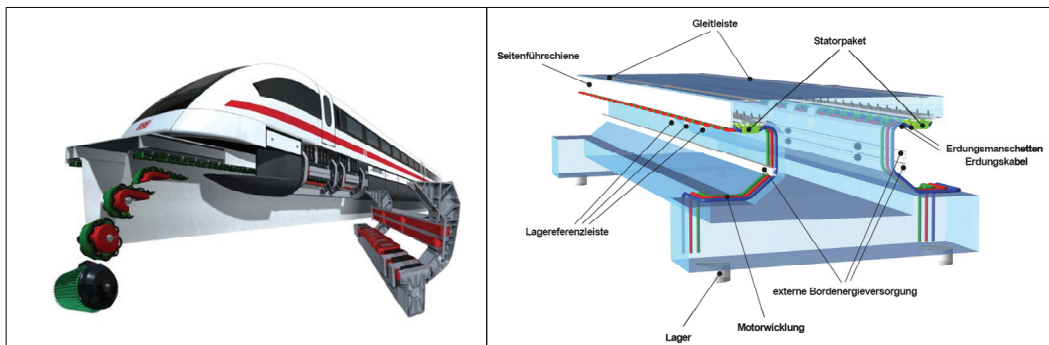


Figure 2.1 Typical Transrapid vehicle and guideway, MSB-AG-Fahrweg Teil I, 2007

## 2.2 Transrapid Vehicle

TR09 is the latest maglev vehicle at present, which has been running at the Test Facility in Emsland (TVE) since April 2007. It contains the following subassemblies.

TR 09	
Magnets	Cable systems
Sensors	Levitation frames
Magnet control units	Secondary suspension
On-board power supply	Carriage body
On-board control/diagnosis system	

Table 2.1 Subassemblies of TR 09

The carriage body is constructed of aluminum frames with sandwich shells of glass fiber reinforced plastic panels. Each single vehicle section is capable of independent operation and has 32 levitation and 30 guidance magnets. The propulsion force is generated by the interaction of the vehicle magnet exciter windings and the guideway stator windings. The primary braking is

## 2 Maglev System

regenerative, through linear motor current reversal in response to phase angle modulation (Michael Tum 2007).

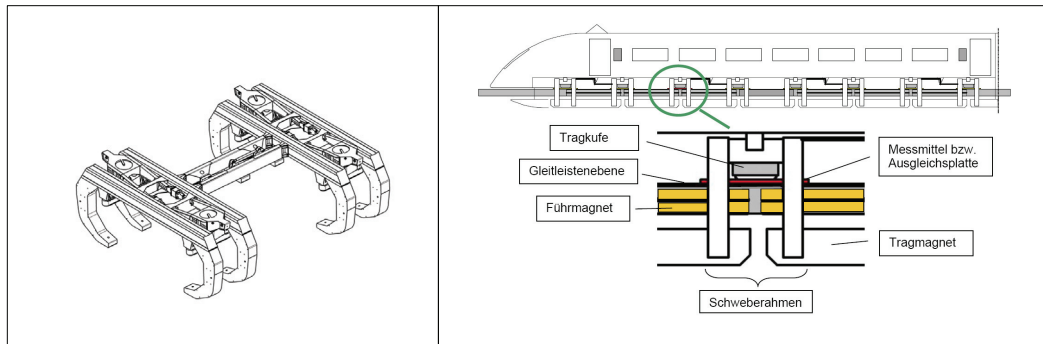


Figure 2.2 Transrapid vehicle and its subassemblies, MSB-AG-Fahrzeug Teil I, 2007

## 2.3 Maglev Guideway

The function of the maglev guideway is to transmit actions due to operation, environment influences and its own load into the subsoil. It supports the vehicles which are suspended on the guideway without contact. Functional components that enable the impelling, levitation and guidance with magnetic force are installed.

Being controlled electronically, the levitation magnets, which are installed on both sides along the total vehicle, will keep the vehicle on the desired vertical distance over magnetic attractive forces. Guidance magnets will keep the vehicle horizontally non-contact with the guidance rails. The driving component is installed on the guideway in form of stator packs. This circumstance distinguishes the maglev guideway from those of all other traffic systems.

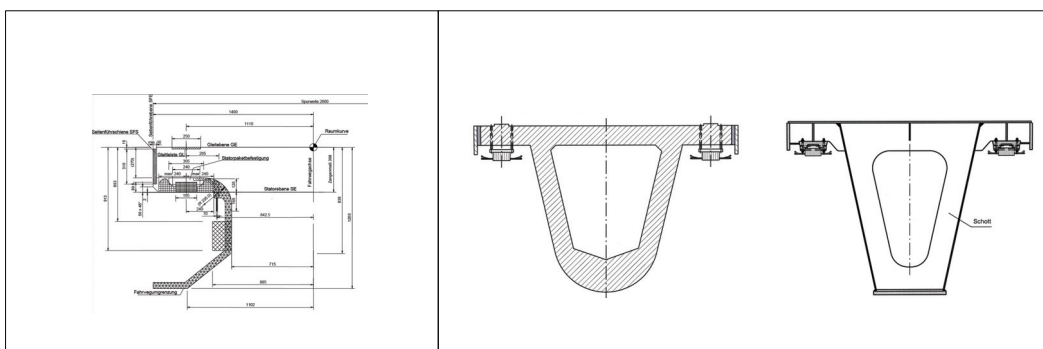


Figure 2.3 Cross sections for typical concrete and steel guideways, MSB-AG-Fahrweg Teil II, 2007

The distances between levitation/guidance magnet and the guideway are very small. Consequently the tolerable deviations of the structural element under all external actions are extraordinarily small. The requirements of the shape accuracy of the construction element lie in a typical order of magnitude in mechanical engineering, within the range of a millimeter, which is almost not possible for most of the building industry (G. Schwindt 2006).

In addition to the common requirements for guideway structure, the design of the Transrapid guideway is determined further by specific requirements of the Maglev system as shown in Table 2.2:

- 
- 
- An open space below the surface of the guideway is needed since the vehicle embraces the cantilever arms of the guideway.
  - The vehicle must be levitated in a designed distance of approximately 10 mm to the guideway and 10 mm to the guidance rails.
  - The vehicle and guideway constitute a coupled system, which leads to precisely defined stiffness requirements for the guideway.
  - The vehicle requires precise positioning of the stator packs and guidance rails, which allow only marginal tolerances for manufacturing and assembly tolerances.
  - The guideway deformation and vibrations when vehicle traversing at high speed
- 

**Table 2.2 Special requirements of maglev guideway**

Gert Schwindt summarized the special requirements for maglev guideway into two aspects, namely the interface between the guideway and the vehicle/propulsion system, and the interface to the environment. The former is resulting from the geometry, the tolerances, the stiffness, the damping, the attachment of the long stator equipment and the maintenance; the latter means the guideway girder has to fulfill environmental criteria such as noise emission levels and must be suitable for all weather conditions.

# 3

---

## Guideway Development 1981~2006

### 3.1 General

The guideway for Transrapid maglev has been developed for more than 25 years at the Test Facility in Emsland (TVE). Since 1981, about 20 types of guideways have been designed, constructed and tested. Figure 3.1 shows most of these guideways which can be found from literatures. They will be studied in this chapter.

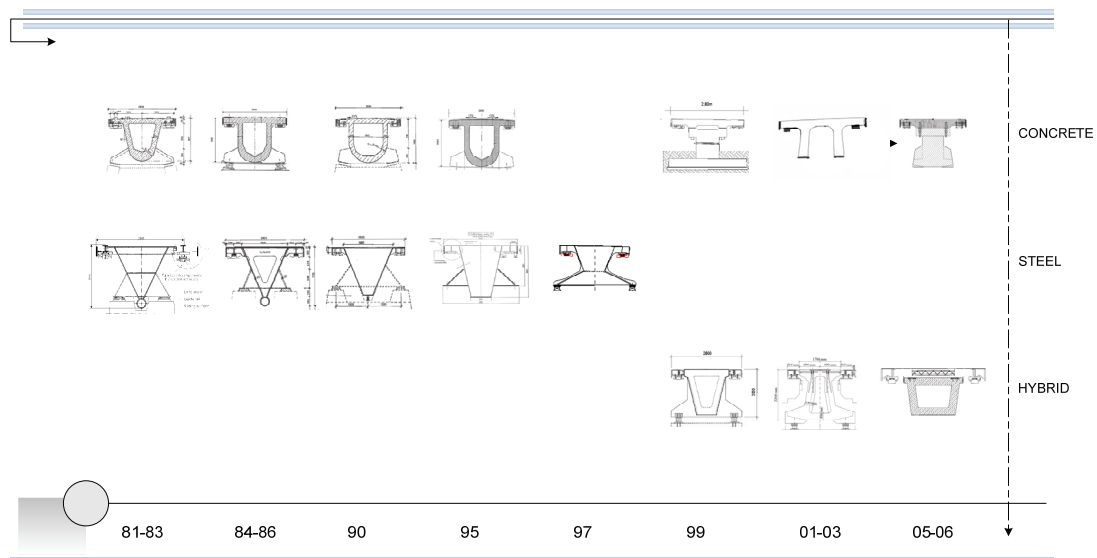


Figure 3.1 Development of maglev guideway

### 3.2 Hamburg-Prelude

Although in a modified form, the first application of Transrapid system took place in the Hamburg international traffic exhibition in 1979. The vehicle Transrapid 05 and a steel guideway with length of 906 m were realized. The girder was simply supported at a span of 24 m. For the constraint region a longer span of up to 50 m was used.

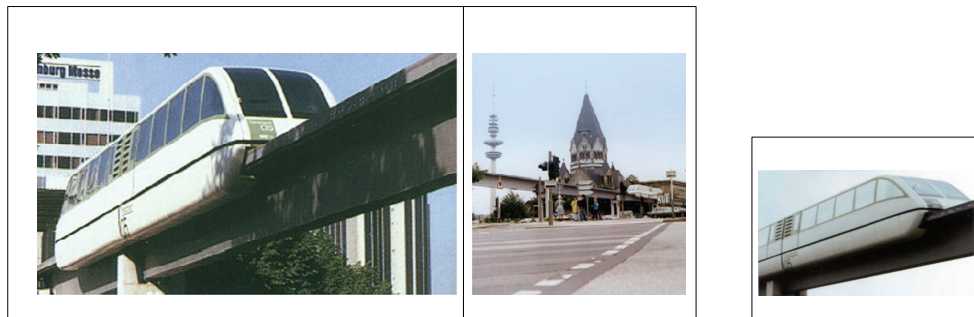


Figure 3.2 The guideway in Hamburg and TR05, I. Mangerig et al., 2002

### 3.3 TVE 1981-1983, C1 & S1

When the Test Facility at Emsland was built in the first construction stage (1981-1983), two guideway types were realized with different design characteristics, referred to as C1 (C for concrete and 1 for first generation) and S1 (S for steel) in this report.

The prestressed concrete guideway C1 was developed by the engineering company Dywidag. The girder was simply supported with a length of 24.8 m and a height of 1.8m. The cross section of the elevated concrete guideway consists of a single-celled box girder with cantilever arms, a circular bottom chord and diaphragms at the ends.

In order to exclude any additional time-dependent distortion arising from dead load and prestressing, the girders are prestressed using the balanced-load concept in both directions for these loadings. The guideway girders were prefabricated since they could be lifted out of the formwork easily due to their shape. The hollow space was obtained by an extractable inner formwork and the diaphragms were cast subsequently (H. Falkner, 1990).

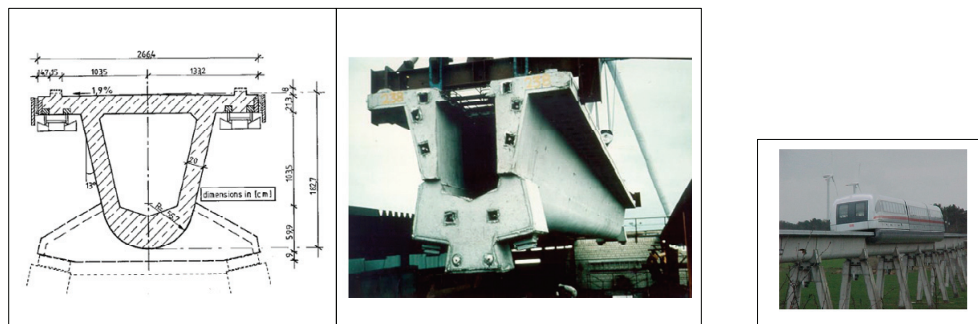
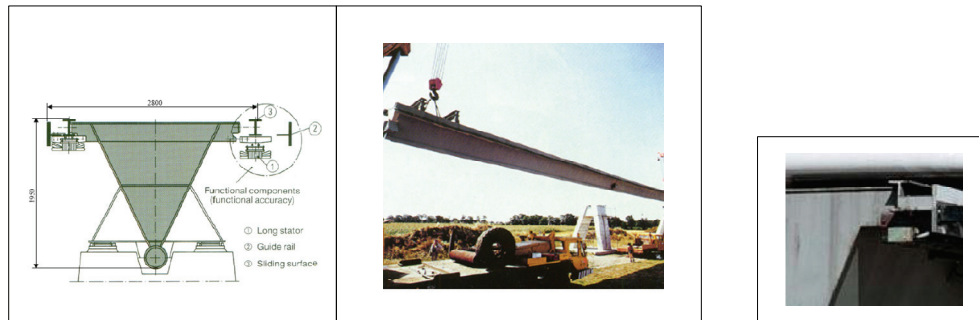


Figure 3.3 Guideway C1, H. Falkner, 1990

The guideway girders rest on steel calotte-bearings. For the first stage of construction between 1981 and 1983 a relatively small distance between these bearings (in the transverse direction) was chosen. Because of the relatively high lateral forces, anchorage at the girder ends was required to secure the positioning of these bearings. Short prestressing rods in a steel pipe duct, protected against corrosion by a cement grout injection, were used as anchors. The starting, acceleration and braking of maglev vehicles induces high longitudinal forces, which have to be carried by the guideway. Vertically positioned elastomeric bearings between the girder ends and a trail spade on top of the supports were used.

The procedure for equipping the guideway C1 with its different components (stator packs, lateral guidance rail and sliding strip) is critical for a rapid construction progress. Mounting of the girders on the supports was carried out with a mobile crane and only roughly positioned. For final positioning, hydraulic jacks were used. Afterwards, a special vehicle was run on top of the girders, from which the sliding strip was cut to its specified size, and the stator packs as well as the lateral guidance rail were fitted. These equipment components were fitted using steel parts to the guideway girders and then fixed in place by grouting. The parts were brought into the exact position by the special equipment vehicle and held in place until the grout was sufficiently hardened. This way of equipping the guideway C1 proved successful but was sensitive against disturbances, e.g. unfavorable weather conditions, machine failure, etc.

With regards to stiffness requirements the first generation of steel guideway S1 was constructed at the same period. A triangular cross-section was chosen, which ensured a high torsional stiffness. The bottom chord consists of a steel pipe. The girder cross-section is stiffened by crossbeams and diaphragms, but longitudinal stiffeners have been avoided as far as possible, with the exception of certain places over the supports.



**Figure 3.4 Guideway S1, H. Falkner, 1990**

The fixing method of the function equipment was designed in such a way that the required exact position of each part could be adjusted by screws. The sliding strip consists of an I-section, which also carries the stator magnets. The guidance rail is formed by a T-section.

Because of the low dead load of the steel guideway girders, an anchorage over the supports is required to secure exact positioning of the girders. These anchors, consisting of steel rods, are designed in such a way that girder elongations do not cause bending stresses in the rods. The anchors are prestressed, in order to avoid lifting force from the bearings.

The guideway girder has double spans with a length of approximately 50 m. Two components with a length of 25 m were delivered and welded together on site. After the mounting of the girder on the supports, the two-span continuous beam was adjusted into its position by hydraulic jacks. After fixing the bearings, the fittings of the guideway equipment could be brought into their precise position by a bolted connection.

The precise fitting tapholes for the stator packs were drilled and the stator packs fixed in the fitting-out hall by the same machine that had been used for the concrete guideway C1. The production of the sliding strip and the lateral guidance rail was carried out with a high degree of precision such that a later readjustment became unnecessary. For the girder assembly, special gauges were used, and most of the welding was carried out by welding robots (Horst Falkner 1990).

### **3.4 TVE 1984-1986, C2 & S2**

Based on knowledge and experience obtained from the first construction stage, two new guideway types, C2 and S2, were designed and constructed as the second construction stage at the south loop line of TVE in the year 1984-1986.

Compared with guideway C1, the new prestressed concrete guideway C2 has been improved in the following aspects:

### 3 Guideway Development 1981-2006



**Figure 3.5 Guideway C2, Gert Schwindt, 2006**

- The distance of bearings was increased transversely to such an extent that the bearing position could be secured without the use of anchors
- Special steel bearings for longitudinal forces were arranged instead of previous elastomeric bearings.
- Since it was learned that it was possible to mount the girders with a high degree of precision, therefore, for the second stage, all works for equipping the guideway girders were carried out in a specially equipped fitting-out hall rather than on the track.
- The lateral prestressed guidance rail was welded to steel parts already set in the girder concrete. For the fixing of the stator packs, steel blocks were set in the concrete, in which fitting tapholes were later cut to hold directly the fixing bolts of the stator packs.



**Figure 3.6 Guideway S2, H. Falkner, 1990**

The cross section of new steel guideway S2 was designed according to the first generation in the shape of polygon with a steel tube lying below. Compared to the first generation, two considerable modifications were made for the steel guideway S2:

- The experience gained during fabrication showed that it is possible to produce these girders with such a degree of precision that the fixing of the guideway equipment could be done without having to compensate for tolerances. Therefore new cross-section of the girders is fully welded. Top plate, lateral guide rail and the longitudinal girders for the fixing of the stator packs are an integral part of the cross-section.
- In order to simplify the time-consuming mounting procedure, instead of a continuous supporting scheme, simply supported girders with length of 25 m were arranged at the second construction stage.

### 3.5 TVE 1990, C3 & S3

The test and research in the 1980s based on the first two generation guideways have shown a problem: the dirt sediments on the top of the guideway girders and solar radiation caused an undesirable high bulging of these girders. This resulted in disturbances of the driving operations, as the allowable deviations of the girders from the gradient are then exceeded. As continuous beams show significantly smaller deflections than the simply supported girders, it is planned to use continuous two-span beams for the new guideway type. Engineers intended to couple two prefabricated guideway girders together after mounting with prestressing tendons. In order to study the behaviour of such a girder in operating conditions, the concrete guideway C3 was constructed at TVE in 1990.

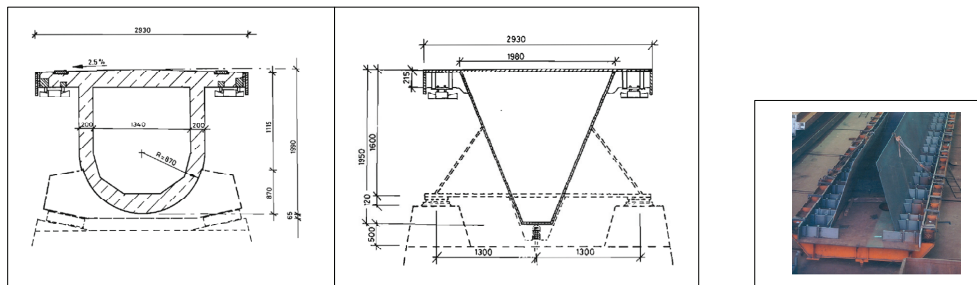


Figure 3.7 Guideway C3 and S3, [www.transrapid.de](http://www.transrapid.de)

Also a third generation of steel guideway S3 was developed with a two-span girder and a trapezoidal cross section. It has almost the same shape as the previous generation. The difference is that for simplification of construction, flat bar steel was used in the bottom, instead of the steel pipe for the bottom cord. The aim is automatic production of the guideway girders according to the track gradient directly, in order to avoid adjustments on the track.

### 3.6 TVE 1995-1999, C4, S4 & H1

Within further development of the program in the years 1995-1999, especially the plan of the maglev line Berlin-Hamburg, came the fourth generation guideway, both in concrete and steel, as well as further guideway types such as the first Hybrid concept H1 (H for hybrid guideway). It was also in this period that the guideway began to be classified according to the construction height.

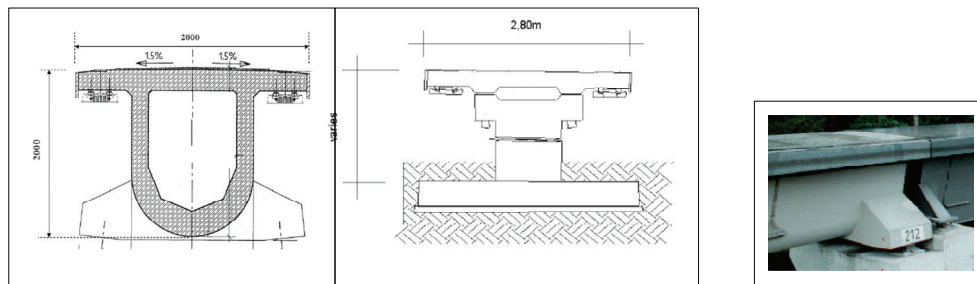
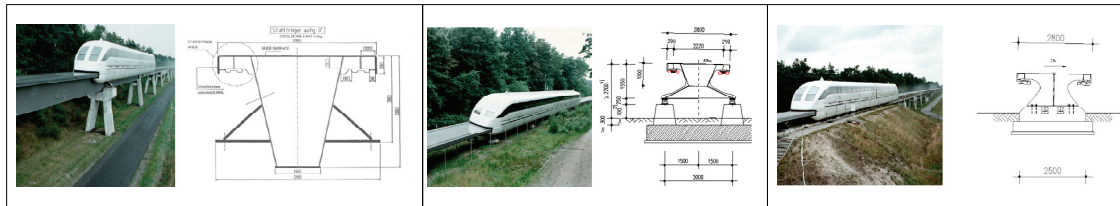


Figure 3.8 Guideway C4, Type I and III, Gert Schwindt, 2006

For different surrounding conditions, e.g. the existing traffic routes, three steel guideway types were developed in this period:

- S4 Type I: Elevated two-span continual girder with a span length between 18 m and 31 m.
- S4 Type II: Elevated two-span continual girder as transition between at-grade and elevated track, also used with soft soil. It has a span length of 12.4 m.
- S4 Type III: Guideway structure mainly used in tunnels or on bridges, with a specific length of 6.2 m.



**Figure 3.9 Guideway S4, Type I, II and III, Gert Schwindt, 2006**

The two-span elevated guideway girder S4-I has a typical span length of 25 m. A trapezoidal cross section is designed instead of the original triangle form. The S4-II has the same height of deck as S4-I. The smaller spans of S4-II however permit a halving of the cross-sectional height and a reduction of the thickness of the bottom plate. Guideway S4-III is a different solution, which rest at grade directly with a two-span girder of 6.2 m. It has a variable stiffness over the length due to the difference of cross section. The girder is seated on prefabricated foundations and is coupled by nut-/spring-connections with the neighbouring girders.

At the same time, an elevated concrete guideway C4, as well as a two-span elevated hybrid guideway H1, were installed at TVE.

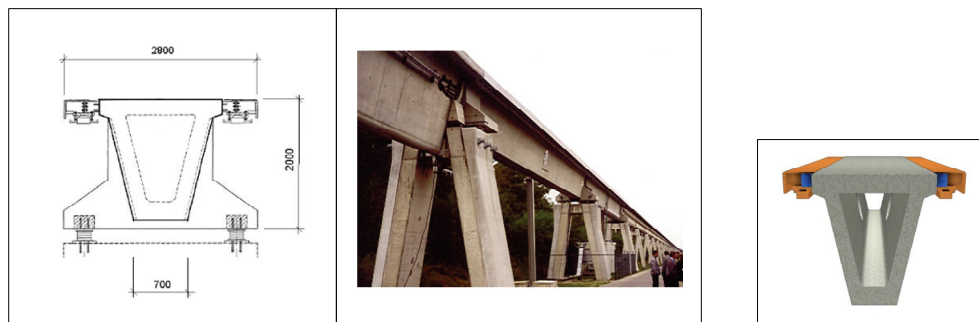


**Figure 3.10 Guideway H1, Gert Schwindt, 2006(left), Mangerig, 2002(right)**

The solution for a Hybrid concept was developed to combine the advantages of prestressed concrete and steel structure and to avoid their respective disadvantages. The task of resistance to all attacking effects into the substructure is to be economically taken by a prestressed concreted box girder. The functional components with sliding strip, lateral guidance rail and stator are combined and designed as functional components by means of modular function unit. It can be adjusted to enable shape accuracy within the range of tolerance, which is unusually not satisfied for the prestressed concrete girder.

During the fabrication of a hybrid girder, a prestressed concrete beam with a lateral steel cantilever is first provided. The functional components are fastened to the steel cantilever with two bolts in a further manufacturing step. The drillings for 4 screws at the lateral side of the cantilever are used for safety reasons as for redundancy, however, at the same time it slightly relocates the attachment (I. Mangerig 2002). According to the test data at TVE, the hybrid girder is particularly characterized with the high precision and decrease of temperature susceptibility for thermal gradients.

### 3.7 TVE 2001-2006, C5, C6 & H2

The Shanghai Transrapid line was realized as a double-track guideway with a length of 30 km in 2001 and 2002. A special feature of the guideway in Shanghai (H2) is its wider base which was implemented on the basis of experience gained with the previous hybrid guideway H1 installed at TVE. In the next chapter this type of guideway will be studied in detail.



Figure 3.11 Guideway H2, Transrapid International, 2002

Two other newly developed guideways are Max Bögl's Munich Girder (C5) and Züblin's MSB-Track-2010 (C6), which will be also introduced in the next chapter.



Figure 3.12 Guideway C5 (Munich Girder), Max Bögl, 2005



Figure 3.13 Guideway C6 (MSB-Track-2010), Züblin, 2006

# 4

---

## The State of the Art in Guideway Design

## 4.1 General

In this chapter the hybrid guideway for the Shanghai project and the recently developed Munich girder and MSB-Track-2010 for Munich project will be briefly introduced:

- the hybrid girder at Shanghai project, Max Bögl
- the Munich girder, Max Bögl
- the MSB-Track-2010, Züblin

## 4.2 Shanghai Project

The construction of Shanghai Transrapid Line began in March, 2001, and public service commenced on January 1, 2004. For the first Chinese Transrapid project, the track between the Pudong Airport and Longyangroad Station in the outskirts of Shanghai was chosen. At this distance of about 30 km the newly-developed hybrid guideway girder was used to build the track. The construction technology is provided by the German syndicate Transrapid Guideway Consulting Group (TGC), which consists of the Munich engineer's office CBP and two German building companies Max Bögl and Gebr.v.d.W.



Figure 4.1 Shanghai Maglev line, adapted from Google Maps, [maps.google.com](https://maps.google.com)

The Maglev Line begins at Longyangroad Station of Metro Line 2 and ends at Pudong Airport, with a total length of 29,88 km plus 2,47 km entry/exit lines and 1,35 km inspection line at the maintenance center.

### 4.2.1 Substructure

The substratum along the Shanghai Transrapid Line is loose deposits which mainly consists of saturated clay, silt and sandy soil. The weak alluvial soil and the site's periodic seismic activity, made it less than ideal for the stable support of the heavy concrete and steel infrastructure. The solution to these instability problems lay in building elevated guideways sitting atop piers, which are supported on a pile foundation.

#### 4 The State of the Art in Guideway Design

The reinforced-concrete support piers, 1.8 by 1.8 m in plan and typically 8 m high, are designed to withstand the seismic forces of earthquakes measuring up to 7.5 on the Richter scale. Each support pier sits atop a pile cap 2 m deep and 10 to 12 m on a side. Apart from some sections, double-column piers have been adopted. Single-column piers are adopted where there is a local restriction or at entry and exit lines of the maintenance center. Piers with steel frames are adopted at oblique road-crossings.

The pile caps cover 20 to 24 piles, each 60 cm in diameter, which are driven to a fine sand/clay stratum at a depth of 30 m to 35 m; the rest are deeper than 58 m. The adopted pile shape is a square of reinforced concrete and prestressed high-strength pipe pile. At the vicinity of existing buildings, drilled hole poured-concrete piles are used. In order to increase the horizontal resistance of the foundation, part of the driven piles have an inclination of 1:8.



Figure 4.2 Guideway substructure, [www.smtdc.com](http://www.smtdc.com)

#### 4.2.2 Bearing

On the soft soil ground of Shanghai, it is unavoidable that settlements of the guideway structure occur after a long time of train operation. Settlements, especially non-uniform ones between the adjacent supporting piers can cause shift or dislocation of guideway girders and bring troubles to the guideway precision control.

For this consideration, bearing for Shanghai Transrapid line is designed to realize the exact positioning of guideway girders and eliminate shift or dislocation of guideway girders. In addition to the performance for general elevated guideway bearings, special requirements such as low compression, two-way adjustment in both vertical and lateral directions have been met for the bearings design.

Two structure types, namely simple girder and simple-continuous girder (first simple supported, coupling later), are applied in the guideway structures of the Shanghai project. Accordingly two types of bearings, typical bearing and fixing-sliding bearing, have been developed to meet requirements in both cases.

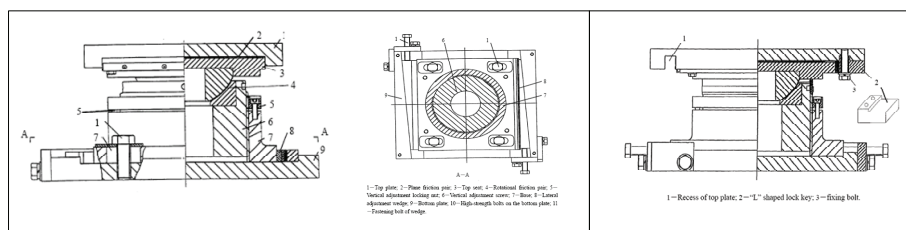


Figure 4.3 The typical bearing (left) and fixing-sliding bearing (right), X. Wu, 2005

A typical bearing has the similar structure and function as the general guideway bearing, to transfer loads from girders to substructures and also to ensure free displacement and rotation of guideway girder in the non-restrained direction under possible environmental impacts and loading cases. During the erection of the girders or in case of unallowable shift or dislocation of guideway girders, it also allows to make the girders' position adjusted vertically and laterally and fallen into the allowable scope by normal maintenance hours.

Vertically, the typical bearings are designed to be adjusted by a trapezoidal screw. The operation and performance of adjustment is believed to be convenient and reliable with reference on adjusting and fixing methods in the bridge anchorage technology. The adjustment range in vertical direction is 20mm upwards, and 10mm downwards. The vertical adjustment of bearings is also designed to be equipped with the locking mechanism, to which only a small compressive force needs to apply to prevent the trapezoidal screws from loosening under the dynamic actions of trains (X. Wu, 2005).

For the lateral adjustment and transfer of horizontal forces, high strength friction bolts are used generally, however, because of the ambiguous horizontal resistance and inconvenient adjustment by loosening and tightening the high strength bolts, Shoulder ridges in the bottom plate plus wedges between the base and shoulder ridges are designed in the Shanghai project. The bolts attached in the bottom plates are used only to position and not to load any lateral forces

The fixing-sliding bearing is a single-way sliding bearing designed for a simple-continuous girder, where the two simple girders are erected and positioned independently and then connected vertically into a two-span quasi-continuous girder. This design can fully utilize the stiffness advantages and overcome the size and weight disadvantage of continuous beams. Perpendicularly to the ledge, a recess cuts into both sides near the top seat of a fixing-sliding bearing. An "L" shaped lock key can be inserted in the recess to lock the bearing and a single-way sliding bearing is changed to be a fixing one.

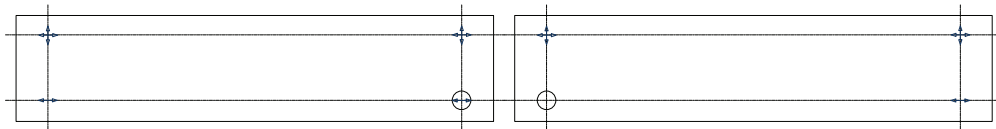


**Figure 4.4 Supporting scheme**

The bearing layout of a two-span continuous girder connected by two simple girders is illustrated in Figure 4.4. When the two girders are simply supported, there is a fixing bearing under each girder; when they are connected to a continuous girder, one fixing bearing should be changed to act as a single-way sliding bearing. Otherwise the horizontal force resulting from the temperature impacts will damage the redundant fixing bearing in the continuous girder. The fixing-sliding bearing enables the guideway girders to be interchanged between a simple beam system and a continuous beams system by locking or unlocking the "L" key in the bearing.

### **4.2.3 Superstructure**

Three types of hybrid guideway were used in the Shanghai project. Those referred to as type I girders were approximately 24.8 m long and weighed approximately 190 Mg. The type II girders were 12.4 m long, and those for the maintenance facility, located near the airport, were 3.1 m

long. Among the total of 2,777 guideway girders, type I girders were mainly used (2,497). 70 type II beams and 210 maintenance facility girders were manufactured and installed.

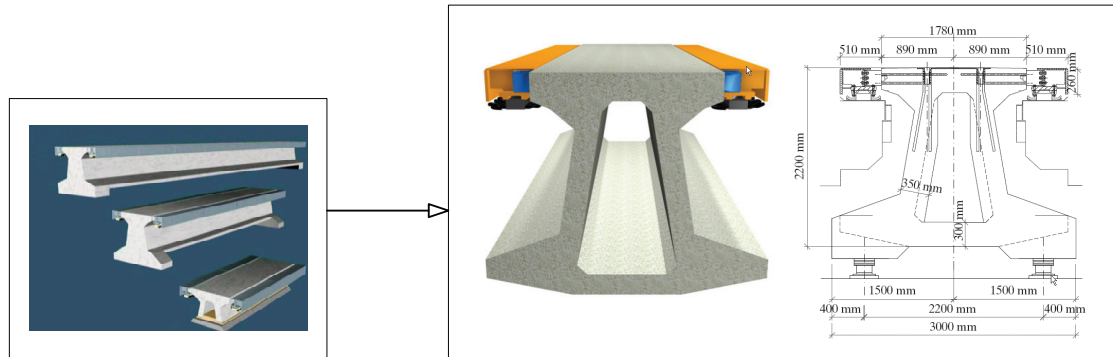


Figure 4.5 Hybrid guideway, J. Feix, IABSE 2003

The hybrid girder design evolved from Max Bögl's considerable experience with steel fabrication and with elements of precast, prestressed concrete. Since 1996, the hybrid guideway girder has been developed on the basis of the characteristics of the steel and concrete guideway. When the hybrid girder was developed, the basic idea was to combine different building materials in order to profit from the advantages of the respective material. At the same time, specific disadvantages of each building material could thus be avoided.

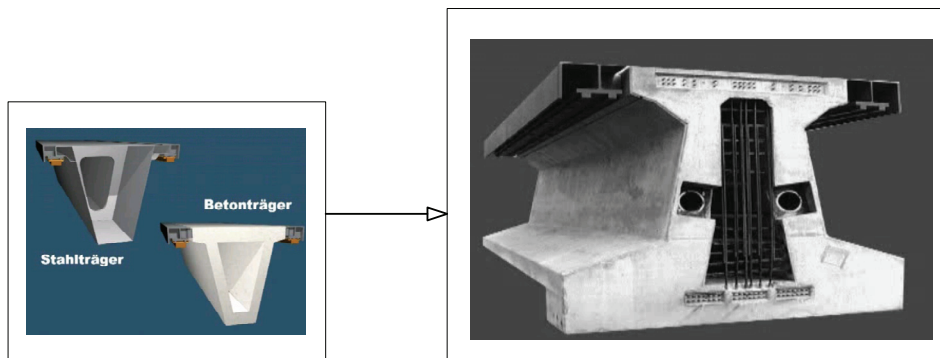


Figure 4.6 Development of hybrid girder, Max Bögl, 2007

For the steel guideway, in addition to its high production costs, higher sound emission is made compared to concrete girders. The vertical stiffness is relatively low. There are also high temperature gradients ( $t_{\text{top}}-t_{\text{bottom}}$ ) or ( $t_{\text{left}}-t_{\text{right}}$ ) in both directions.

For girders with prestressed concrete, it doesn't prove profitable to attach the functional components by means of grout based on cement. The grouting material was not durable enough and caused high restoration expenses.

The disadvantages of the two girder types described above led to the development of the hybrid girder, which was to unite the advantages of the existing constructions. In contrast to the prestressed concrete girder that is apt to carry loads most effectively, the steel construction

perfectly meets the system-specific demands on exactness, especially in the functional areas (J. Feix, 2003).

The hybrid guideway consists of three major subassemblies:

- prestressed concrete main girder
- brackets as a connecting element
- modular function unit girders

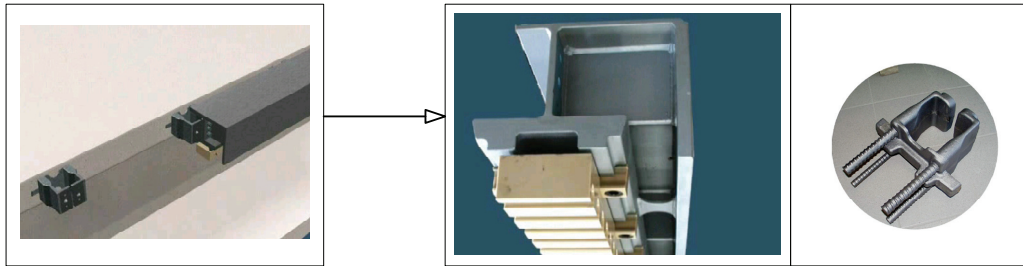


**Figure 4.7 Modular function unit and bracket, Max Bögl, 2007**

An essential part is the application of the modular function unit. It is produced with a module length of approximately 3.10 m according to the triple system length of the stator packs. The three important elements of the Transrapid, i.e. sliding strip, guidance rail and stator-pack-fastening, are combined into the modular function unit. Before assembly of the function-unit-girders only the bracket heads have to be machined and installed. This system makes possible a serial production as well as precision work to the finest tolerances. Therefore it is considered as a highly economical solution.

The brackets connect the main structure (precast pre-stressed concrete girders) and the function unit girders (welded steel structure). It transfers the loads from the functional unit girders into the main girder. A redundant system of bolts and screws is used here. The material for brackets has been developed from welded steel to the final cast iron.

### 4.3 Munich Project – Munich Girder

The Munich Maglev Project is a connection between the Main Station and Munich Airport, which was close to being built but was announced to be canceled on March 27, 2008, due to rising costs associated with constructing the track. The line is planned to be 37.8 km long and it would take 10 minutes at a maximum speed of 350 km/h for the trains to travel it. Several developments were made especially for this line, including a new Vehicle, Transrapid 09 and a new guideway girder, the so called "Munich Girder", by Max Bögl and MSB-Track-2010 by Züblin.

The route consists of at-grade and elevated double-track guideways. The track length is divided in approx. 5.8 km elevated guideway, approx. 22.9 km at-grade guideway and 3 tunnels with a total length of approx. 9.1 km (E. Grossert, 2004).

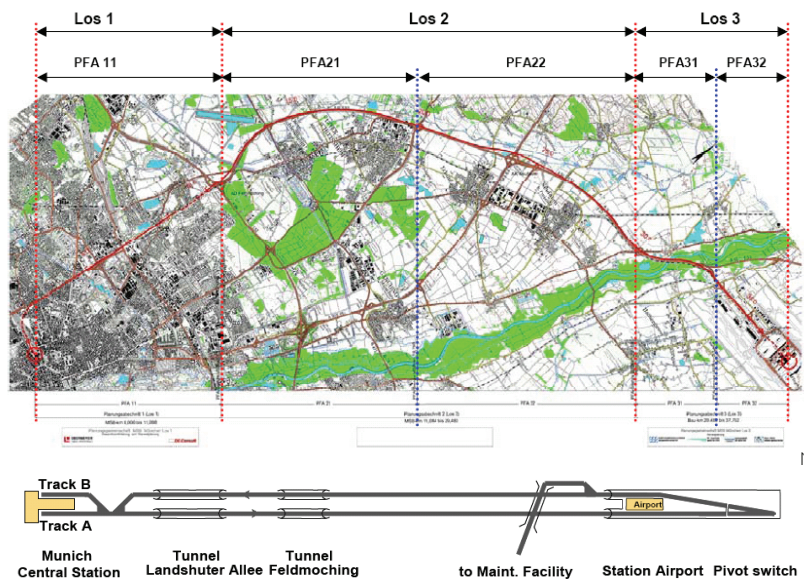


Figure 4.8 Munich Project, E. Grossert, 2004

In the Munich planning process, three types of guideway are utilized:

- Type I: system length 24.768 m, girder height  $\leq 2.50$  m
- Type II: system length 12.384 m, girder height  $\leq 1.60$  m
- Type III: system length 6.192 m, plate construction, construction height  $\leq 0.40$  m

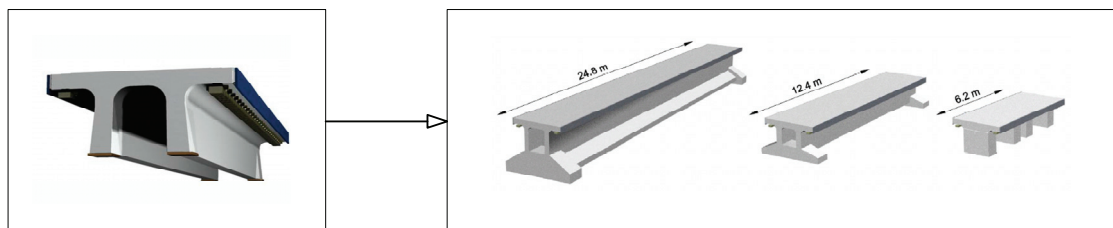


Figure 4.9 Munich Girder, Max Bögl, 2007

Based on the previous experience gained from Shanghai project and the fixed track system FF-Bögl, the engineering company Max Bögl continues to work on the development of the guideway structure. The optimization mainly focuses on how the high precision requirement could be met while achieving low production costs. In 2004 a guideway girder named Munich girder was developed for Munich Transrapid line.

### 4.3.1 Superstructure

The main girder consists of a cross-section which resembles a  $\pi$  slab, constructed using the prestressed concrete method. It is pre-tensioned with directly bonded lengthwise lacing. Due to the stiffness, ratio garland-shaped pre-stressing similar to that for the long girders is not necessary.

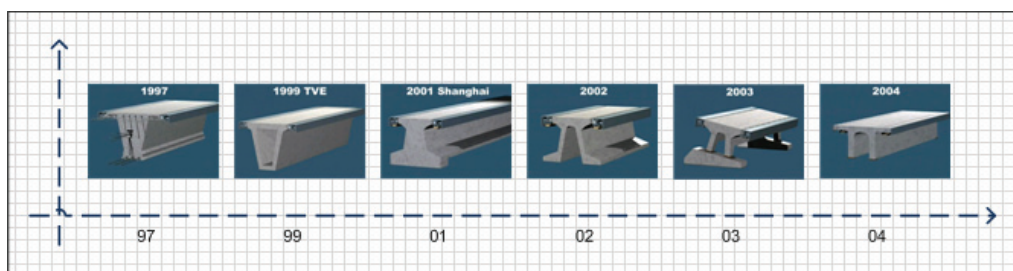


Figure 4.10 Guideway development, adapted from Max Bögl, 2007

In earlier hybrid concepts, precision could only be reached while connecting bracket units inserted in the main girder. However, due to the costly welding work during the module's manufacturing and also its corrosion protection, it is believed that the brackets and the steel function level modules account for over 60% of the price of hybrid guideways (W. Antlauf 2006). Additionally, each module is fastened to four brackets with 12 screws and 6 bolts, which are relatively expensive and require quality control during the production process and must be continually inspected during operation. Similar factors apply to the manufacture and monitoring of the brackets themselves.

Based on the idea of saving on steel and reduction in fastening materials, the steel function levels area for the Munich girder was substituted with a concrete upper flange which is grinded directly. Small holes laterally and on the downside of the girder cantilevers are worked by computer-aided grinding machines after creeping and shrinkage had taken place.

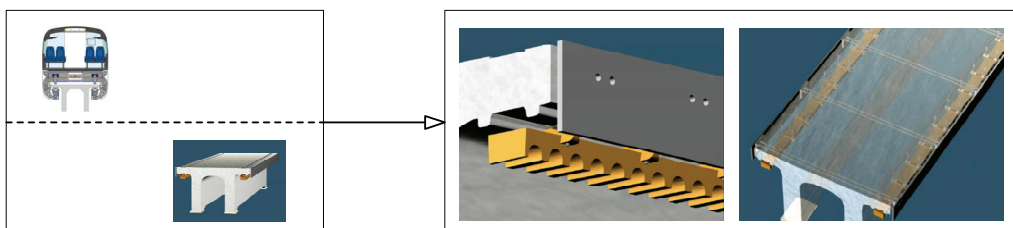


Figure 4.11 Subassemblies of Munich Girder, adapted from Max Bögl, 2007

The lateral guidance rail still consist of 30 mm thick sheet steel, which is screwed onto the upper flange of the girder with the normal length of approx 3 m. It rests on concrete humps which are similarly mechanically processed. The screws are twisted and prestressed into concrete embedded

long nuts. Two opposite long nuts are each connected to one another by a thread rod, so that the pre-tensioning force achieved is effective across the whole width of the girder.

The girder is completed by the availability of new slide strip and coating by ThyssenKrupp. The strip plane is replaced by coated concrete, which has a width of approx. 18 cm, and runs continually over the whole length of the girder.

The stator cores are connected to the cantilever where 3 transverse beams each are screwed onto anchors built into the concrete. On both sides of the underneath of the cantilever two over-dimensioned parallel concrete ledges running lengthwise are arranged, which ensure the exact position of the stator cores after the grinding process.

This development eliminates previously necessary devices fixing the connecting bracket units, and only remains the anchorage system to which the modules of the function level are attached. Fastening of the guidance rail and stator packs allows a quick and efficient adjustment. Additionally, the computer-controlled grinding equipment guarantees reliable, constant quality without the need for extensive monitoring. Defects due to faulty measurement are thereby excluded.

#### 4.3.2 Bearing and Substructure

Depending on the soil conditions, spread foundations or pile foundations are produced at span intervals. The foot support at the end of each girder consists of a concrete prefabricated part, the so-called support wedge with an integrated lower bearing plate. Using these prefabricated parts the cross incline of the girders can be adjusted.

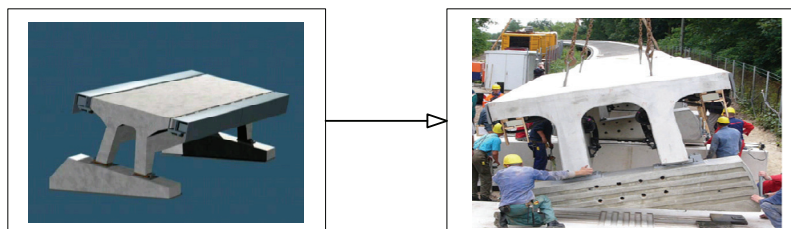


**Figure 4.12 Support wedge, Max Bögl, 2007**

The girders are connected to these support wedges via simply constructed elastomer bearings. The bearings are economical to manufacture and monitor. They permit readjustments using a chuck flange and may be completely replaced if necessary.

Before delivery the girders are connected tightly with two support wedges. They can be brought to the stipulated site without the need for special means of transport. With lifting gear, the approx. 45 ton girders are placed on the prepared foundations and adjusted with hydraulic presses. Based on Max Bögl's previous experience from FF Bögl track supporting layers, the planned remaining gap between the foundation and support wedge is later grouted with erosion and frost resistant solid concrete (Antlauf Walter 2006).

### **4.3.3 Summary**

The improvement made to Munich Girder when compared with the Shanghai hybrid girder can be summarized as:

- Saving on steel function level module and fastening material.
- Wide cross section leads to an increased lateral stiffness.
- Assembly and adjustment can be achieved efficiently via various ways, e.g. the bearings, the separation of grouting layer, and mechanical processing of the slide planes, the plant surfaces for the guidance rails and the stator cores.
- Comfort of traveling is improved due to well adjustment.
- Use of self-compacting concrete eliminates the need for vibrating thereby simplifying the concreting while improving the quality and lowering costs at the same time.
- Use of steel fiber in the concrete minimizes the time-consuming process of assembling the rebars and shows its advantage with respect to Transrapid High frequency loads.

## 4.4 Munich project - MSB Track 2010

With the aim of further developing the magnetic levitation system, a new guideway named MSB-Track-2010 has been designed by another building company Züblin AG for the planned Munich line. The installation of the system at the TVE was completed by June 2006 and the guideway is currently undergoing test procedures.

The essential idea of this new guideway is based on the traditional railroad track, e.g. the Züblin slab track system, whereby a reinforced concrete beam is simply founded on the soil with small plies at regular distances. The system consists in three main components:

- the guideway beam
- the bearing
- the precast guideway slab

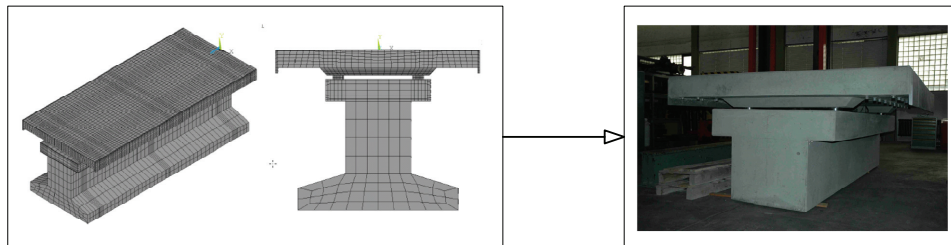


Figure 4.13 MSB-Track 2010, Züblin AG, 2005

### 4.4.1 The guideway beam

The guideway beam is a continuous reinforced concrete beam poured in situ. It is constructed without joints and supported on the soil continuously. Small crack widths are allowed due to proper reinforcement. Therefore the constraining stresses resulting from creep, shrinkage and differences in temperature is compensated alone by cracking and the elastic dilatation of the concrete beam. In addition, local soil subsidence can also be compensated by the system (H. Bachmann 2007).

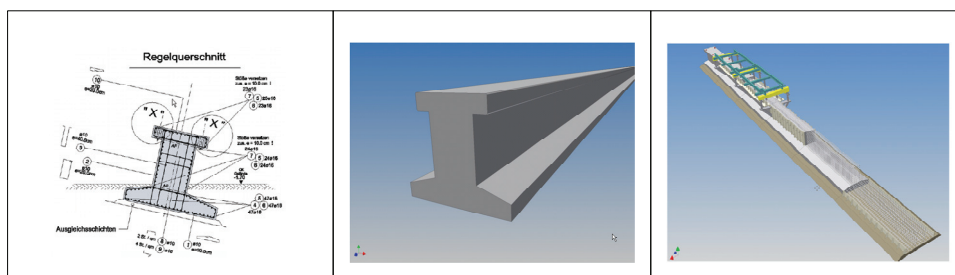


Figure 4.14 The guideway beam, Züblin AG, 2005

The resistance against sliding or overturning of the guideway beam, due to extreme horizontal loads from wind or from centrifugal forces of the vehicle, is taken up by the bottom torsional resistance component. With a widened base, the horizontal loads on the guideway beam can be

well controlled. Considering the different demands, four different cross sections were specified. The transverse gradient lies between  $2^\circ$  and  $12^\circ$ .

#### 4.4.2 The bearing

The guideway slab is supported by six non-compressible steel bearings. Because of the small dimensions of the slab, each individual bearing does not need to compensate any large deformations and are therefore constructed as rigid steel bearings. Anchor plates which are milled to their nominal dimensions with extreme precision can be found both in the guideway slab and in the guideway beam. The guideway slab is then bolted to the beam.

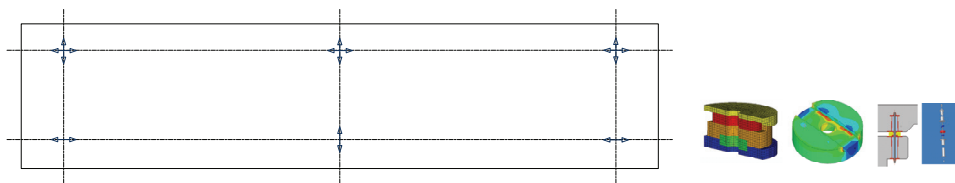


Figure 4.15 The bearings, adapted from Züblin AG, 2005

The bearing is set in the vicinity of the telescopic duct embedded in guideway beam and guideway slab. The anchor plates, steel bearing, the anchor bolts and the concrete component are then connected together. With the aim of corrosion protection, the duct is injected with the slushing grease.

Each individual plate is statically determinate on six bearings on the local concrete bar. Constraint stress as result of temperature and tolerances when assembling can be avoided by the statically determined system. According to the test by Züblin, the deformation caused by creep, shrinkage and thermal effect is relatively low due to the small slab dimensions (H. Bachmann, 2006).

One advantage of the system is that both the bolts and the bearings are replaceable, which make it also possible to replace the guideway slab in case of failure of individual component.

#### 4.4.3 The guideway slab

The guideway slab designed by Züblin consists of a concrete slab with dimensions of  $6.192 \text{ m} \times 2.80 \text{ m}$  and a thickness of  $25 \text{ cm}$ . The slab is strengthened by a haunch in the region of the supports. The relatively small dimensions of the slab allow for a constraint-free support on the steel bearings. The guidance rail on the side and the stator pack fastenings are anchored in the concrete by means of steel butt strap joints.

Two important load bearing items within the concrete slab are the steel butt straps to anchor the guidance rail and the stator pack fastenings. Both type of anchorage are connected in the interior of the concrete. The guidance-rail anchor consists of totally six butt straps which are retained by the sleeves used for the stator pack fastenings. Simultaneously the stator pack fastening is fixed with the steel butt strap using a screw nut. The tensile stress can then be transferred through the screw nut and butt straps to the concrete (H. Bachmann, 2006).

The selected combined anchorage of stator pack and guidance rail does not only bring advantages with the reasonable flow of force, but also leads also to match with the production to the concrete slab. All anchorage elements can be bolted to only one special component, so that a relatively simple installation is possible in the concrete fabrication.

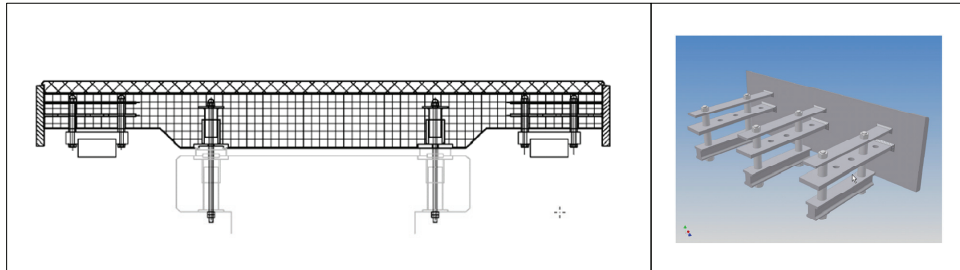


**Figure 4.16** The guideway slab, Züblin AG, 2005

Compared with previous solutions that the guidance rails are divided into relatively short sections, the new anchorage component has a length of 1.03 m. Engineers from Züblin believe that this arrangement can avoid the deformation caused by temperature differences between the steel and the concrete and creep and shrinkage of concrete. Amount of reinforcement steel in slab are accordingly decreased. The test has shown that the maximum shift between steel and concrete is only 0.02 mm at the end of guidance rail (H. Bachmann 2007).

#### **4.4.4 Summary**

The advantages of MSB-Track-2010 can be summarized as:

- The system is continuously supported, therefore local subsoil deformation, both horizontal and vertical, does not lead to any discontinuity in the guideway.
- In case of unacceptable deformation, it can be equalized by the adjustable bearings.
- Production process is simple and economical due to combined anchorage system.
- Replacement of bearing and guideway slab can be achieved conveniently.
- The guideway slabs can be used on the regular beam at ground level as well as in every tunnel and on every bridge by means of a modified beam.



# 5

---

## Actions on Guideway

## 5.1 General

According to EN1990, the load on the maglev guideway can be divided into three types: permanent action (G), variable action (Q) and accidental action (A). These actions will be summarized in this chapter. The global and local coordinate systems that will be used to describe the loads are defined as in Figure 5.1.

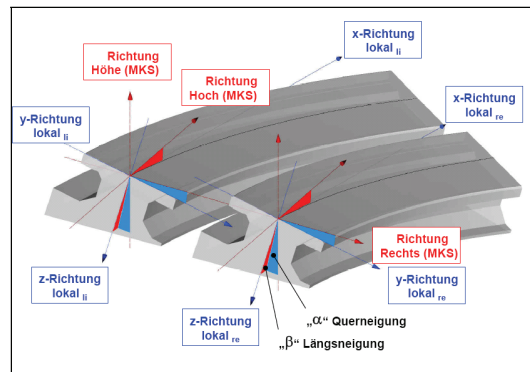


Figure 5.1 Coordinate system, MSB-AG-Fahrweg Teil I, 2007

## 5.2 Permanent Action

A permanent action (G) is an effect which works during the entire service life and their temporal change is negligible in relation to the average value, or always takes place with a change within a certain limit value in the same direction. Based on *Magnetschnellbahn Ausführungsgrundlage Fahrweg Teil II*, The permanent actions on guideways can be defined as:

	<b>Permanent Action</b>
G1	Self weight
G2	Prestress
G3	Creep and shrinkage
G4	Permanent water pressure
G5	Possible foundation settlement
G6	Earth pressure

Table 5.1 Permanent actions on guideway

The dead loads of the structure components (G1) should be determined according to the relevant standards and regulations. For the specific equipments of the Transrapid System, the following values are to be taken:

Long stator incl. motor winding, grounding and other attachment	1.40 kN/m
Components for external power supply incl. attachment	0.25 kN/m
Lateral guidance, sliding strip	N/A
Other attachments	0.10 kN/m

Table 5.2 Dead load of structural components (G1)

The prestressing in the concrete girder (G2) is considered as a permanent action. However for practical reasons it may be treated differently (see EN1992). The effects from creeping and shrinking (G3) must be considered if the actions are unfavorable (MSB-AG-Fahrweg Teil II, 2007).

The water pressure (G4) and earth pressure (G6) should be considered according to generally accepted regulations. The possible foundation settlement (G5) corresponds with the limit value of permissible deformation of the substructure. These values are to be set in the most unfavorable case in each situation.

### 5.3 Variable Action

A variable action (Q) is an effect whose temporal change cannot be negligible in relation to the average value. For the variable action on the guideway, the following cases are to be considered:

	<i>Variable Action</i>
Q1	Self weight of vehicle
Q2	Live load
Q3	Non-uniformly distributed load in x-direction
Q4	Non-uniformly distributed load in y-direction
Q5	Lateral force due to guidance dynamic response
Q6	Restraint action from guidance magnet due to horizontal radius
Q7a	Aerodynamic action-Trains encounter
Q7b	Aerodynamic action-Driving in tunnel
Q8a	Headwind-Lift action
Q8b	Headwind-Pressure and suction
Q9a	Crosswind-Lateral action
Q9b	Crosswind-Lift action
Q10	Temperature

Table 5.3 Variable actions on guideway

#### 5.3.1 Vehicle weight and live load, Q1 & Q2

The static action due to the vehicle weight (self weight of vehicle and live load),  $P_z$ , can be determined according to Table 5.4 from MSB-AG-Fahrweg Teil II. It is distributed over the levitation magnet length  $L_{TM-B}$  as shown in Figure 5.2.

Bezeichnung	Gemittelte, statische Streckenlast [kN/m]	Häufigkeit *
Fahrzeugeigengewicht EG (minimales Fahrzeuggewicht)	$\bar{p}_{z, EG} = 21,0$ **	-
mittleres Fahrzeuggewicht MG (bei Normalauslastung)	$\bar{p}_{z, MG} = 26,0$ ***	80 %
zulässiges Fahrzeuggewicht ZG (bei Maximalauslastung)	$\bar{p}_{z, ZG} = 29,0$ ***	20 %
maximales Fahrzeuggewicht HG (z.B. im Brandfall, Evakuierung einer Sektion) ****	$\bar{p}_{z, HG} = 31,0$	-

Table 5.4 Average static action due to vehicle weight, MSB-AG-Fahrweg Teil II

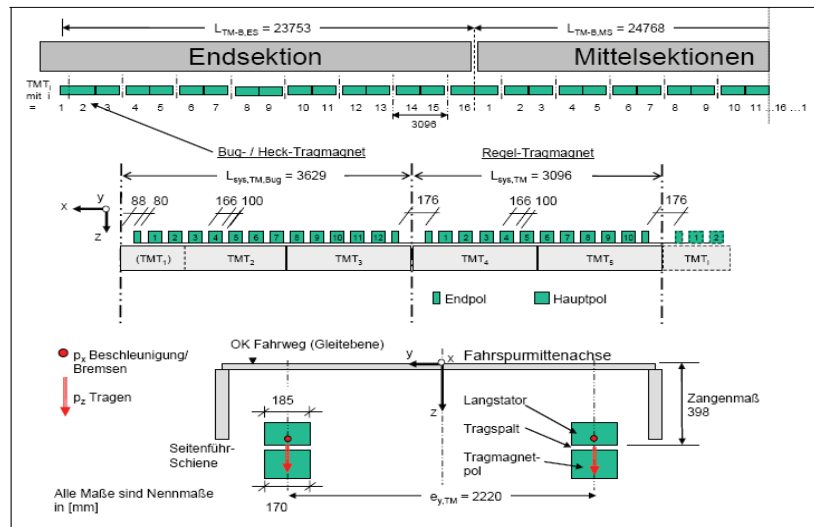


Figure 5.2 Action between levitation magnet and long stator, MSB-AG-Fahrweg Teil II

### 5.3.2 Dynamic Action, Q1 & Q2

The maximum velocity of the maglev vehicle at the current stage is 500 km/m. The limit values of the accelerations for both frequent and non-frequent situations are taken from Table 5.5.

Richtung	Bezeichnung	Grenzwerte
x	Beschleunigen und Bremsen	$-1,5 \text{ m/s}^2 \leq a_x \leq +1,5 \text{ m/s}^2$
y	freie Seitenbeschleunigung	$-1,5 \text{ m/s}^2 \leq a_y \leq +1,5 \text{ m/s}^2$
z	Normalbeschleunigung (inkl. $g = 9,81 \text{ m/s}^2$ )	$+9,21 \text{ m/s}^2 \leq a_z \leq +11,01 \text{ m/s}^2$ (aus $g - 0,6 \text{ m/s}^2$ bzw. $g + 1,2 \text{ m/s}^2$ )

Table 5.5 Limit of acceleration in x, y and z direction, MSB-AG-Fahrweg Teil II

The relation between the driving velocity and the acceleration are defined as:

- Acceleration  $a_x(x)$  in the x-direction due to start and brake

$$|a_x(x)| \leq 1.5 \text{ m/s}^2$$

- Acceleration  $a_y(x)$  in the y-direction

$$a_y(x) = \frac{v(x)^2}{|R_H(x)|} \cdot \cos \alpha(x) \cdot \cos^2 \beta(x) - \left( g \cdot \cos \beta(x) + \frac{v(x)^2}{-R_{V,K/W}(x)} \right) \cdot \sin \alpha(x)$$

- Acceleration  $a_z(x)$  in the z-direction

$$a_z(x) = \frac{v(x)^2}{|R_H(x)|} \cdot \sin \alpha(x) \cdot \cos^2 \beta(x) + \left( g \cdot \cos \beta(x) + \frac{v(x)^2}{-R_{V,K/W}(x)} \right) \cdot \cos \alpha(x)$$

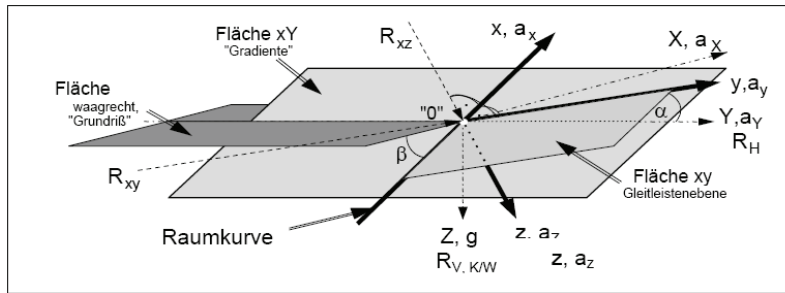


Figure 5.3 The relation between acceleration and the drawing parameters, MSB-AG-Fahrweg Teil II

**X-direction [Dynamic action due to brake and acceleration]**

The maximum permissible longitudinal force indicated in Table 5.7 is determined by the maximum acceleration in the x-direction from Table 5.5 ( $a = 1.5 \text{ m/s}^2$ ). In the range outside the motor section, a reduction factor 0.5 is taken into account:

$$P_{x,links} = P_{x,rechts} = 0.5 \cdot P_x \tag{5.1}$$

Statische Einwirkungen max $p_{x,Schub}$ bei häufigen Bemessungssituationen aus:		
1	minimalem Fahrzeuggewicht	$\max p_{x,Q1/Q2,EG} = \bar{p}_{Z,EG} / g \cdot \max a_x = 3,2 \text{ kN/m}$
2	mittlerem Fahrzeuggewicht	$\max p_{x,Q1/Q2,MG} = \bar{p}_{Z,MG} / g \cdot \max a_x = 4,0 \text{ kN/m}$
3	zulässigem Fahrzeuggewicht	$\max p_{x,Q1/Q2,ZG} = \bar{p}_{Z,ZG} / g \cdot \max a_x = 4,5 \text{ kN/m}$ (Grenzwert)
4	maximalem Fahrzeuggewicht	$\max p_{x,Q1/Q2,HG} = \max p_{x,Q1/Q2,ZG} = 4,5 \text{ kN/m}$ (Grenzwert)

Table 5.6 Maximum force in x direction due to acceleration and braking, MSB-AG-Fahrweg Teil II

**Y-direction [Dynamic action due to lateral acceleration]**

The action on each guidance magnet section  $F_{MTi}$  is given by:

$$P_{y,ay,i} = \bar{P}_{Z,EG/ MG/ ZG/ HG} \cdot \frac{L_{ES/MS}}{L_{FMT}} \cdot \frac{a_y(x)}{g} \cdot \frac{k_{y,ay,i}}{100} \text{ in [kN/m]} \tag{5.2}$$

$k_{y,ay,i}$  represents the distribution of the guidance magnetic force over the vehicle length, which can be determined from Table 5.7 according to the magnet allocation

FMT <sub>i</sub> TMT <sub>i</sub>	Endsektionen															
	(1) *	2	3	4	5	6	7	BM	10	11	12	13	14	15	16	
$k_{y,ay,i}$ [%]	-	7	7	8	7	8	11	-	-	11	8	7	9	8	5	4
$k_{z,ay,i}$ [%]		5	10	6	6	6	7	9	8	6	6	6	6	5	7	7
FMT <sub>i</sub> TMT <sub>i</sub>	Mittelsektionen															
	1	2	3	4	5	6	7	BM	10	11	12	13	14	15	16	
$k_{y,ay,i}$ [%]	4	5	7	8	7	8	11	-	-	11	8	7	8	7	5	4
$k_{z,ay,i}$ [%]	7	7	5	6	5	5	7	8	8	7	5	5	6	5	7	7

\* TMT<sub>1</sub> entspricht als typische Ausführung der Verlängerung des TMT<sub>2</sub> (siehe Abbildung 3).

Table 5.7 Distribution of the magnet force caused by  $a_y$ , MSB-AG-Fahrweg Teil II



## 5 Actions on Guideway

TMT <sub>i</sub>	Endsektionen															
	1*	2	3	4	5	6	7	8	9	10	11	12	13	14	15	16
k <sub>z,az,i</sub> [%]	10	10	5	7	7	7	7	7	7	7	6	6	6	6	6	6
TMT <sub>i</sub>	Mittelsektionen															
	1	2	3	4	5	6	7	8	9	10	11	12	13	14	15	16
k <sub>z,az,i</sub> [%]	6	6	6	6	6	6	7	7	7	7	6	6	6	6	6	6

\* TMT<sub>1</sub> entspricht als typische Ausführung der Verlängerung des TMT<sub>2</sub> (siehe Abbildung 3).

**Table 5.8 Distribution of levitation magnet force, MSB-AG-Fahrweg Teil II**

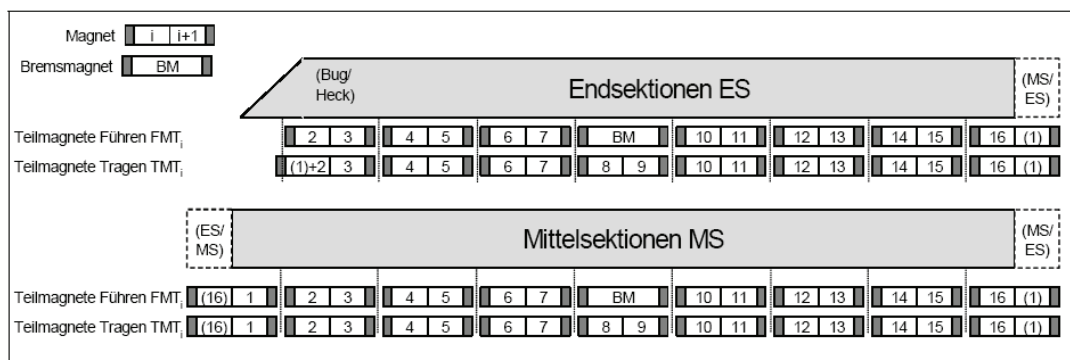


**Figure 5.5 Designation for levitation magnet and guidance magnet, MSB-AG-Fahrweg Teil II**

Due to the braking and acceleration, moments around y-axis on carriage body will be generated, as illustrated in Figure 5.6. This load should be considered with the previous static vehicle load together.

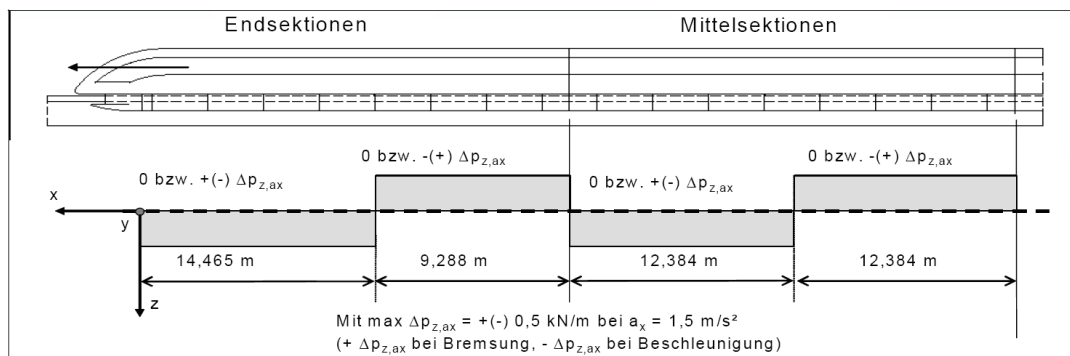


**Figure 5.6 The additional force in z direction due to acceleration and braking, MSB-AG-Fahrweg Teil II**

### 5.3.3 Non-uniformly distributed load in x-direction, Q3

The centre of gravity of the vehicle can shift due to non-uniform distributed live load and self weight of vehicle in x-direction (Q3). This unequal distribution is introduced over the vehicle structure (e.g. distribution of the loads over air cushion systems) to the levitation and guidance magnets.

In case of vehicles for goods transport it should be guaranteed by a project-specific loading regulation that the non-uniformly distributed load in x-direction will be less unfavorable than that in Table 5.8.

### 5.3.4 Non-uniformly distributed load in y-direction, Q4

The centre of gravity of the vehicle can shift due to non-uniform distributed live load in y-direction (Q4). This shift is however negligible compared with the average static action indicated in Table 5.4. In case of vehicles for goods transport, it should be also guaranteed by a project-specific loading regulation that in the y-direction no non-uniform loading takes place.

### 5.3.5 Lateral force due to guidance dynamic response, Q5

Dynamic lateral force (SK) due to the lateral guidance dynamics can be determined by:

$$\pm P_{y,SK} = \pm \left( 1 + \frac{v_{Fzg} [\text{km/h}]}{500 [\text{km/h}]} \right) \text{ in [kN/m]} \quad (5.8)$$

Note that for  $v_{Fzg} = 0$ , the lateral force  $P_{y,SK} = 0$ .

### 5.3.6 Restraint action due to horizontal radius, Q6

The restraint action due to the guidance magnet in the y-direction with a small horizontal radius is determined by the vehicle geometry. The characteristic value for relevant radius can be obtained from Table 5.9. The distribution of the action over the vehicle length is represented in Figure 5.7.

$p_{y,ZWG,i}$ [kN/m]	Endsektionen		Mittelsektionen	
	$R_H = 350 \text{ m}$	$R_H = 1000 \text{ m}$	$R_H = 350 \text{ m}$	$R_H = 1000 \text{ m}$
$p_{y,ZWG,1}$	-	-	18,0	7
$p_{y,ZWG,2}$	21,0	7	0	0
$p_{y,ZWG,3}$	0	0	0	0
$p_{y,ZWG,4}$	1,0	0	6,0	0
$p_{y,ZWG,5}$	2,0	0	1,0	0
$p_{y,ZWG,6}$	-4,5	0	-5	-1
$p_{y,ZWG,7}$	-21,0	-7	-21,0	-6
BM	-	-	-	-
$p_{y,ZWG,10}$	-21,0	-7	-21,0	-6
$p_{y,ZWG,11}$	-4,5	0	-5	-1
$p_{y,ZWG,12}$	1,0	0	1,0	0
$p_{y,ZWG,13}$	7,0	0	6,0	0
$p_{y,ZWG,14}$	0	0	0	0
$p_{y,ZWG,15}$	1,0	0	1,0	0
$p_{y,ZWG,16}$	18,0	7	18,0	7

Zwischenwerte dürfen linear inter- bzw. extrapoliert werden.

Table 5.9 Distribution of the restraint action with a horizontal radius  $R$ , MSB-AG-Fahrweg Teil II

## 5 Actions on Guideway

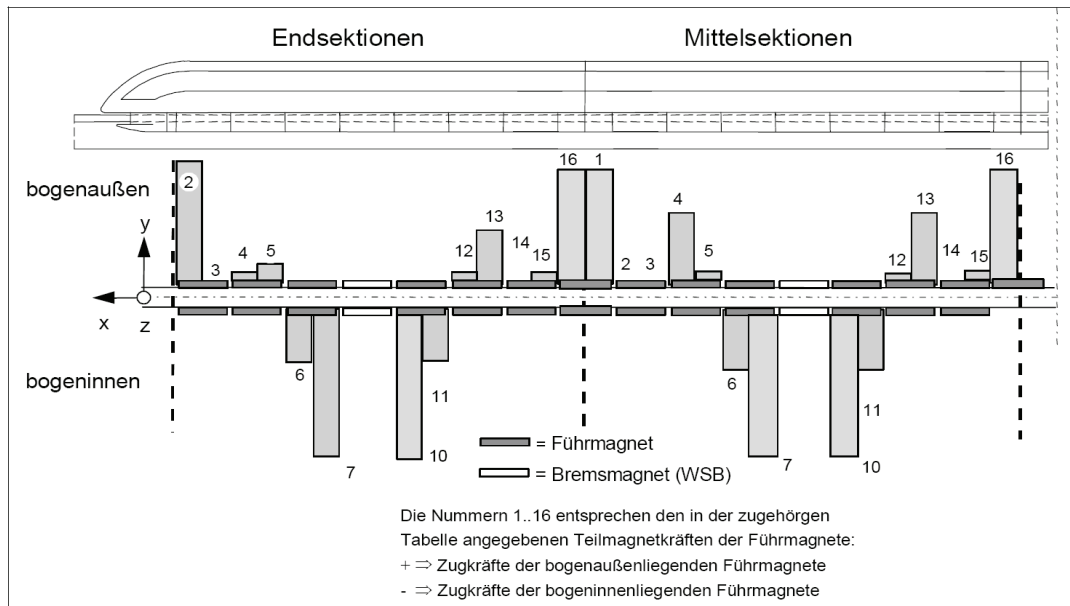


Figure 5.7 Distribution of the restraint action with horizontal radius  $R$ , MSB-AG-Fahrweg Teil II

### 5.3.7 Aerodynamic action $Q7$

The guidance magnet force due to train encounters may be neglected on the basis of enough tracks spacing.

Vehicle driving in tunnel will cause a reduced space for air expulsion. Therefore the values for pressure and suction indicated in Table 5.11 should be increased by 10 %.

### 5.3.8 Headwind Action $Q8$

The lift forces in the  $z$ -direction by headwind ( $Q8a$ ) are indicated in Figure 5.8. For the foremost/end sections, the force can be calculated according to Table 5.10.

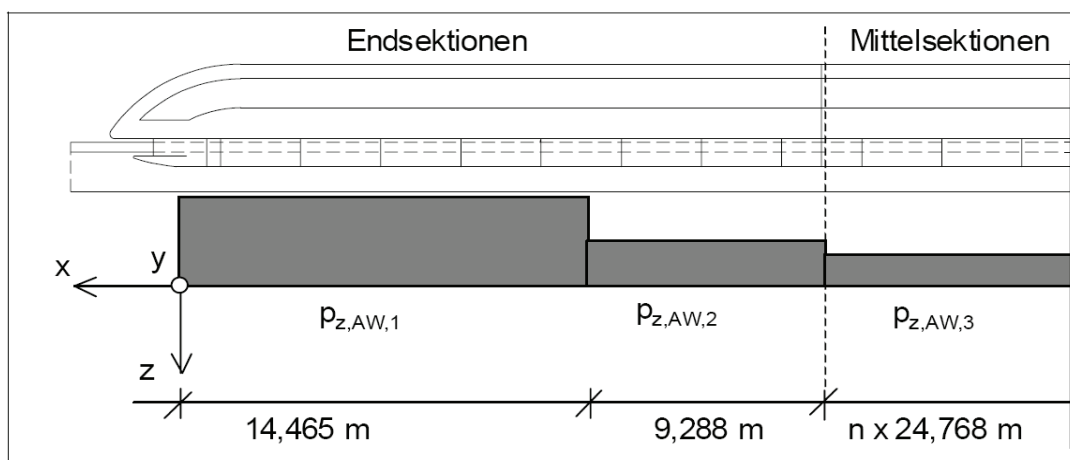


Figure 5.8 Load distribution for aerodynamic lift action, MSB-AG-Fahrweg Teil II

$v$	$P_{z,A,1}$	$P_{z,A,2}$
[km/h]	[kN/m]	[kN/m]
0	0	0
200	-0.8	0.5
300	-1.8	1.2
400	-3.2	2.1
500	-5.0	3.2

Table 5.10 Lift force for foremost section and end section of maglev vehicle

For the middle sections, Equation (5.9) can be used:

$$P_{z,A,3}(v) = \frac{P_{z,A,1}(v)}{3} \quad \text{in [kN/m]} \quad (5.9)$$

It is noted that the lift forces are considered only if they work unfavorably. The lift action due to headwind (Q8a) and that due to crosswind (Q9b) are not considered at the same time.

The wind pressure and suction due to headwind (Q8b) are applied on the top surface of the guideway. They are dependent on the driving speed and the location in longitudinal and transverse direction. The load distribution is shown in Figure 5.9. The relevant magnitude can be obtained from Table 5.11 for  $v = 500$  km/h (530 km/h).

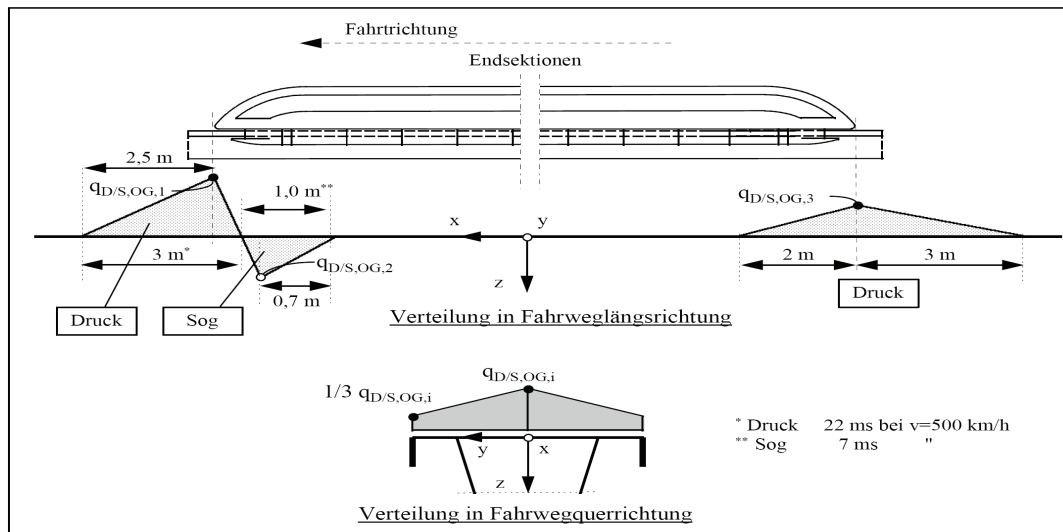


Figure 5.9 Distribution of pressure/suction on guideway due to headwind, MSB-AG-Fahrweg Teil II

$v$	$Q_{D/S,OG,1}$	$Q_{D/S,OG,2}$	$Q_{D/S,OG,3}$
[km/h]	[kN/m <sup>2</sup> ]	[kN/m <sup>2</sup> ]	[kN/m <sup>2</sup> ]
0	0	0	0
500	+14	-7	+7
530	+16	-8	+8

Table 5.11 The pressure (+) and suction (-) on guideway due to headwind, MSB-AG-Fahrweg Teil II

The magnitudes under other velocities can be calculated by linear interpolation in the relationship of the square of the speed.

### 5.3.9 Crosswind Action Q9

The action due to crosswind on standing and moving vehicles contains the lateral force in y-direction, moments around the x- and z-axis, and the lift forces in z-direction. The magnitude of the force and the points of application depend on:

- Driving velocity  $v_{Fzg}$
- Wind velocity  $v_{w,b}$
- Geometry of the maglev vehicle

The nominal wind speeds (5-seconds average value for 10m in 1 year)  $v_{b,10}$  are defined:

- Wind zone I  $v_{W,b,10} = 27$  m/s
- Wind zone II  $v_{W,b,10} = 30$  m/s
- Wind zone III  $v_{W,b,10} = 34$  m/s
- Wind zone IV  $v_{W,b,10} = 38$  m/s

Next the wind factor is defined. For instance, at Wind zone II, the ground speed  $v_{W,m,10}$  (10-min average value for 10 m in 10 years) is 25 m/s, therefore the factor is 1,44 ( $30/25 = 1.44$ ).

Nominal wind speeds with other heights  $h_w$  (in m) on terrain surface can be determined by Equation (5.10) with  $Z_w =$  approx. 1.3 m.

$$\frac{v_{W,b,h_w}}{v_{W,b,10}} = \left(\frac{h_w}{10}\right)^{0.11} \tag{5.10}$$

where

$$h_w = h_{G,Gelände} + z_w$$

In addition, a moment about the x-axis will be caused. The resulting forces are transferred from the levitation magnets to the guideway in z-direction.

With the driving speed and wind speed (see Table 5.12), the force on the guidance magnet and levitation magnet can be determined from *Tabelle 28-26* in *Anhang* of *MSB-AG-Fahrweg Teil II*. Then the lateral force and vertical force on the magnets can be obtained by linear interpolation for  $v_{Fzg} < 500$  km/h. When  $v_{Fzg} > 500$  km/h, it can be extrapolated in the relationship of the square of driving speed.

Windgeschwindigkeit bei $h_{G,Gelände} \leq 4,0$ m in Windzone				Windgeschwindigkeit bei $4,0 \text{ m} < h_{G,Gelände} \leq 13,0$ m in Windzone				Windgeschwindigkeit bei $13,0 \text{ m} < h_{G,Gelände} \leq 20,0$ m in Windzone			
I	II	III	IV	I	II	III	IV	I	II	III	IV
25	28	32	36	28	31	36	40	29	33	37	42

**Table 5.12 Wind speed for relevant guideway height [m/s]**

The lift forces caused by the crosswind can be determined from *Tabelle 19* in *MSB-AG-Fahrweg Teil II* for various driving speeds and wind speeds. The load is distributed in the same way as the Headwind action (Q8a), which has been shown in Figure 5.8.

Note that the lift forces reduce the vertical loads and thus are only considered if they work unfavorably. For the middle sections of the vehicle, Equation (5.11) is used.

$$P_{z,AW,3}(v) = \frac{P_{z,AW,1}(v)}{3} \quad \text{in [kN/m]} \quad (5.11)$$

### 5.3.10 Temperature Action Q10

The maximum temperature difference between the stator packages of long stator and the cantilever is

$$\max \Delta T_{antrieb} = 15 \text{ K}$$

# 6

---

## Vehicle/Guideway Interaction Analysis

## 6.1 General

A maglev vehicle-guideway interaction analysis consists of two complex dynamic systems: the vehicle with its suspension and active control characteristics; and the guideway with its flexibility characteristics. Figure 6.1 shows the essential elements of an interaction model.



**Figure 6.1** Maglev dynamic model

As the vehicle moves along the guideway, it is acted upon by the external forces and suspension system forces, which cause linear and rotational accelerations of the vehicle body. The suspension system responds to vehicle motion and guideway dynamics and surface irregularity. The guideway girder deforms in response to the moving suspension forces and the support dynamics. The support motions are related to the foundation dynamic characteristics and the guideway reaction forces and moments (James C. Ray et al, 1995). These systems interact with each other through time varying interfaces. The strongly coupled process is extremely complicated.

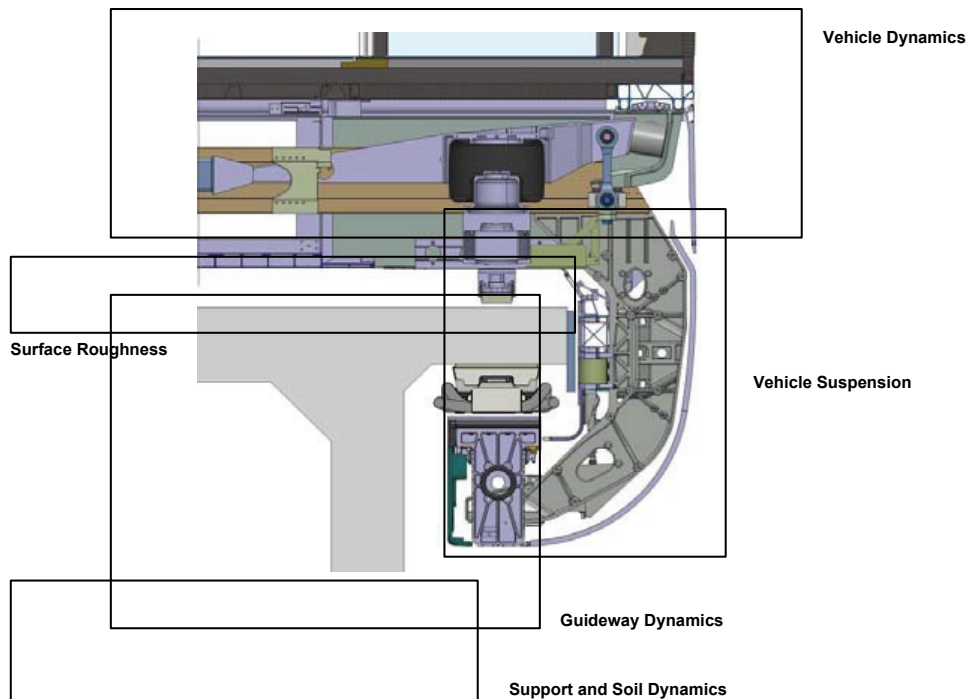


**Figure 6.2** Coupled Maglev Model, adapted from MSB-AG-Fahrzeug Teil III, 2007

To control the magnitude of the guideway displacement and vibration, it is important to be able to accurately predict guideway response to the action of crossing maglev vehicle. Furthermore, the guideway must provide acceptable ride quality and should be economically feasible. To evaluate a wide range of guideway designs for various operating condition, it is necessary to develop a reliable simulation technique for the interaction system.

The dynamic interaction process can be modeled in different levels of accuracy. This study includes five different dynamic models for maglev vehicles moving at a constant speed on a simply supported guideway.

These models fall into two types, those considering vehicle as moving forces, and those that model the vehicle as a multiple degrees-of-freedom system incorporating the dynamics of the suspension by lumped masses, linear springs and dampings.

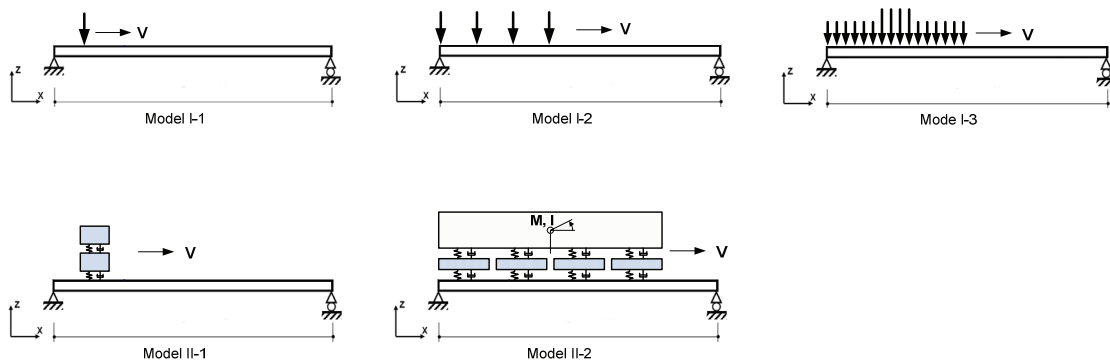


**Figure 6.3 Vehicle/guideway interaction models**

Numerical simulations for different models are performed by **Matlab/Simulink**, with an emphasis on the guideway deflection under a moving vehicle at various velocities. Simulink can provide the graphical environment and a customized set of block libraries that let the user design, simulate and test a variety of time-varying systems (The Mathworks Inc., 2007). The complex interaction model, which consists of the guideway, the car body, the bogies, the electromagnetic suspension system, and the guideway surface irregularity, can be built and simulated using numerical integration algorithms that compute the system dynamics over time using information contained in the model.

Alternatively, the first three models can also be created by the Finite Element Software like **Midas/Civil**. By performing a time-history analysis, the dynamic responses of the guideway under a moving load or multiple loads can be obtained. This way is closely related to other design issues during the design process, and is able to account for non-uniform properties of the guideway. But due to the limitation of the software package, it can only analyze the models of the first type.

The surface roughness model is obtained by **Simulink** as well. Using the Signal Processing Tools a Gaussian White Noise is generated and is passed through a specified Infinite Impulse Response (IIR) filter to get the desired road surface profile.

## 6.2 Guideway Model

The dynamic deflection of the simply supported guideway can be computed by using the Modal analysis method (Biggs, 1964). The Bernoulli-Euler equation is the basis of this method. The space- and time-varying guideway motion  $y(x,t)$  is represented as an infinite summation of its natural modes. Normally a finite number of modes are used to represent the guideway motion in accordance with the required level of accuracy.

The technique is appropriate to solve one-dimension oscillation problem. Based on the assumption that vertical motion is dominant and that the vertical, lateral and twist motions of the guideway are independent with each other, attention will be mainly focused on the vertical guideway deflection when vehicle/guideway interaction is analyzed in this report.

The equation of motion for a Bernoulli-Euler beam where a multiple-load vehicle is traveling along is given by:

$$EI \frac{\partial^4 y}{\partial x^4} + C \frac{\partial y}{\partial t} + m \frac{\partial^2 y}{\partial t^2} = F(x,t) \quad (6.1)$$

where

$y$	guideway vertical displacement;
$x$	axial coordinate;
$EI$	bending stiffness of the guideway;
$C$	viscous damping coefficient;
$m$	guideway mass per unit length;
$F(x,t)$	electromagnetic interaction forces between vehicle bogies and guideway

The interaction forces  $F(x,t)$  can be derived as:

$$F(x,t) = \sum_{i=1}^n F_i(t) \delta(x_i - vt) \quad (6.2)$$

where

$x_i$	actual coordinate of the electromagnetic interaction force;
$\delta$	Dirac delta function
$n$	number of electromagnetic interaction forces

The boundary conditions are:

$$\begin{aligned} x=0 \quad y(0,t) &= 0, \quad \frac{\partial^2 y(0,t)}{\partial x^2} = 0 \\ x=L \quad y(L,t) &= 0, \quad \frac{\partial^2 y(L,t)}{\partial x^2} = 0 \end{aligned} \quad (6.3)$$

The initial conditions are:

$$t=0 \quad y(x,0) = 0, \quad \frac{\partial y(x,0)}{\partial t} = 0 \quad (6.4)$$

The problem specified by above equations can be solved with a modal analysis method. The displacement of the guideway is expressed as:

$$y(x,t) = \sum_{k=1}^{\infty} A_k(t) \phi_k(x) \quad (6.5)$$

where

$k$	mode number, 1, 2, 3...
$A_k(t)$	$k$ -th modal amplitude
$\phi_k(x)$	$k$ -th modal shape function

The orthonormal modal shape function  $\phi_k(x)$  of the  $k$ -th mode for a single-span guideway can be expressed as:

$$\phi_k(x) = \sqrt{2} \sin\left(\frac{k\pi x}{L}\right) \quad (6.6)$$

The modal amplitude  $A_k(t)$  of the  $k$ -th mode is the solution of the following differential equation:

$$\frac{d^2 A_k(t)}{dt^2} + 2\zeta_k \omega_k \frac{dA_k(t)}{dt} + \omega_k^2 A_k(t) = \frac{\int_0^L F(x,t) \phi_k(x) dx}{\int_0^L m \phi_k^2(x) dx} \quad (6.7)$$

where

$\zeta_k$	modal damping ratio of the $k$ -th mode
$\omega_k$	circular natural frequency of the $k$ -th mode

The circular natural frequency of the  $k$ -th mode for a simply supported guideway is given by:

$$\omega_k = \left(\frac{k\pi}{L}\right)^2 \sqrt{\frac{EI}{m}} \quad (6.8)$$

Using the orthogonality property of  $\phi_k(x)$  and assuming the shape functions are normalized, the following equation is obtained:

$$\frac{1}{L} \int_0^L \phi_k^2(x) dx = 1 \quad (6.9)$$

Substituting Equation (6.9) into Equation (6.7), the equation of motion of the guideway in terms of the modal amplitude is written as:

$$\frac{d^2 A_k(t)}{dt^2} + 2\zeta_k \omega_k \frac{dA_k(t)}{dt} + \omega_k^2 A_k(t) = \frac{1}{mL} \int_0^L F(x,t) \phi_k(x) dx \quad (6.10)$$

For a Maglev system, the guideway loading usually consists of a specified pressure profile which moves with the vehicle velocity  $v$  (James C. Ray et al, 1994), and then the right side of Equation (6.10) can be integrated explicitly to obtain a function of time only:

$$\frac{d^2 A_k(t)}{dt^2} + 2\zeta_k \omega_k \frac{dA_k(t)}{dt} + \omega_k^2 A_k(t) = \frac{1}{mL} \sum_{i=1}^n F_i(t) \phi_k(x_i) \quad (6.11)$$

In Figure 6.4 the elevated maglev guideway used in the dynamic interaction model is shown. It is designed mainly based on the first generation of concrete guideway at Test Facility Emsland. Its prototype was originally developed by the engineering company Dywidag early in 1981.

The guideway is simply supported with a span length  $L = 24.768$  m and a height  $H = 1.827$  m. The cross-section consists of a single-celled box girder with cantilever arms and diaphragms at the ends. The guideway parameters that will be used for the simulation are listed in the following table:

$L = 24.768$	Length of guideway [m]
$A = 1.44565$	Area of cross section [m <sup>2</sup> ]
$I = 0.543244$	Moment of inertia [m <sup>4</sup> ]
$E = 35.684 \times 10^9$	Young's Modulus [N/m <sup>2</sup> ]
$W = 23540$	Weight of guideway [N/m <sup>3</sup> ]
$m = 3470.4$	Guideway mass per unit length [kg/m]
$\zeta_k = 0.006$	Damping ratio for $k$ -th mode [/]

**Table 6.1** Guideway parameters



**Figure 6.4** Guideway model

### 6.3 Vehicle Model and Suspension system

The Transrapid vehicle consists of a carriage body, eight C-shape levitation frames, secondary suspensions, 32 levitation magnets and 30 guidance magnets. The magnetic interaction forces are distributed uniformly over the total vehicle length. In case of a simplified model, the finite forces are used to replace the vehicle loads on the condition that they can provide an equal static action and an approximate dynamic action. In Figure 6.6 five vehicle models are shown from a moving constant load to a multiple degree-of-freedom system at different levels of accuracy.

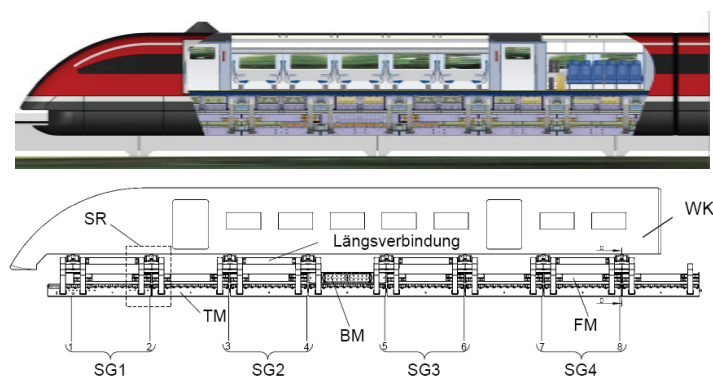


Figure 6.5 TR09, MSB-AG-Fahrzeug Teil IV, 2007

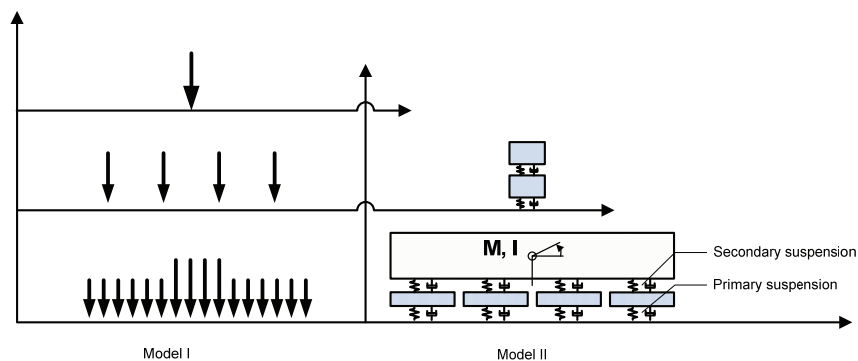


Figure 6.6 Maglev vehicle models

In case of a multiple degree-of-freedom system, for instance the 2 degree-of-freedom model and 6 degree-of-freedom model, the spring and the shock absorber in the secondary suspension are characterized by spring stiffness  $k_s$  and damping coincident  $c_s$  respectively. These parameters can be obtained from literature based on the test data at TVE, which are listed in Table 6.2.

For the primary suspension, the force to support the vehicle is developed by electromagnets interacting with the stator packs. This interaction results in the force that attracts the electromagnet to the guideway and is related to the air gap and the coils current.

The dotted lines in Figure 6.7 show the force-gap relation when the current in the electromagnets were kept constant (James H. Lever, 1998). A decrease in air gap would result in an increase in the attractive force that would accelerate the electromagnet into the guideway. An increase in gap would similarly lead to a decrease in the force and the force would no longer be large enough to support the maglev vehicle. Therefore the levitation provided by a constant current magnet is unstable and an active control system is desirable. As the gap becomes smaller, the current is decreased to reduce the attractive force. The electromagnet is then driven away from the guideway. On the other sides, as the gap becomes larger, the current is increased, resulting in an increase in force and acting to return the vehicle to the nominal gap.

The solid curve in Figure 6.7 shows the force as a function of the gap that result from an active control strategy. For each millimeter of gap change the current would be changed by 20%. Since this process appears highly nonlinear and is difficult to describe mathematically, the tangent slope of the force-gap curve on a nominal steady point is used to represent the stiffness for primary suspension. The magnetic force is expressed as:

$$F_{EMS} = F_0 + k_p (s - s_0) + c_p s' \tag{6.12}$$

- $F_{EMS}$  total electromagnetic force
- $F_0$  static electromagnetic force
- $k_p$  tangent stiffness for primary suspension
- $c_p$  damping for primary suspension
- $s$  air gap
- $s_0$  nominal air gap, 8 mm for the TR06 system

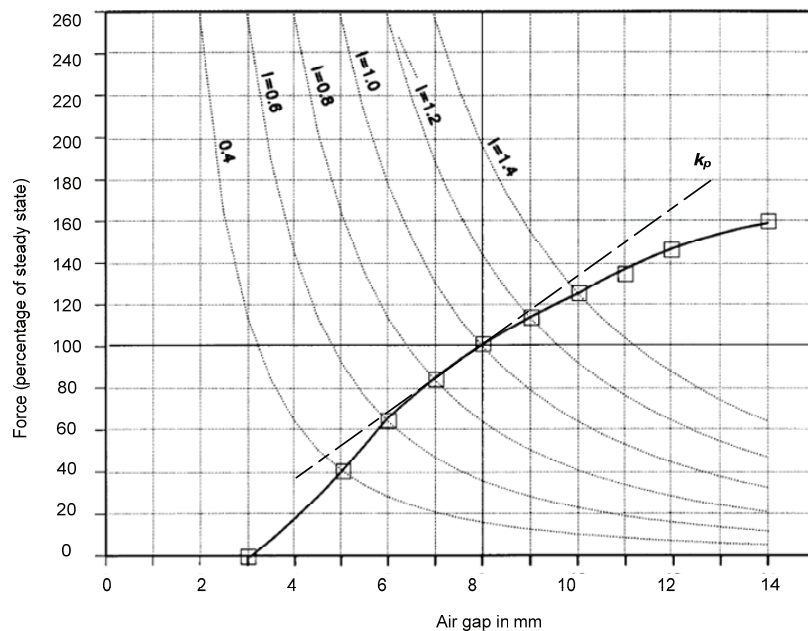


Figure 6.7 Force-gap characteristics for a typical EMS suspension, adapted from J.H. Lever, 1998

The vehicle parameters used in the Matlab code are listed in Table 6.2. Note that these characteristics are believed to be able to represent the Transrapid TR06 system only. For the new TR08 and TR09 vehicle system, the data collected at this moment is not sufficient to make a numerical model.

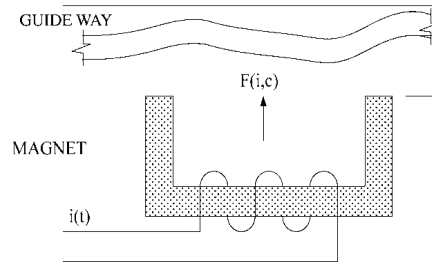
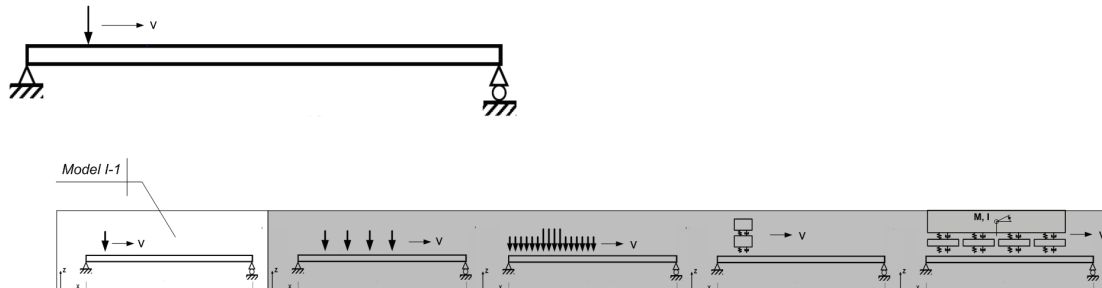


Figure 6.8 Electromagnetic suspension system, Jin Shi et al., 2007

$L_v = 24.768$	Maglev vehicle length [m]
$m_v = 29200$	Carriage body mass [kg]
$I_v = 1.75 \times 10^6$	Carriage body pitch inertia [kg m <sup>2</sup> ]
$m_f = 32000$	Total Levitation frame mass [kg]
$k_p = 1.18 \times 10^8$	Total primary stiffness [N/m]
$k_s = 6.812 \times 10^5$	Total secondary stiffness [N/m]
$c_p = 2.15 \times 10^6$	Total primary damping [N s/m]
$c_s = 8.46 \times 10^4$	Total secondary damping [N s/m]

Table 6.2 Maglev vehicle parameters

### 6.4 Dynamic Interaction Model I-1



The modeling of a maglev vehicle traveling along a guideway as a moving force neglects the inertia of the moving subsystem and no dynamic interaction between magnet and guideway is considered. In that case, the equation of motion of the guideway in terms of the modal amplitude (6.11) is written as:

$$\frac{d^2 A_k(t)}{dt^2} + 2\zeta_k \omega_k \frac{dA_k(t)}{dt} + \omega_k^2 A_k(t) = \frac{F}{mL} \sqrt{2} \sin\left(\frac{k\pi vt}{L}\right) \tag{6.13}$$

where

- $F$  moving constant force,  $F = (m_v + m_f)g$
- $v$  velocity of maglev vehicle
- $m$  guideway mass per unit length

The displacement of the guideway at mid span can be derived from Equation (6.5):

$$y\left(\frac{L}{2}, t\right) = \sum_{k=1}^{\infty} A_k(t) \phi_k\left(\frac{L}{2}\right) = \sum_{k=1}^{\infty} A_k(t) \sqrt{2} \sin\left(\frac{k\pi}{2}\right) \tag{6.14}$$

Equation (6.13) and (6.14) are functions of time only and therefore can be simulated by Simulink. Firstly only the first mode of the guideway is considered, so  $k=1$ . The Simulink model is shown in Figure 6.9. During the simulation, four parameters are defined for simplicity:

$$a = 2\zeta_1 \omega_1, \quad b = \omega_1^2, \quad c = \frac{\sqrt{2}}{mL}, \quad d = \frac{k\pi v}{L} \tag{6.15}$$

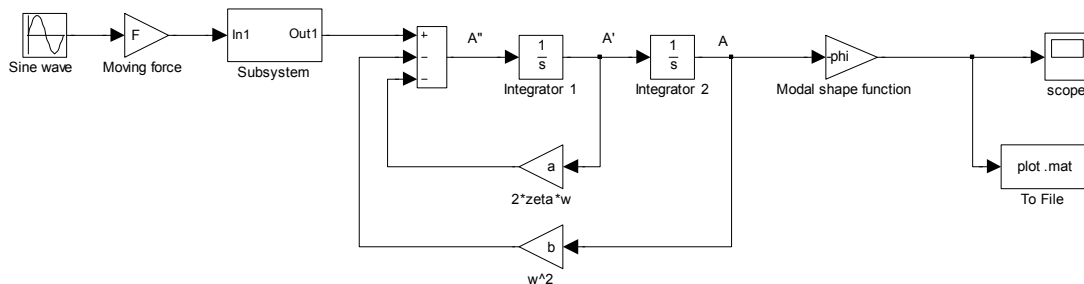


Figure 6.9 Simulink model

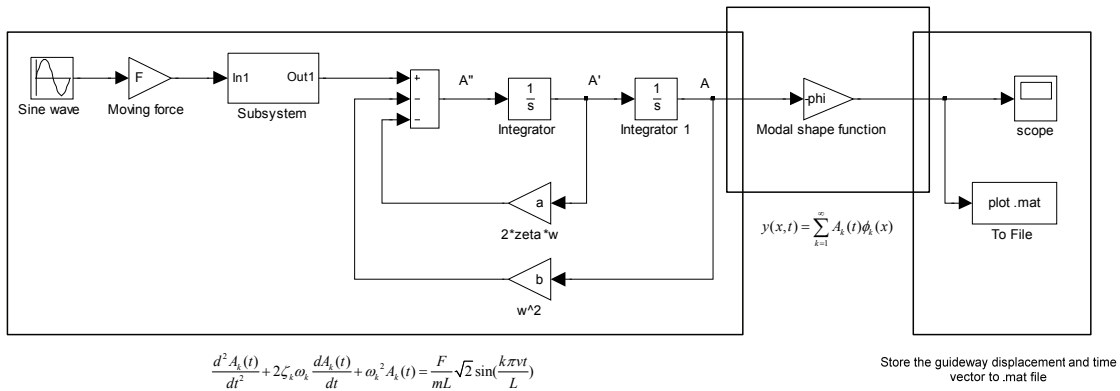


Figure 6.10 Simulink Model I-1

A Matlab code consisting of the parameters and variables is written first. It provides the necessary input to Simulink for the simulation in time domain. When Simulink is running, the state will be recalculated for every time step. The first block from the left introduces a sine wave with the amplitude  $c$  and the frequency  $d$ . After multiplied by the moving force  $F$ , it will be passed through a subsystem as shown in Figure 6.11.

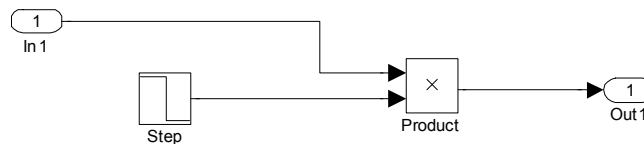


Figure 6.11 Step subsystem

The Step block in the subsystem provides a step between two definable levels at a specified time. A step time  $t = L/v$ , which is the travelling time of the vehicle on the guideway, an initial value 1, and a final value 0 are defined respectively. If the simulation time is less than the Step time  $t$ , which means the vehicle is still moving on the guideway, the block's output is the initial parameter value 1. For simulation time greater than or equal to the Step time  $t$ , the output is the final parameter value 0. This subsystem behaves similarly as the Dirac delta function in Equation (6.2).

The output of the subsystem is stored into the Sum block. By using two Integrator blocks, a loop can be built based on Equation (6.13) within a given period  $T$ . The output is multiplied by the modal shape function  $\phi_k(L/2)$  according to Equation (6.14). The blocks at far right will store the guideway displacement vector and time vector to let Matlab make plots of these.

### 6.4.1 Validation of the model

The model can easily be validated by applying a force moving at a very slow velocity. In that case the maximum displacement at mid span should be approximately equal to the static situation, where:

$$u_{static,mid} = \frac{FL^3}{48EI} = 9.8 \times 10^{-3} \text{ m} \quad (6.16)$$

By taking  $v = 0.1$  m/s the simulation is performed and the result is shown in Figure 6.12. The displacement at mid span is plotted as a function of the location of the moving force  $x_i$ .

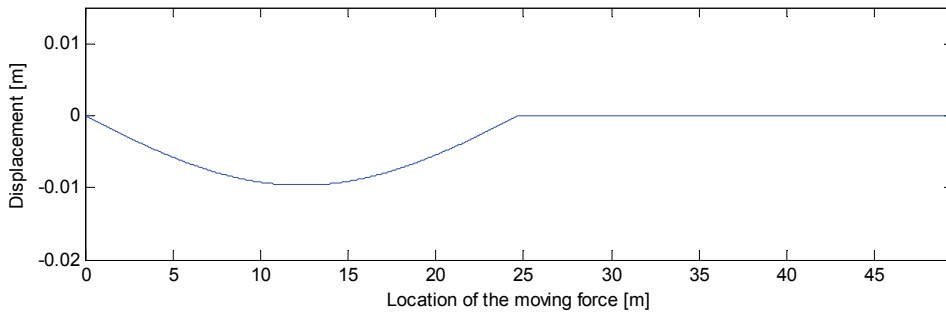


Figure 6.12 Guideway displacement-location of the moving force at  $v=0.1$ m/s

As can be seen from the figure, the maximum displacement at mid span is:

$$u_{dynamic,v=0.1} = 9.659 \times 10^{-3} \text{ m} \quad (6.17)$$

It occurs when the load moves to the middle of the guideway and is quite closed to the static case with a difference of 1.44% only. A possible reason for this small difference is the assumption that the first mode is dominant and thus any other higher modes are neglected.

Alternatively the numerical model can be validated by applying a force moving at the first critical velocity  $v_{critical,1}$ , where the maximum displacement should occur at the moment when the moving force is about to leave the guideway (Li Guohao, 1992), and the magnitude should be equal to:

$$u_{critical,1} = \frac{FL^3}{EI\pi^3} = 15.20 \times 10^{-3} \text{ m} \quad (6.18)$$

The critical velocity can be derived when the crossing frequency  $\Omega_k = k\pi v/L$  is equal to the natural frequency of the guideway  $\omega_k$ :

$$\Omega_k = \omega_k = \left( \frac{k\pi}{L} \right)^2 \sqrt{\frac{EI}{m}} \quad (6.19)$$

Then the critical velocity can be written as:

$$v_{critical,k} = \frac{L}{k\pi} \omega_k = \left( \frac{k\pi}{L} \right) \sqrt{\frac{EI}{m}} \quad (6.20)$$

So the first critical velocity  $v_{critical,1}$  is:

$$v_{critical,1} = \left(\frac{\pi}{L}\right) \sqrt{\frac{EI}{m}} = 299.78 \text{ m/s} \quad (6.21)$$

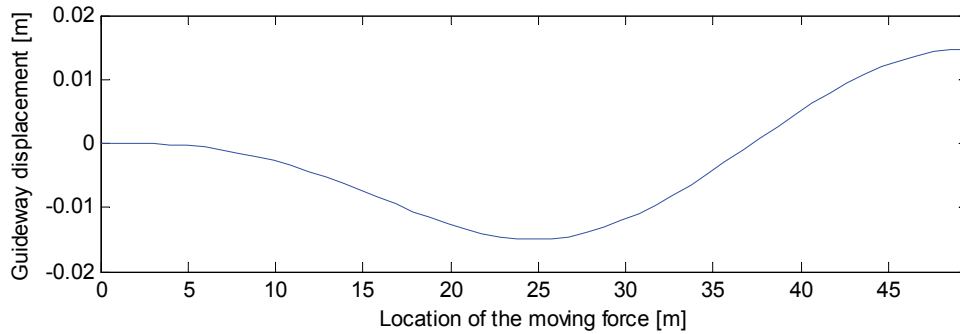


Figure 6.13 Guideway displacement-location of the moving force at  $v=299.78\text{m/s}$

By taking  $v = 299.78 \text{ m/s}$  Simulink results in the plot shown in Figure 6.13. The maximum guideway displacement at mid-span occurs when the location of the moving force is 24.77 m. Note that the guideway length is 24.768 m so this is exactly the moment when the force is leaving the guideway. The maximum guideway displacement for first critical velocity is:

$$u_{dynamic, v=299.78} = 15.02 \times 10^{-3} \text{ m} \quad (6.22)$$

It is also quite close to the analytical solution in Equation (6.18), so the numerical model is well constructed.

### 6.4.2 Dynamic response

The guideway responses under a moving force at various velocities are studied using the numerical model. The time histories of the displacement at mid span as a function of the location of the moving force is shown in Figure 6.14 for various velocities ( $\zeta_k = 0.006$ ).

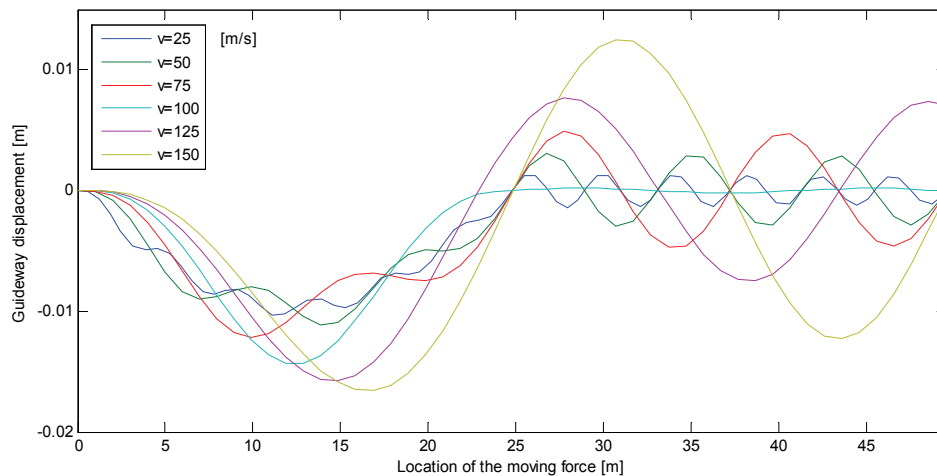


Figure 6.14 Guideway displacement-location of the moving force for various velocities

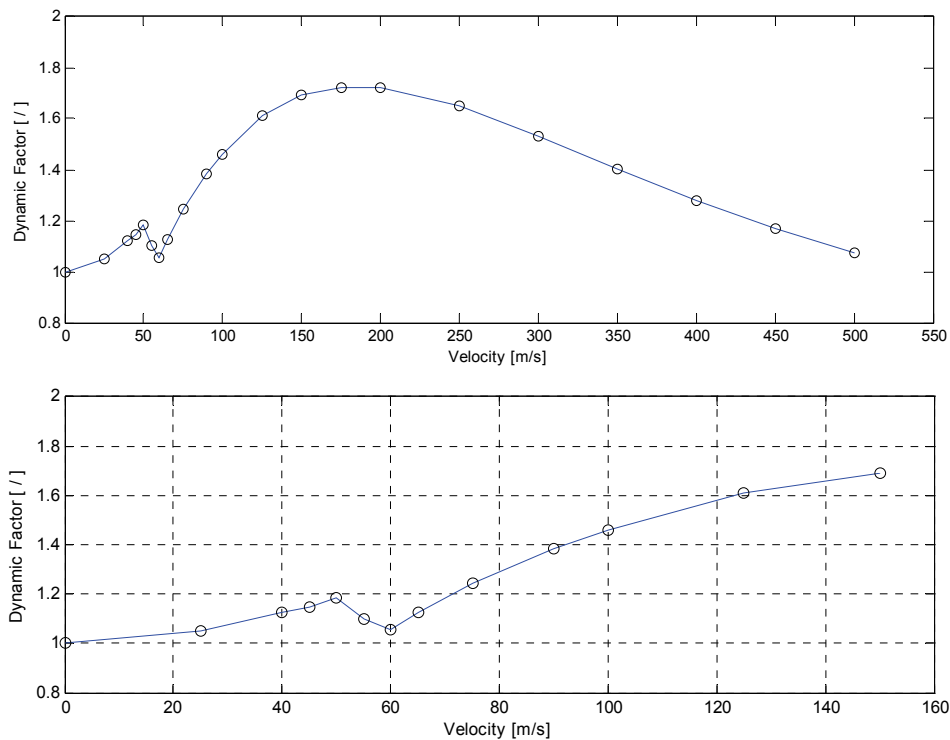


Figure 6.15 Dynamic factor as a function of velocity

The dynamic factor is defined based on *Magnetschnellbahn Ausführungsgrundlage Fahrweg Teil II*:

$$\varphi_{Bg,z} = \frac{u_{dynamic,max}}{u_{static,max}} \quad (6.22)$$

Figure 6.15 shows the dynamic factor vs. velocity of the moving force. The maximum dynamic factor is 1.723 which is attained for  $v = 200$  m/s. Note that the critical velocity  $v_{critical,1}$  is 299.78 m/s. Thus the velocity for maximum dynamic factor can be expressed in term of critical velocity as:

$$v = 0.67 v_{critical,1} \quad (6.23)$$

However, this velocity is unlikely to be seen in the maglev application, for which the maximum allowed velocity is 500 km/h (138.89 m/s) at the current stage.

### 6.4.3 Influence of damping

A number of simulations are performed to study the effect of damping on the guideway displacement. Four damping factors, 0, 0.3%, 0.6% and 1.6% are chosen according to the German design guideline.

In Figure 6.16 the guideway displacement at mid span is plotted as a function of location of the moving force for various dampings and various velocities. Only a slight change can be seen in the figure when damping varies. Therefore the effect of damping ratio on guideway displacement can be neglected when it ranges between 0 and 1.6%. This shows an agreement with the German design guideline where only one design curve is available for four damping ratios.

## 6 Vehicle/Guideway Interaction Analysis

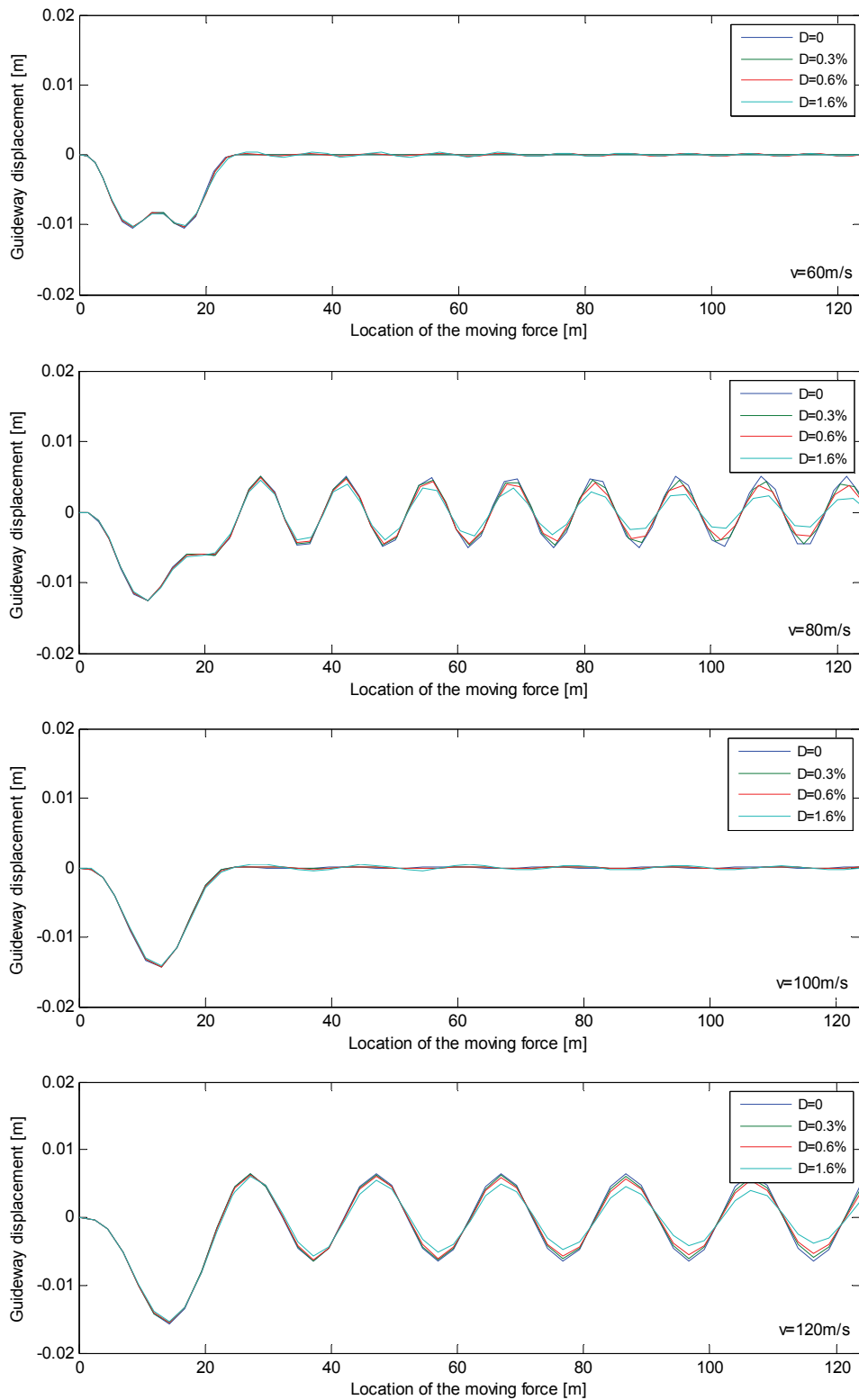
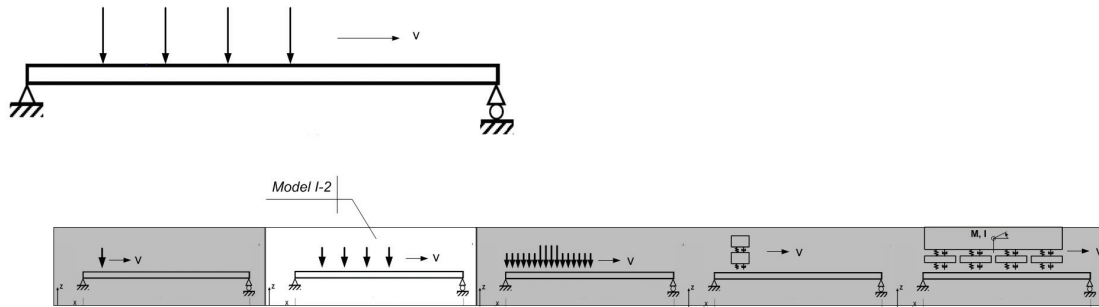


Figure 6.16 Guideway displacement-location of the moving force for various damping ratios

### 6.5 Dynamic Interaction Model I-2



For a Maglev system, the vehicle loading usually consists of a distributed pressure rather than a single concentrated load. In the Model I-2, four moving forces will be used to represent the loading of the maglev vehicle.

$$F_i = \frac{1}{n}(m_v + m_f)g \tag{6.24}$$

where

- $F_i$  moving constant force
- $m_v$  carriage body mass
- $m_f$  levitation frame mass
- $n$  number of moving force,  $n = 4$
- $i$  1, 2, 3 ...  $n$

The equation of motion of the guideway in terms of the modal amplitude (6.11) is written as:

$$\frac{d^2 A_k(t)}{dt^2} + 2\zeta_k \omega_k \frac{dA_k(t)}{dt} + \omega_k^2 A_k(t) = \frac{\sqrt{2}}{mL} \sum_{i=1}^4 F_i \sin\left(\frac{k\pi x_i}{L}\right) \tag{6.25}$$

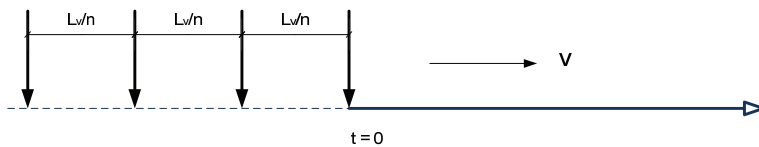


Figure 6.17 Dynamic interaction model

If the moment at which the first force is about to move onto the guideway is denoted as the starting point of the time domain, then the location of  $i$ -th force,  $x_i$ , can be calculated as:

$$x_i = vt_i = v \left[ t - (i-1) \frac{L_v}{4v} \right] \tag{6.26}$$

Equation (6.25) is now expressed as:

$$\frac{d^2 A_k(t)}{dt^2} + 2\zeta_k \omega_k \frac{dA_k(t)}{dt} + \omega_k^2 A_k(t) = \frac{\sqrt{2}}{mL} \sum_{i=1}^4 F_i \sin\left(\frac{k\pi v}{L} \left[ t - (i-1) \frac{L_v}{4v} \right] \right) \quad (6.27)$$

where

- $L_v$  length of maglev vehicle
- $L$  length of simply supported guideway

The displacement of the guideway at mid span can be derived from Equation (6.5):

$$y\left(\frac{L}{2}, t\right) = \sum_{k=1}^{\infty} A_k(t) \phi_k\left(\frac{L}{2}\right) = \sum_{k=1}^{\infty} A_k(t) \sqrt{2} \sin\left(\frac{k\pi}{2}\right) \quad (6.28)$$

Equation (6.27) and (6.28) are functions of time only and therefore can be simulated by Simulink. Only the first mode of the guideway is considered so  $k = 1$ . Again four parameters are defined for simplicity of the simulation:

$$a = 2\zeta_1 \omega_1, \quad b = \omega_1^2, \quad c = \frac{\sqrt{2}}{mL}, \quad d = \frac{k\pi v}{L} \quad (6.29)$$

The Simulink model is shown in Figure 6.18.

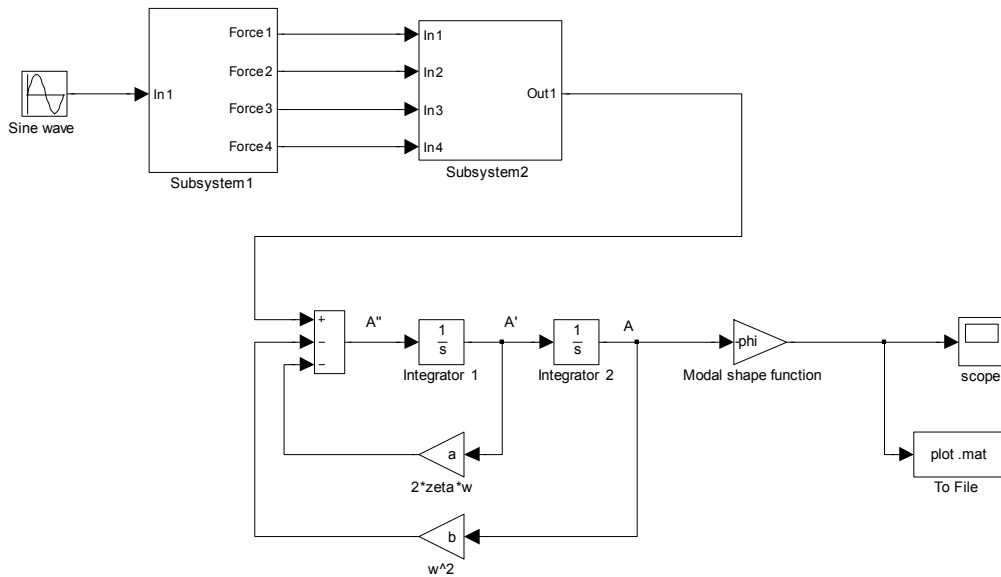


Figure 6.18 Simulink Model I-2

The right-hand side of Equation (6.27) can be simulated by constructing a subsystem using the Transport Delay block. Transport Delay block delays the input by a specified amount of time. It can be used to simulate the time delay between two neighboring forces, as shown in Figure 6.19.

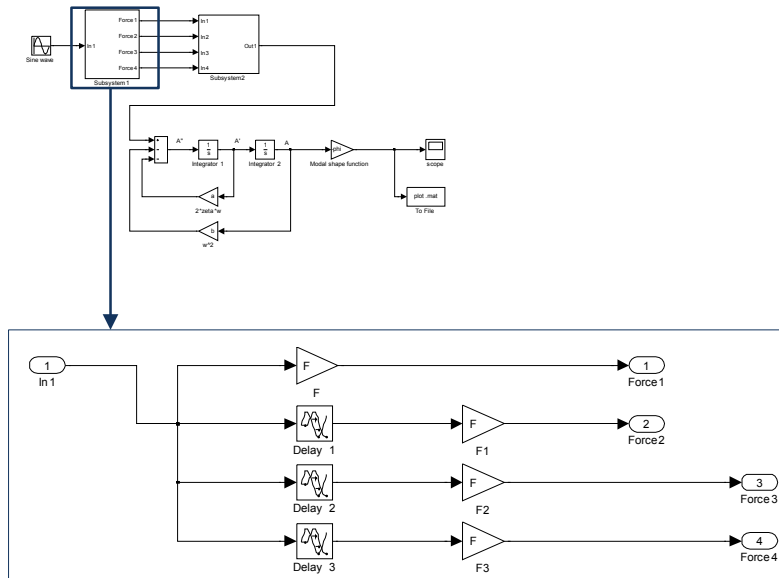


Figure 6.19 Subsystem-Transport Delay

The input of this subsystem is a sine wave with the amplitude  $c$  and frequency  $d$ . The time delay parameters for each Transport Delay block can be obtained from Equation (6.26):

$$T_{delay} = (i - 1) \frac{L_v}{nv} \tag{6.30}$$

thus

$$T_{delay1} = \frac{L_v}{nv}, T_{delay2} = \frac{2L_v}{nv}, T_{delay3} = \frac{3L_v}{nv} \tag{6.31}$$

The four outputs are then passed through another subsystem as shown in Figure 6.20. These block sets can have the forces cease to excite when they have already left the guideway. It consists of a number of Step blocks to provide the step between two definable levels at a specified time step.

Note that the time steps for each block are different and can be expressed as:

$$T_{time,step} = \frac{L}{v} + T_{delay} \tag{6.32}$$

thus

$$T_{step} = \frac{L}{v}, T_{step,1} = \frac{L}{v} + \frac{L_v}{nv}, T_{step,2} = \frac{L}{v} + \frac{2L_v}{nv}, T_{step,3} = \frac{L}{v} + \frac{3L_v}{nv} \tag{6.33}$$

## 6 Vehicle/Guideway Interaction Analysis

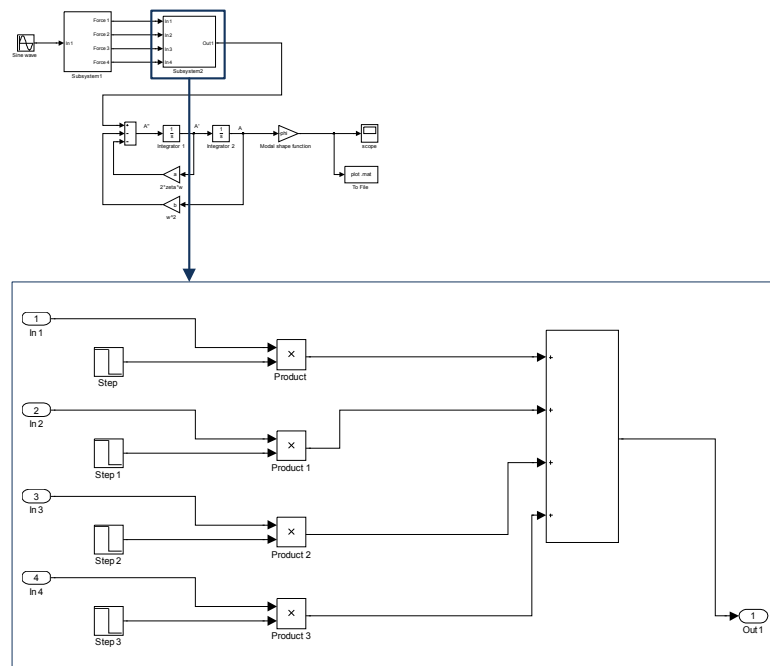


**Figure 6.20 Subsystem-Step**

The output of this system is stored into a Sum block. A loop then can be build with the help of two Integrator blocks based on Equation (6.27). The output will be multiplied by the modal shape function with  $x = L/2$  according to Equation (6.28). The entire simulation process can be monitored by the Scope block at far right and the displacement and time vector will be stored by the To File block.

### 6.5.1 Validation of the model

Model I-2 is validated in the same way as in Section 6.4.1, by applying multiple forces moving at a very slow velocity and then comparing the simulation result with the static result. A short script is written to calculate the static displacement with the help of Finite Element software ANSYS.

```

/filename, 1x4
/title, 1x4
/UNITS, SI
/PREP7

n=4
L=24.768
mv=29200
mf=32000
g=9.806
F=(mv+mf)*g/n

A=1.44565
E=35.684e9
I=0.543244

ET, 1, BEAM3
R, 1, A, I, 2
MP, ex, 1, E
MP, prxy, 1, 0.3

*DO, i, 1, 2*n+1
K, i, (i-1)*L/(2*n), 0, 0
*ENDDO

*DO, j, 1, 2*n
L, j, j+1
*ENDDO

ALLSEL
LESIZE, all, L/(2*n)
LMESH, all
FINISH

/SOLU

DK, 1, UX, 0, , , UY,
UZ
DK, 2*n+1, UY, 0, , ,
UZ

*DO, k, 1, n
FK, 2*k, FY, -F
*ENDDO
SOLVE
/POST1
PLNSOL, u, y
    
```

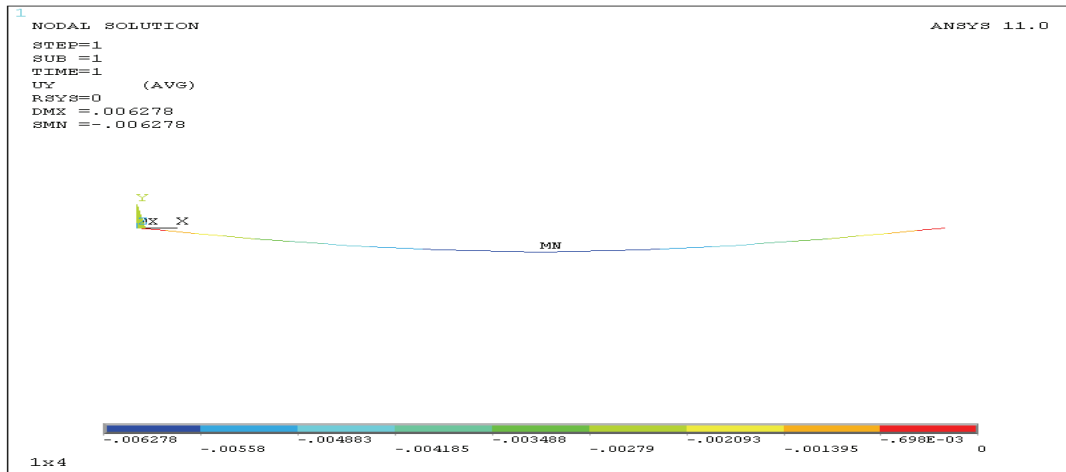


Figure 6.21 Static guideway displacement [m]

From Figure 6.21 the static displacement at mid span can be obtained:

$$u_{static,mid} = 6.278 \times 10^{-3} \text{ m} \tag{6.34}$$

The numerical simulation is then performed by taking  $v = 0.1$  m/s. The guideway dynamic displacement at mid span is plotted as a function of the location of the first moving force  $x_1$ :

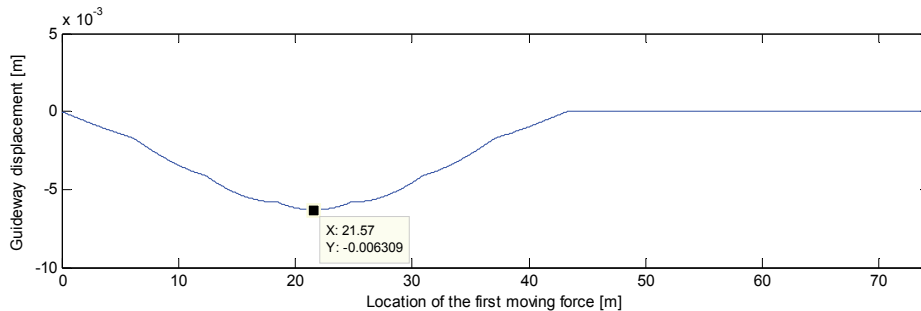


Figure 6.22 Guideway displacement-location of the moving force at  $v=0.1$ m/s

$$u_{dynamic,v=0.1} = 6.309 \times 10^{-3} \text{ m} \tag{6.35}$$

The maximum dynamic displacements for static and dynamic cases give closed results. Two possible reasons may lead to the slight difference: the assumption that the first mode is dominant and the influence from the slow velocity.

### 6.5.2 Dynamic response and influence of damping

The guideway responses under multiple moving forces at various velocities are studied using this numerical model ( $\zeta_k = 0.006$ ). The time histories of the displacement at mid span as a function of the location of the first moving force for various velocities are shown in Figure 6.23.

## 6 Vehicle/Guideway Interaction Analysis

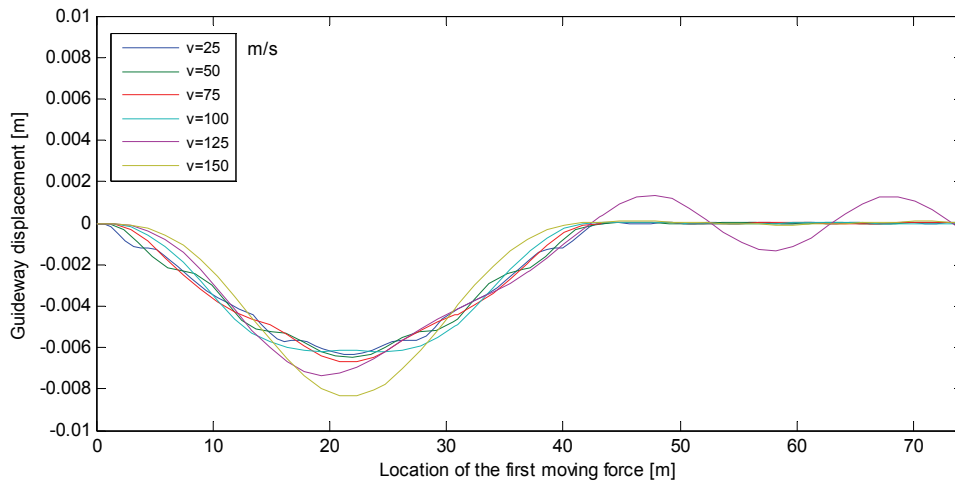


**Figure 6.23** Guideway displacement-location of the moving force for various velocities

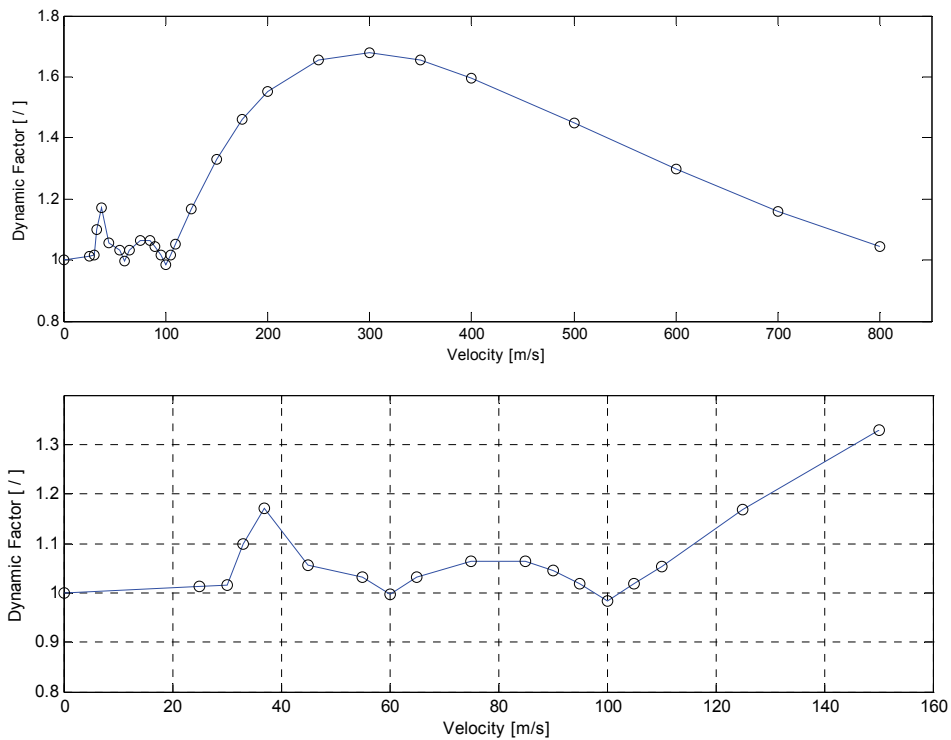


**Figure 6.24**Figure 6.15 Dynamic factor as a function of velocity

Figure 6.24 shows the dynamic factor vs. velocity of the moving forces. The maximum dynamic factor is 1.679 and is attained for approx.  $v = 300$  m/s.

The influence of damping ratio is studied using Model I-2. Four damping parameters,  $\zeta_k = 0, 0.3\%, 0.6\%$  and  $1.6\%$  are chosen as in Section 6.4.3. From the results shown in Figure 6.25 we can get the same conclusion that when the damping ratio varies between 0 and  $1.6\%$ , it makes little influence on the guideway displacement.

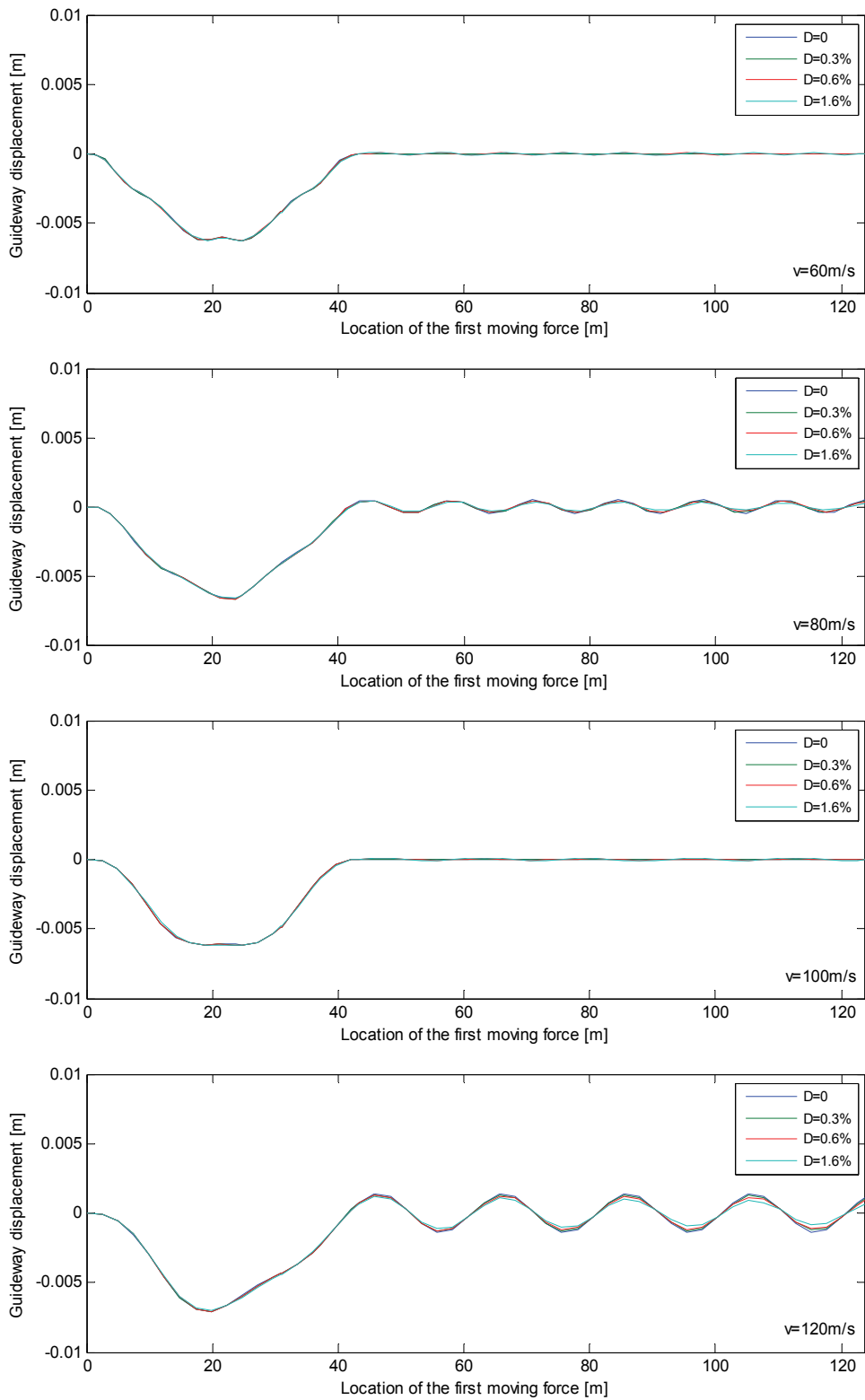
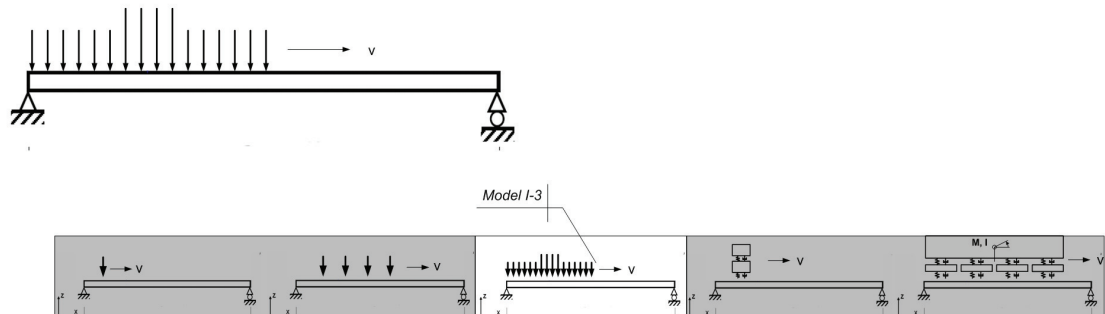


Figure 6.25 Guideway displacement-location of the moving force for various damping ratios

### 6.6 Dynamic Interaction Model I-3



For a Transrapid system, the magnetic levitation force is transferred from the vehicle to the guideway through the levitation magnet and the stator packs. This force is distributed over the length of the vehicle. Therefore the model can be made more real by using multiple forces distributed similarly as the levitation magnets.

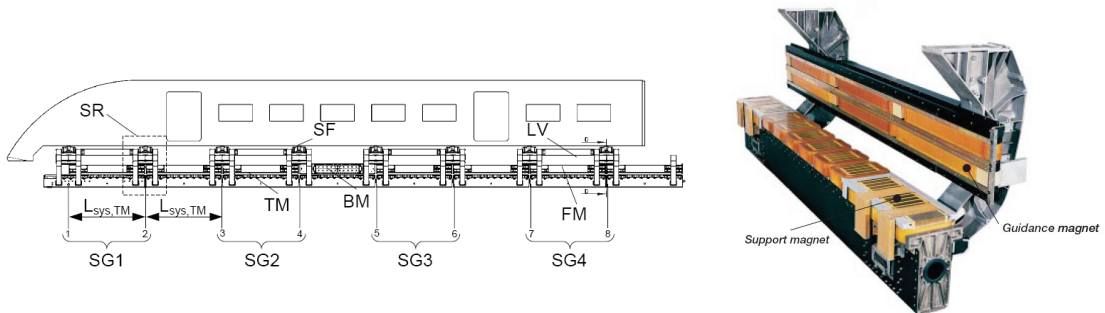


Figure 6.26 Transrapid vehicle, MSB-AG-Fahrzeug II, 2007

A standard Transrapid vehicle (middle section) consists of 16 levitation magnets at both sides. It can be simplified by 16 constant forces moving at certain velocity. The distance between two neighboring forces equal to half of the levitation magnet system length  $L_{sys, TM}$ .

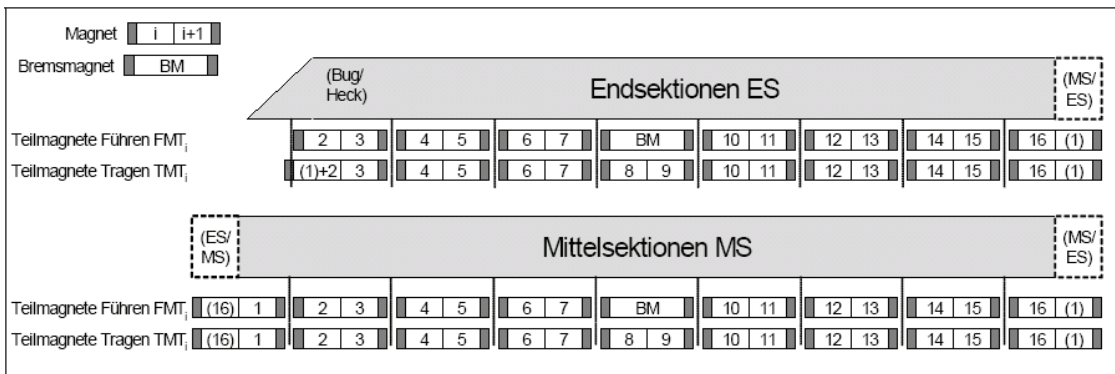


Figure 6.27 Levitation magnets, MSB-AG-Fahrweg Teil II, 2007

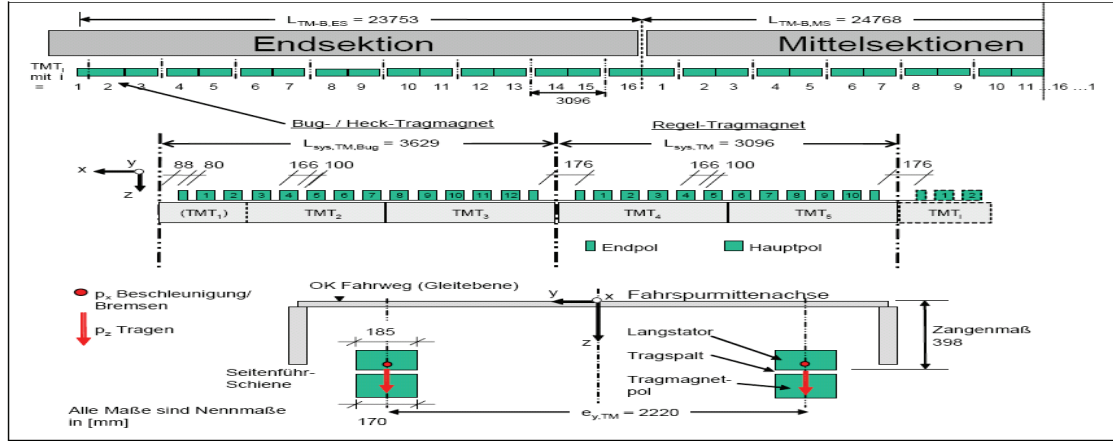


Figure 6.28 Levitation magnets, MSB-AG-Fahrweg Teil II, 2007

Endsektionen																
TMT <sub>i</sub>	1	2	3	4	5	6	7	8	9	10	11	12	13	14	15	16
k <sub>z,az,i</sub> [%]	10	10	5	7	7	7	7	7	7	7	6	6	6	6	6	6
Mittelsektionen																
TMT <sub>i</sub>	1	2	3	4	5	6	7	8	9	10	11	12	13	14	15	16
k <sub>z,az,i</sub> [%]	6	6	6	6	6	6	7	7	7	7	6	6	6	6	6	6

Table 6.3 Force distribution on levitation magnets, MSB-AG-Fahrweg Teil II, 2007

$$d_{\text{Model I-3}} = \frac{1}{2} L_{\text{sys, TM}} = \frac{1}{2} \times 3096 \times 10^{-3} = 1.548 \text{ m} \quad (6.36)$$

According to the design guideline, the magnetic force between single levitation magnet and guideway can be calculated as:

$$p_{z, a_z, \text{TMT}_i, \text{EG/MG/ZG/HG}} = 0.5 \bar{p}_{z, \text{EG/MG/ZG/HG}} \cdot \frac{L_{\text{ES/MS}}}{L_{\text{TMT}_i}} \cdot \frac{a_z}{g} \cdot \frac{k_{z, a_z, i}}{100} \quad (6.37)$$

$k_{z, a_z, i}$  is the percentage of the total force for  $i$ -th levitation magnet which is obtained from Table 6.3.  $\bar{p}_{z, a_z, \text{TMT}_i, \text{EG/MG/ZG/HG}}$  is the static force that can be obtained from *Tabelle 10* of *Magnetschnellban Ausführungsgrundlage, Fahrweg Teil II*.

The percentage for middle section is used in Model I-3. Therefore the magnitude of each force can be calculated as:

$$F_i = \begin{cases} (m_v + m_f)g \times 6\% & 1 \leq i \leq 6 \\ (m_v + m_f)g \times 7\% & 7 \leq i \leq 10 \\ (m_v + m_f)g \times 6\% & 11 \leq i \leq 16 \end{cases} \quad (6.38)$$

where

$F_i$	$i$ -th moving force
$m_v$	carriage body mass
$m_f$	levitation frame mass
$n$	number of moving force, $n = 16$
$i$	1, 2, 3 ... $n$

In this case the equation of motion of the guideway in terms of the modal amplitude (6.11) is written as:

$$\frac{d^2 A_k(t)}{dt^2} + 2\zeta_k \omega_k \frac{dA_k(t)}{dt} + \omega_k^2 A_k(t) = \frac{\sqrt{2}}{mL} \sum_{i=1}^{16} F_i \sin\left(\frac{k\pi x_i}{L}\right) \quad (6.39)$$

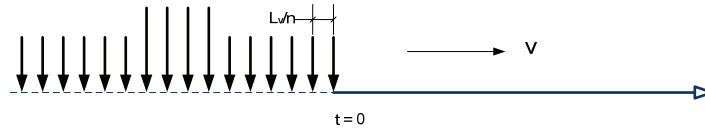


Figure 6.29 Dynamic interaction model

$x_i$  is the location of  $i$ -th force and can be calculated by:

$$x_i = vt_i = v \left[ t - (i-1) \frac{L_v}{16v} \right] \quad (6.40)$$

Equation (6.39) is now expressed as:

$$\frac{d^2 A_k(t)}{dt^2} + 2\zeta_k \omega_k \frac{dA_k(t)}{dt} + \omega_k^2 A_k(t) = \frac{\sqrt{2}}{mL} \sum_{i=1}^{16} F_i \sin\left(\frac{k\pi v}{L} \left[ t - (i-1) \frac{L_v}{16v} \right] \right) \quad (6.41)$$

where

- $L_v$  length of maglev vehicle
- $L$  length of simply supported guideway

The displacement of the guideway at mid span can be derived from Equation (6.5):

$$y\left(\frac{L}{2}, t\right) = \sum_{k=1}^{\infty} A_k(t) \phi_k\left(\frac{L}{2}\right) = \sum_{k=1}^{\infty} A_k(t) \sqrt{2} \sin\left(\frac{k\pi}{2}\right) \quad (6.42)$$

Equation (6.41) and (6.42) are functions of time only and therefore a dynamic model can be created in Simulink as shown in Figure 6.30.

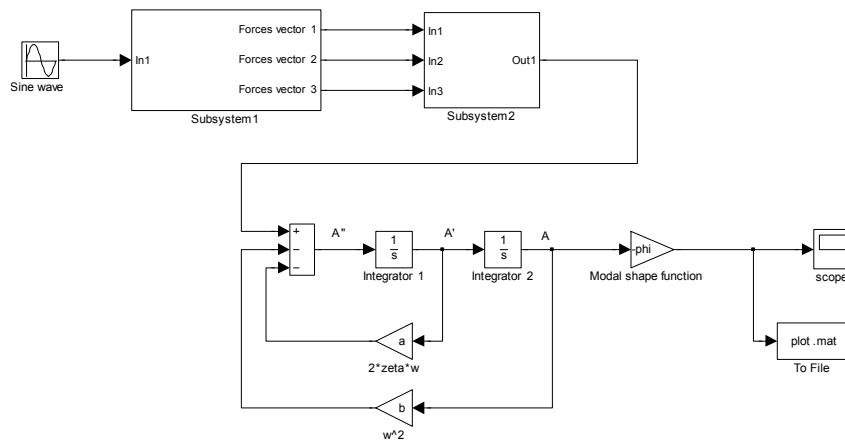


Figure 6.30 Simulink Model-I-3

Model I-3 contains two subsystems. The first subsystem consists of a number of Transport Delay blocks to delay the input signal by a specified amount of time, which can be calculated as Equation (6.44). For simplicity the results are combined into three vector outputs.

$$T_{delay} = (i - 1) \frac{L_v}{16 \cdot v} \quad (i = 1, 2, 3, \dots, 16) \tag{6.44}$$

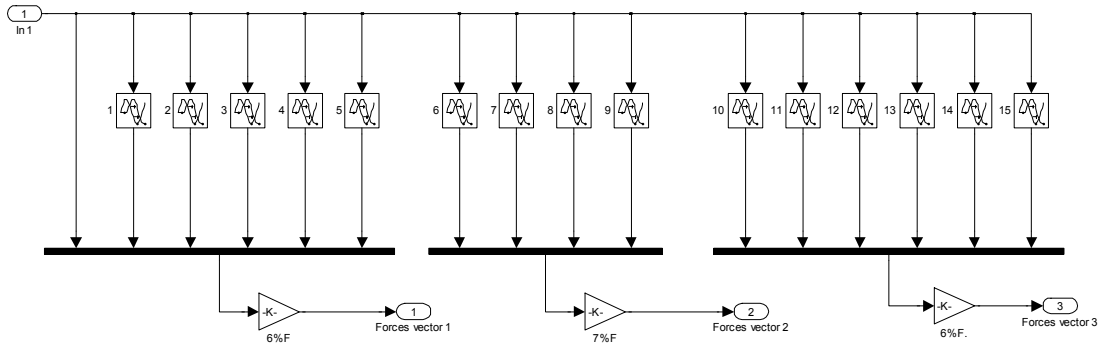


Figure 6.31 Subsystem1-Transport Delay

The second subsystem use the Step blocks to simulate the Dirac Delta function in Equation (6.2). It will generate a zero output after the specified step time, which can be calculated as:

$$T_{time\ step} = \frac{L}{v} + T_{delay} \tag{6.45}$$

By substitution of Equation (6.44), the time step is expressed as:

$$T_{time,step} = \frac{L}{v} + (i - 1) \frac{L_v}{16 \cdot v} \quad (i = 1, 2, \dots, 16) \tag{6.46}$$

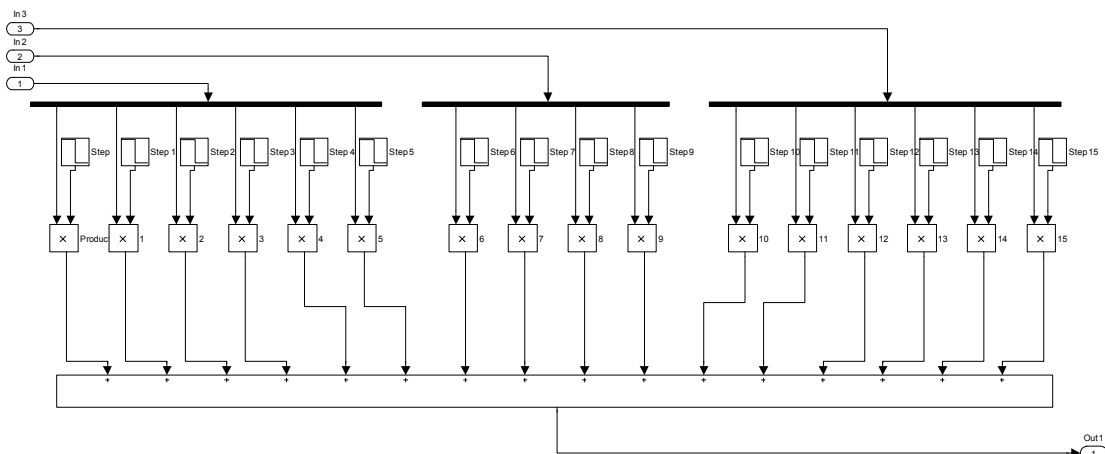


Figure 6.32 Subsystem2-Step

### 6.6.1 Validation of the model

By performing a simulation with a very slow velocity and comparing the result with the static displacement, the model numerical model we have created can be validated.

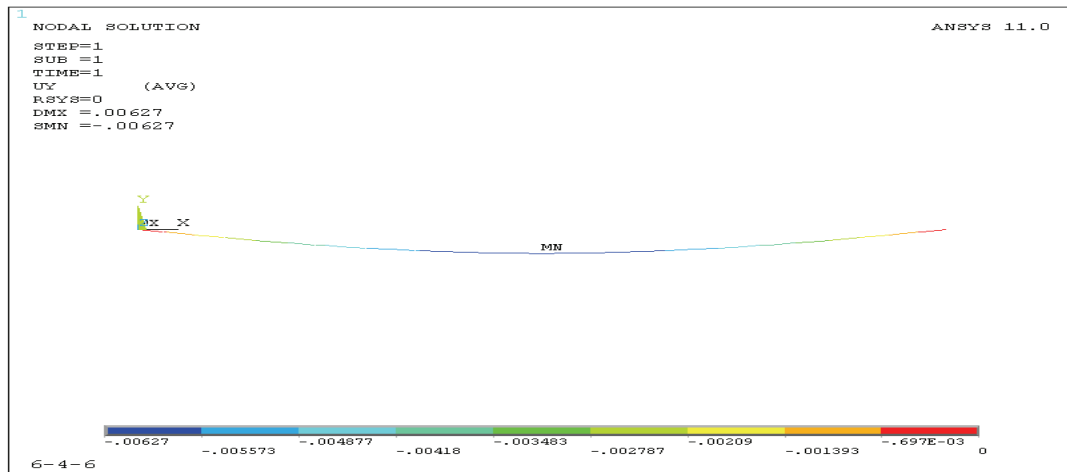


Figure 6.33 Static guideway displacement [m]

Figure 6.33 shows the static displacement of the guideway and the maximum value at mid span is:

$$u_{static,mid} = 6.27 \times 10^{-3} \text{ m} \quad (6.47)$$

The numerical simulation is then performed by taking  $v = 0.1$  m/s. The guideway dynamic displacement at mid span is plotted as a function of the location of the first moving force  $x_1$ :

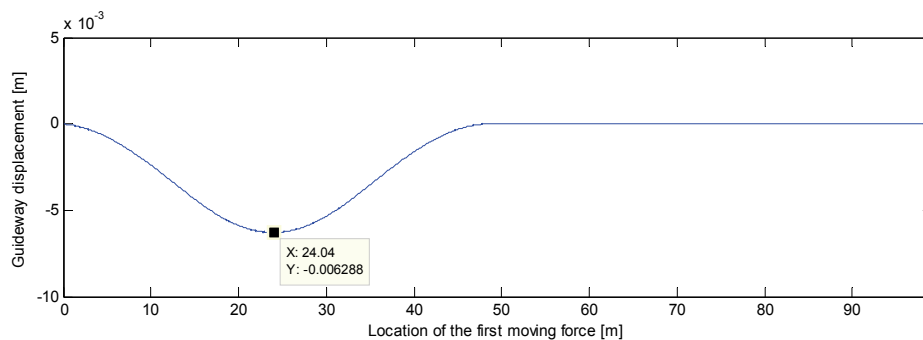


Figure 6.34 Guideway displacement-location of the moving force at  $v=0.1$ m/s

As can be seen in Figure 6.34, the dynamic displacement at mid span for  $v = 0.1$  m/s is very closed to the static result.

$$u_{static,v=0.1} = 6.288 \times 10^{-3} \text{ m} \quad (6.48)$$

### 6.6.2 Dynamic response and influence of damping

A number of simulations are performed in the same way as in Section 6.4 and 6.5 to study the guideway responses under multiple moving forces at various velocities. The time histories of the displacement at mid span as a function of the location of the force are shown in Figure 6.35. Based on these the dynamic factor can be calculated and plotted as a function of velocity as shown in Figure 6.35. A maximum dynamic factor, 1.668, is attained when  $v=300\text{m/s}$ .

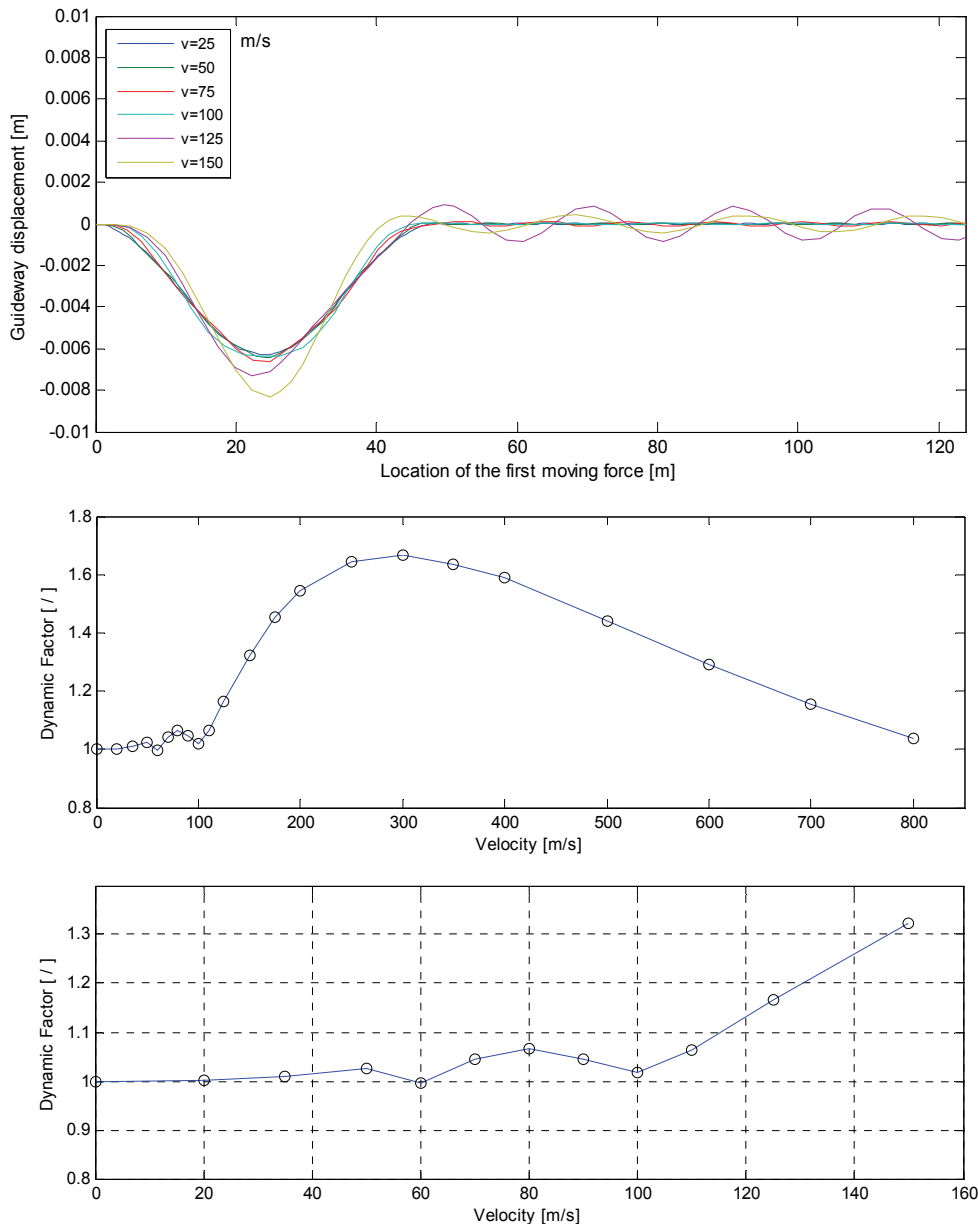
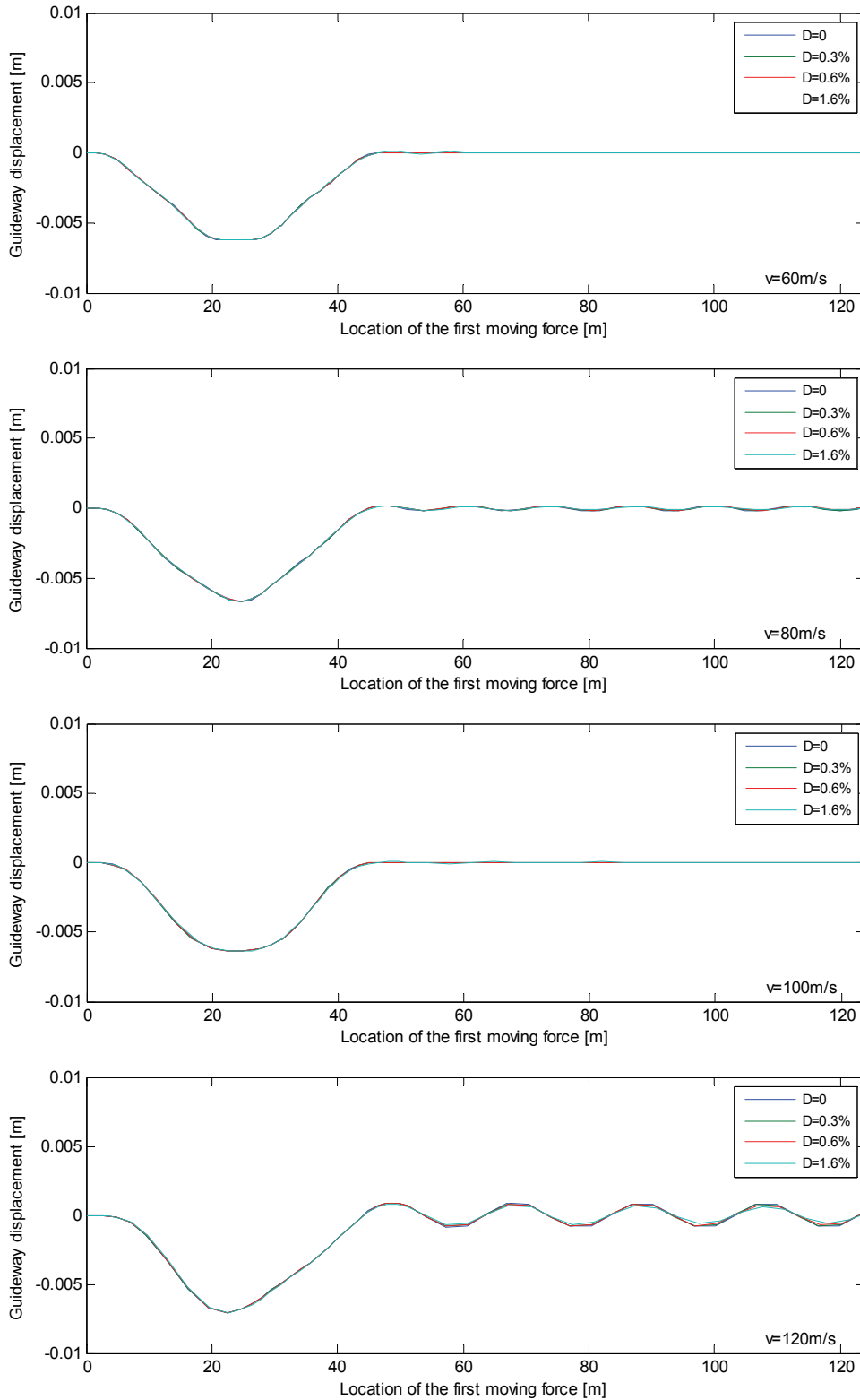


Figure 6.35 Dynamic factor as a function of velocity

The influence of damping ratio is also studied using Model I-3. As can be seen from the

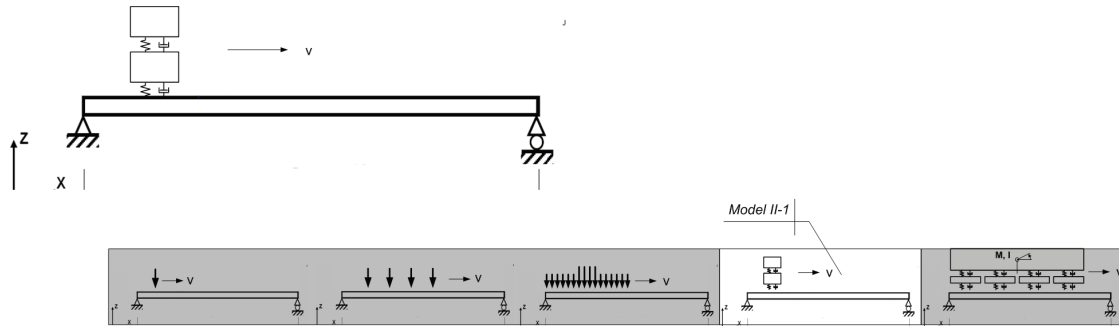
## 6 Vehicle/Guideway Interaction Analysis

simulation results in Figure 6.x2, there is little difference when the damping ratio  $\zeta_k$  varies between 0 and 1.6%.



**Figure 6.36** Guideway displacement-location of the moving force for various damping ratios

### 6.7 Dynamic Interaction Model II-1



Model II-1 uses two lumped masses to represent the carriage body and the levitation frames. The primary and secondary suspensions are modeled by linear springs and dampings. These parameters can be obtained from Table 6.2. The vertical motion of this vehicle system can be described by the basic motion equation.

We will use three subsystems to represent the motion of carriage body, levitation frame and guideway respectively. For the carriage body the equation of motion can be expressed as:

$$m_v \frac{d^2 y_v}{dt^2} + c_s \left( \frac{dy_v}{dt} - \frac{dy_f}{dt} \right) + k_s (y_v - y_f) = 0 \tag{6.49}$$

where

- $m_v$  mass of carriage body
- $y_v$  vertical displacement of carriage body
- $y_f$  vertical displacement of levitation frame
- $c_s$  damping constant of secondary suspension system
- $k_s$  stiffness constant of secondary suspension system

The equation of motion of the levitation frame is:

$$m_f \frac{d^2 y_f}{dt^2} - c_s \left( \frac{dy_v}{dt} - \frac{dy_f}{dt} \right) - k_s (y_v - y_f) + c_p \left( \frac{dy_f}{dt} - \frac{dy(x,t)}{dt} \right) + k_p (y_f - y(x,t)) = 0 \tag{6.50}$$

where

- $m_f$  mass of levitation frame
- $y(x,t)$  vertical displacement of guideway at location  $x$  and time  $t$
- $c_p$  damping constant of primary suspension system
- $k_p$  stiffness constant of primary suspension system

6 Vehicle/Guideway Interaction Analysis

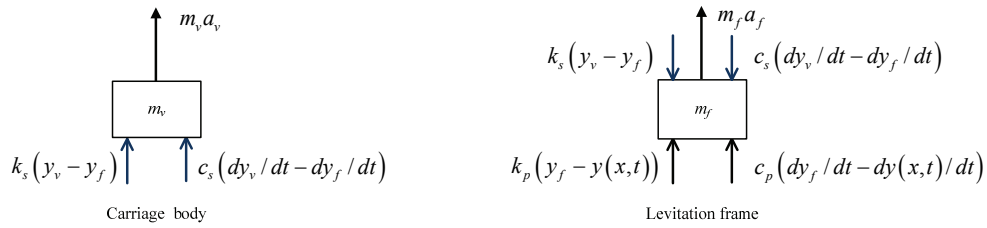


Figure 6.37 Carriage body and levitation frame model

Based on Equation (6.49), the dynamic model for motion of carriage body can be built as:

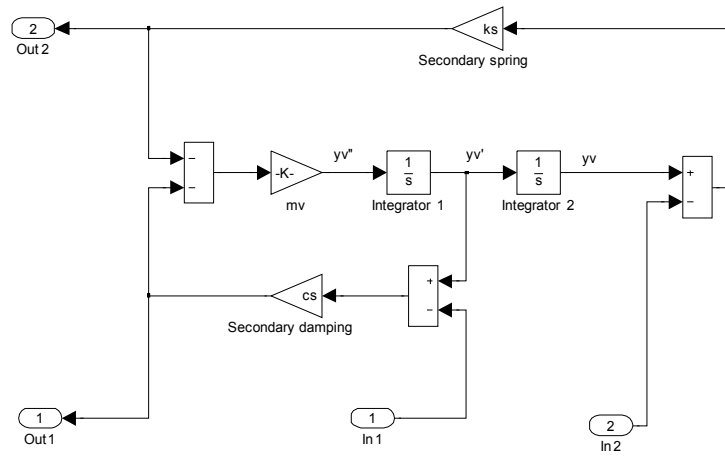


Figure 6.38 Simulink model-carriage body

Similarly the dynamic model for motion of levitation frame can be created in accordance with Equation (6.50):

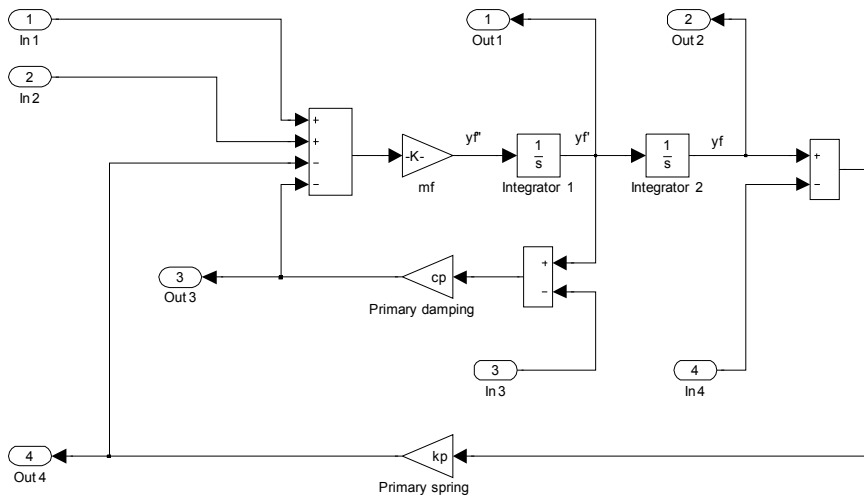


Figure 6.39 Simulink model-levitation frame

The equation of motion of the guideway in terms of the modal amplitude (6.11) now is written as:

$$\frac{d^2 A_k(t)}{dt^2} + 2\zeta_k \omega_k \frac{dA_k(t)}{dt} + \omega_k^2 A_k(t) = \left( (m_v + m_f)g + c_p \left( \frac{dy_f}{dt} - \frac{dy(x,t)}{dt} \right) + k_p (y_f - y(x,t)) \right) \frac{\sqrt{2}}{mL} \sin\left(\frac{k\pi vt}{L}\right) \quad (6.51)$$

The displacement of the guideway can be derived from Equation (6.5) and (6.6):

$$y(x,t) = \sum_{k=1}^{\infty} A_k(t) \phi_k(x) = \sum_{k=1}^{\infty} A_k(t) \sqrt{2} \sin\left(\frac{k\pi vt}{L}\right) \quad (6.52)$$

Based on Equation (6.51) and (6.52) the following dynamic model is created:

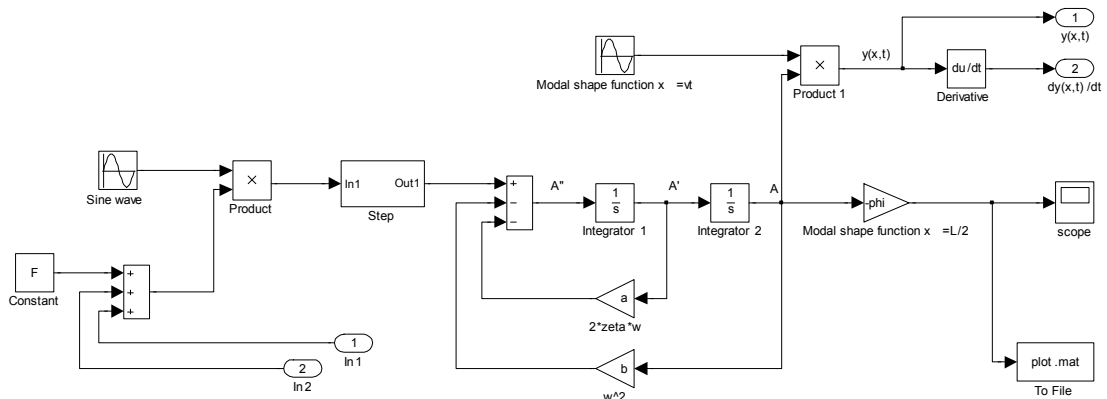


Figure 6.40 Simulink model-guideway

All of these dynamic models are stored as subsystems and linked together so that they can interact with each other:

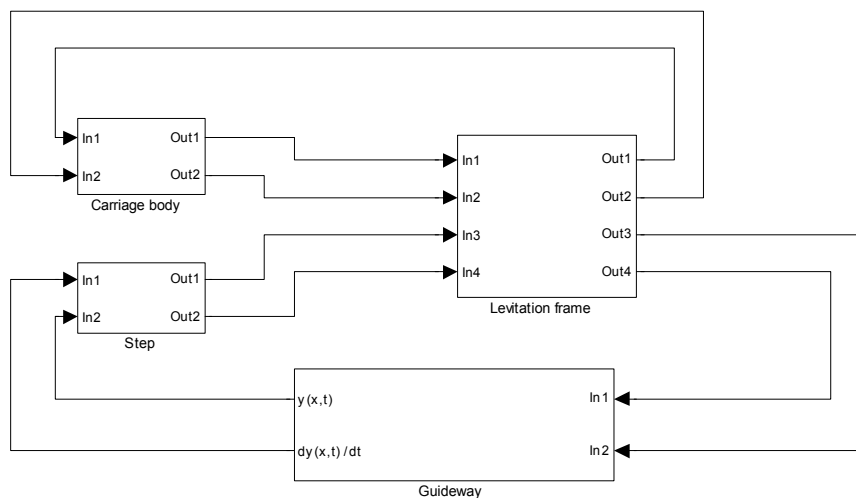


Figure 6.41 Simulink Modle-II-1

### 6.7.1 Validation of the model

The static displacement at mid span is:

$$u_{static,mid} = \frac{(m_v + m_f)gL^3}{48EI} = 9.8 \times 10^{-3} \text{ m} \quad (6.53)$$

By taking a slow velocity  $v = 0.1 \text{ m/s}$ , the numerical model can be validated:

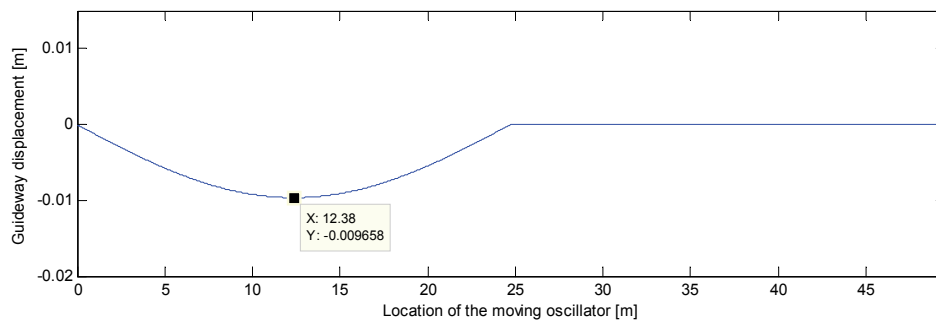


**Figure 6.42** Guideway displacement-location of the moving force at  $v=0.1\text{m/s}$

$$u_{dynamic,v=0.1} = 9.658 \times 10^{-3} \text{ m} \quad (6.54)$$

We can also check the vertical accelerations of the carriage body and levitation frame when  $v = 0.1 \text{ m/s}$ . In a quasi-static case the magnitudes of the acceleration should be ‘quasi-static’ as well.

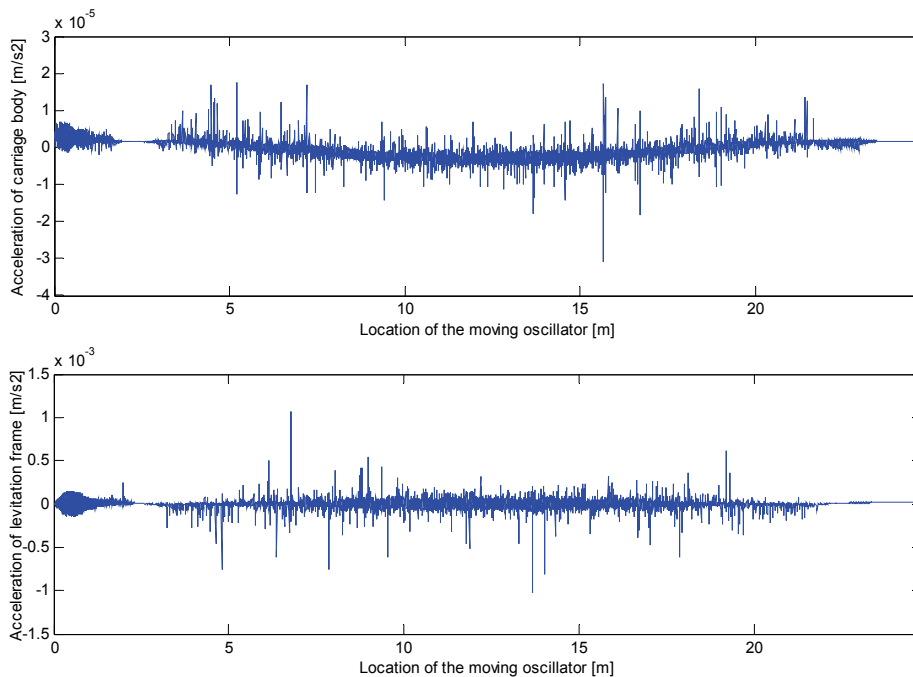


**Figure 6.43** Acceleration of carriage body and levitation frame

### 6.7.2 Dynamic response

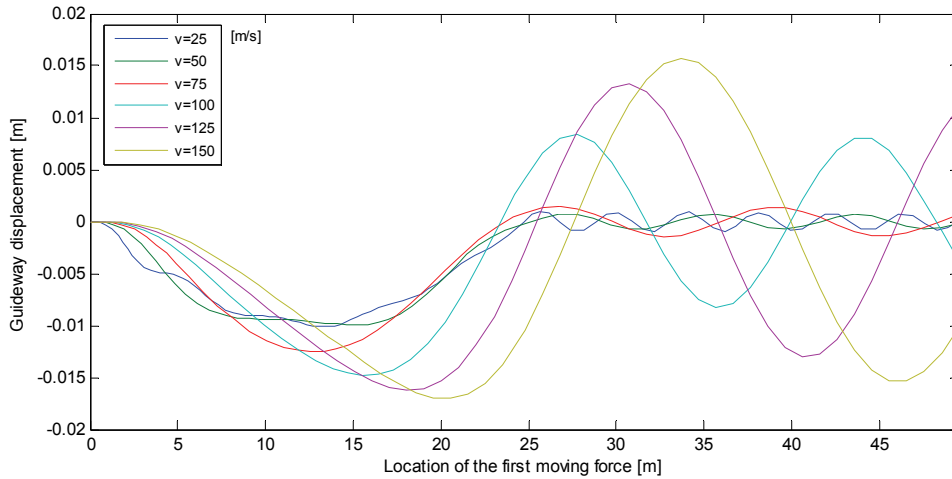


Figure 6.44 Guideway displacement-location of the moving force for various velocities

Simulations are performed to study the guideway displacement for various velocities. The time histories of the displacement at mid span as a function of the location of the moving oscillator is shown in Figure 6.44 ( $\zeta_k = 0.006$ ).

The dynamic factor,  $\phi_{Bg,z}$ , can be calculated based on these simulations. Figure 6.45 shows the dynamic factor as a function of velocity. A maximum value of 1.7633 is attained for  $v = 175$  m/s.

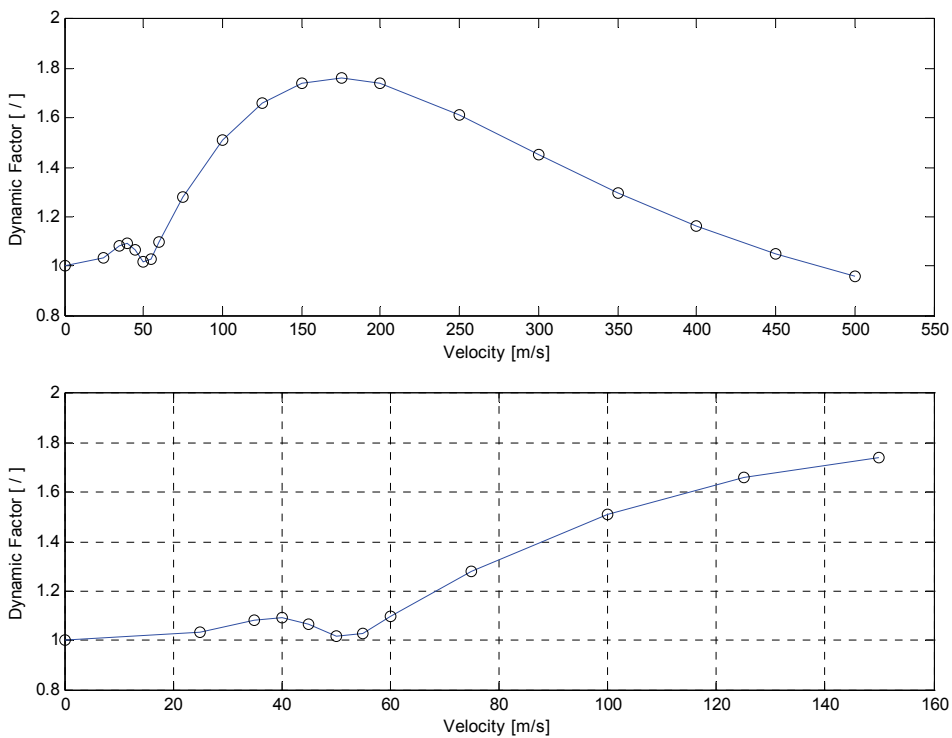
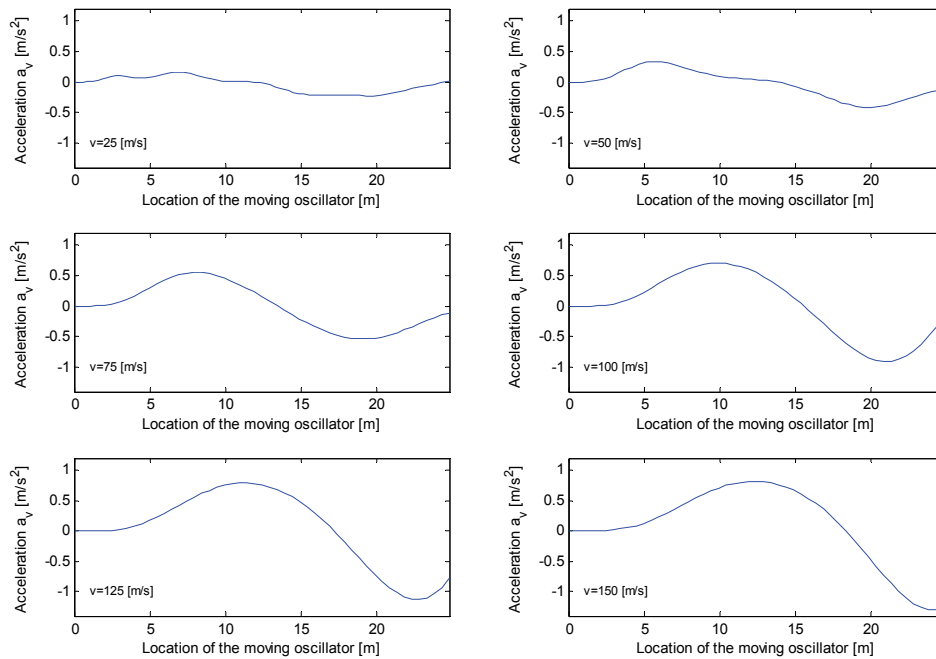


Figure 6.45 Dynamic factor as a function of velocity

## 6 Vehicle/Guideway Interaction Analysis



**Figure 6.46 Acceleration of carriage body at various velocities**

A number of simulations are performed to study the vertical acceleration of the carriage body. As can be seen in Figure 6.46, the magnitudes of maximum and minimum accelerations increase when the velocity varies from 25 to 150 m/s. Therefore we can perform a simulation with the maximum allowed velocity for Maglev vehicle to check the maximum/minimum acceleration of the carriage body.

$$v_{\max} = 500 \text{ km/h} = 138.889 \text{ m/s} \quad (6.55)$$

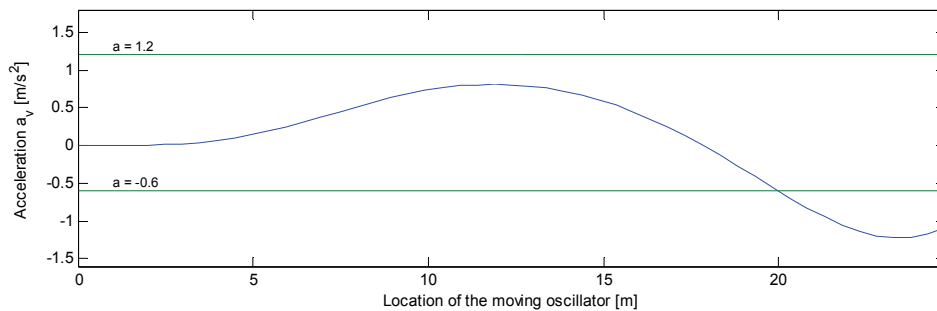


**Figure 6.47 Acceleration of carriage body at  $v=500$ km/h**

The limit acceleration for passenger ride comfort is defined in Section 8.1.1.2 of *Magnetschnellbahn Ausführungsgrundlage, Fahrzeug Teil II*:

$$-0.6 \text{ m/s}^2 \leq a_z \leq 1.2 \text{ m/s}^2 \quad (6.56)$$

Note that a minimum acceleration of  $-1.224 \text{ m/s}^2$  is reached in Figure 6.47 and the limit value has been exceeded.

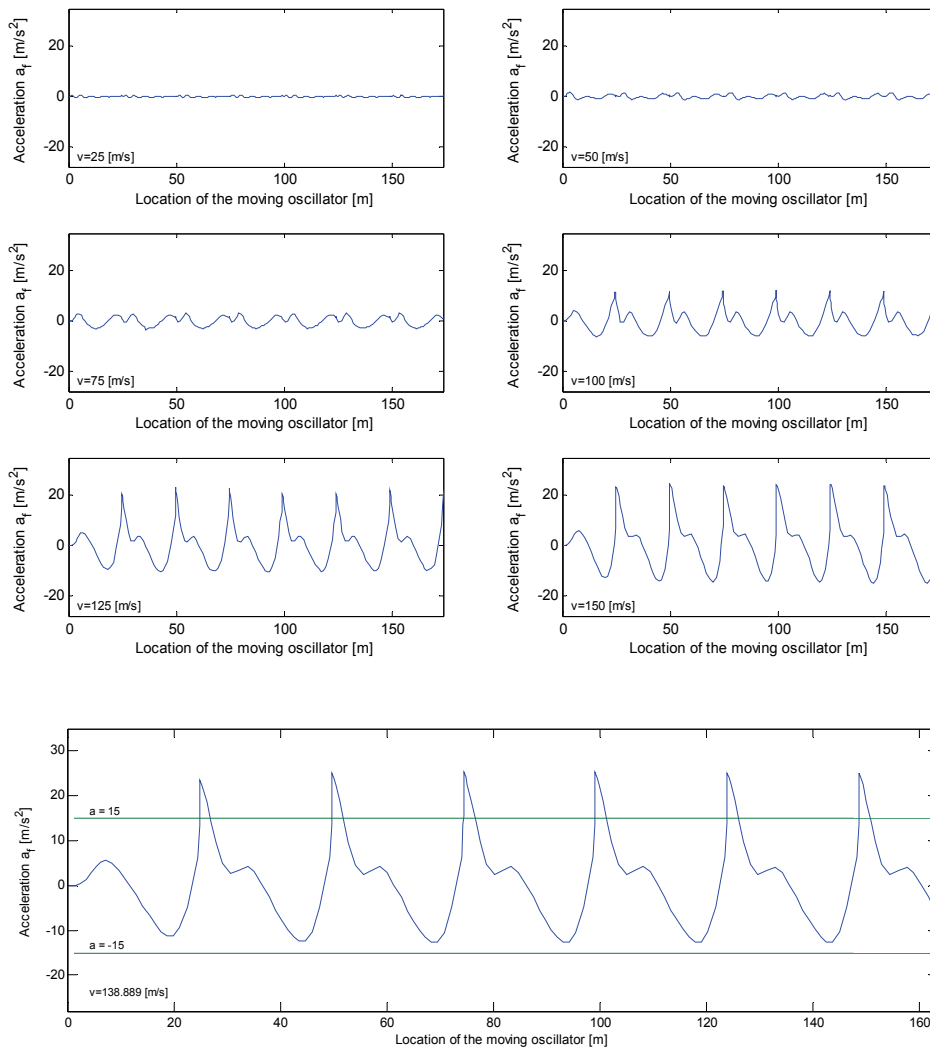


**Figure 6.48 Acceleration of carriage body at various velocities**

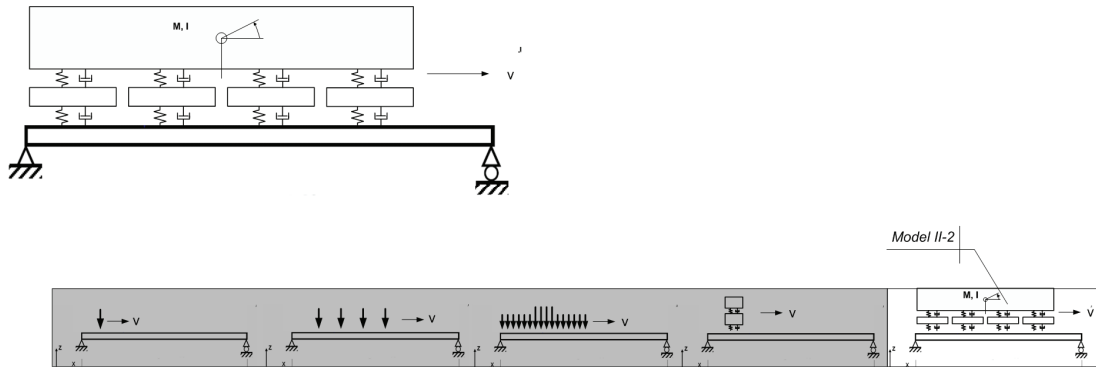
The vertical accelerations of levitation frame as a function of location of the moving oscillator for various velocities are shown in Figure 6.48. The maximum acceleration increases when the driving velocity varies from 25 m/s to 150 m/s.

The limit vertical acceleration of levitation frame can be obtained in Section 8.1.1.7 *Magnetschnellbahn Ausführungsgrundlage Fahrzeug Teil II*:

$$-15 \text{ m/s}^2 \leq a_z \leq 15 \text{ m/s}^2 \quad (6.57)$$

As can be seen in Figure 6.xx, when  $v_{\max} = 500 \text{ km/h} = 138.889 \text{ m/s}$ , a maximum acceleration of  $-25.22 \text{ m/s}^2$  is reached and it also exceeds the limit value in the design guideline.

## 6.8 Dynamic Interaction Model II-2



Model II-2 is created based on the mechanical structure of the Transrapid vehicle. A rigid carriage body is supported by four springs and dashpots which form the secondary suspension. The primary suspension consists of four levitation frames. Four springs and dashpots are used to represent the interaction between the levitation magnets and the stator packs. This model has 6 degree of freedom including one translational and one rotational displacement at the center of the carriage body, and four translational displacements at the levitation frames.

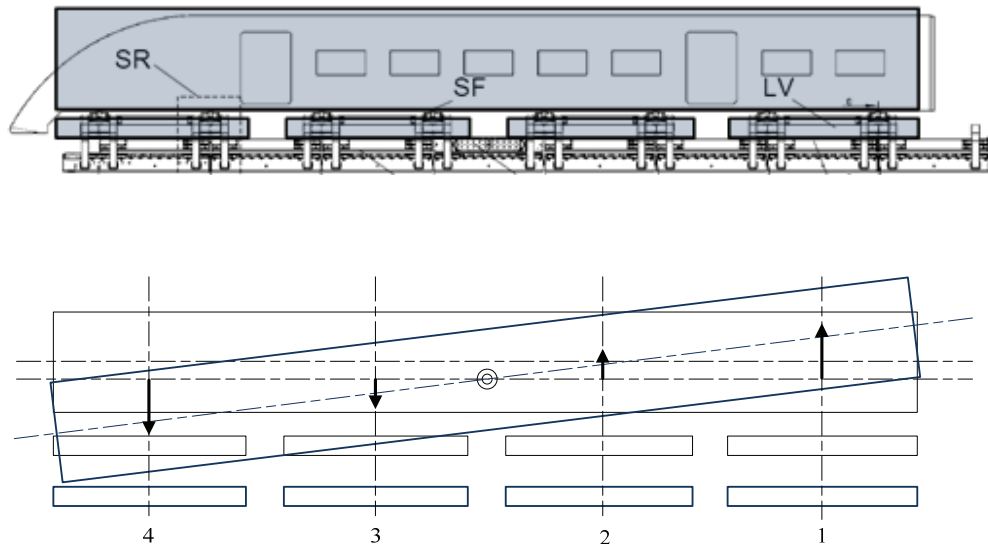
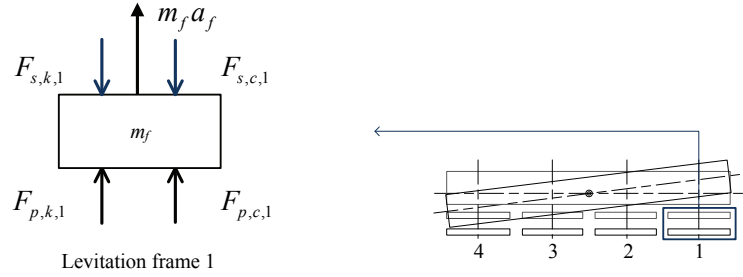


Figure 6.49 Six-degree-of-freedom maglev vehicle model

The equations of motion of four levitation frames and carriage body are derived first.



**Figure 6.50 Levitation frame 1**

The equation of motion of levitation frame 1 can be expressed as:

$$m_f \frac{d^2 y_{f,1}}{dt^2} - F_{s,c,1} - F_{s,k,1} + F_{p,c,1} + F_{p,k,1} = 0 \quad (6.58)$$

where

$$F_{s,c,1} = c_s \left( \frac{dy_v}{dt} - \frac{3}{8} L_v \frac{d\theta_v}{dt} - \frac{dy_{f,1}}{dt} \right) \quad F_{s,k,1} = k_s \left( y_v - \frac{3}{8} L_v \theta_v - y_{f,1} \right)$$

$$F_{p,c,1} = c_p \left( \frac{dy_{f,1}}{dt} - \frac{dy(x_1, t)}{dt} \right) \quad F_{p,k,1} = k_p (y_{f,1} - y(x_1, t))$$

$m_f$	mass of levitation frame 1
$y_{f,1}$	vertical displacement of levitation frame 1
$y_v$	vertical displacement of carriage body at the center of gravity
$\theta_v$	angular displacement of the carriage body
$L_v$	length of carriage body
$y(x_1, t)$	vertical displacement of guideway at location $x_1$ and time $t$

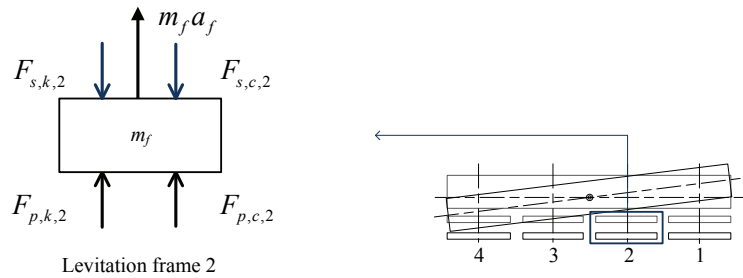


**Figure 6.51 Levitation frame 2**

The equation of motion of levitation frame 2 can be derived as:

$$m_f \frac{d^2 y_{f,2}}{dt^2} - F_{s,c,2} - F_{s,k,2} + F_{p,c,2} + F_{p,k,2} = 0 \quad (6.59)$$

where

## 6 Vehicle/Guideway Interaction Analysis

$$F_{s,c,2} = c_s \left( \frac{dy_v}{dt} - \frac{1}{8} L_v \frac{d\theta_v}{dt} - \frac{dy_{f,2}}{dt} \right) \quad F_{s,k,2} = k_s \left( y_v - \frac{1}{8} L_v \theta_v - y_{f,2} \right)$$

$$F_{p,c,2} = c_p \left( \frac{dy_{f,2}}{dt} - \frac{dy(x_2, t)}{dt} \right) \quad F_{p,k,2} = k_p (y_{f,2} - y(x_2, t))$$

$y_{f,2}$  vertical displacement of levitation frame 2  
 $y(x_2, t)$  vertical displacement of guideway at location  $x_2$  and time  $t$

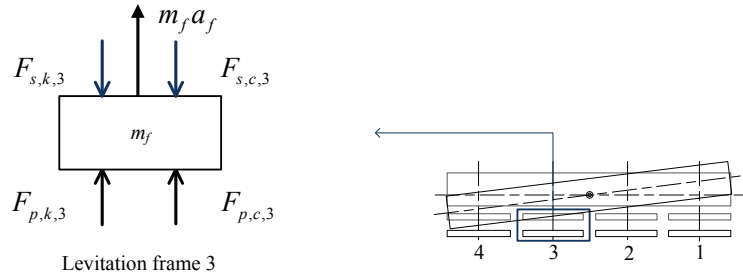


**Figure 6.52 Levitation frame 3**

The equation of motion of levitation frame 3 can be derived as:

$$m_f \frac{d^2 y_{f,3}}{dt^2} - F_{s,c,3} - F_{s,k,3} + F_{p,c,3} + F_{p,k,3} = 0 \quad (6.60)$$

where

$$F_{s,c,3} = c_s \left( \frac{dy_v}{dt} + \frac{1}{8} L_v \frac{d\theta_v}{dt} - \frac{dy_{f,3}}{dt} \right) \quad F_{s,k,3} = k_s \left( y_v + \frac{1}{8} L_v \theta_v - y_{f,3} \right)$$

$$F_{p,c,3} = c_p \left( \frac{dy_{f,3}}{dt} - \frac{dy(x_3, t)}{dt} \right) \quad F_{p,k,3} = k_p (y_{f,3} - y(x_3, t))$$

$y_{f,3}$  vertical displacement of levitation frame 3  
 $y(x_3, t)$  vertical displacement of guideway at location  $x_3$  and time  $t$

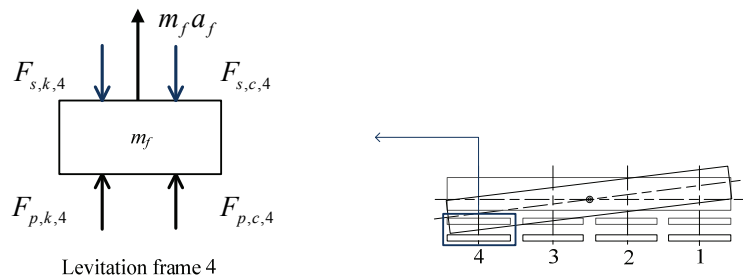


**Figure 6.53 Levitation frame 4**

The equation of motion of levitation frame 4 can be derived as:

$$m_f \frac{d^2 y_{f,4}}{dt^2} - F_{s,c,4} - F_{s,k,4} + F_{p,c,4} + F_{p,k,4} = 0 \quad (6.61)$$

where

$$F_{s,c,4} = c_s \left( \frac{dy_v}{dt} + \frac{3}{8} L_v \frac{d\theta_v}{dt} - \frac{dy_{f,4}}{dt} \right) \quad F_{s,k,4} = k_s \left( y_v + \frac{3}{8} L_v \theta_v - y_{f,4} \right)$$

$$F_{p,c,4} = c_p \left( \frac{dy_{f,4}}{dt} - \frac{dy(x_4, t)}{dt} \right) \quad F_{p,k,4} = k_p (y_{f,4} - y(x_4, t))$$

$y_{f,4}$  vertical displacement of levitation frame 4  
 $y(x_4, t)$  vertical displacement of guideway at location  $x_4$  and time  $t$

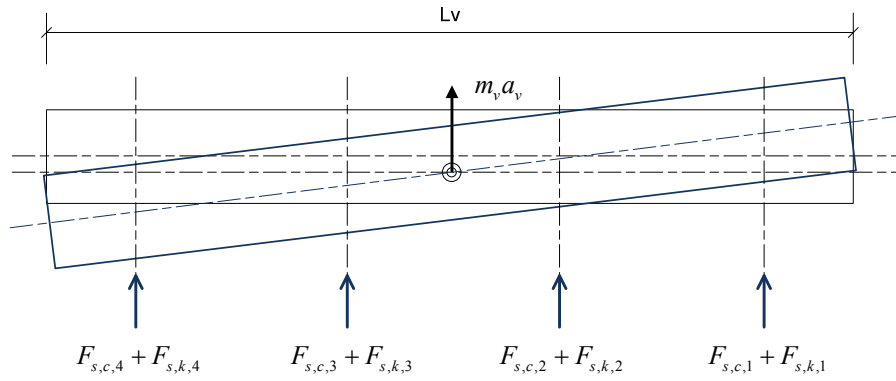


**Figure 6.54 Equilibrium of Carriage body**

The equation of motion of carriage body can be derived as:

$$m_v \frac{d^2 y_v}{dt^2} + F_{s,c,1} + F_{s,k,1} + F_{s,c,2} + F_{s,k,2} + F_{s,c,3} + F_{s,k,3} + F_{s,c,4} + F_{s,k,4} = 0 \quad (6.62)$$

$$I_v \frac{d^2 \theta_v}{dt^2} - (F_{s,c,1} + F_{s,k,1}) \cdot \frac{3}{8} L_v - (F_{s,c,2} + F_{s,k,2}) \cdot \frac{1}{8} L_v +$$

$$(F_{s,c,3} + F_{s,k,3}) \cdot \frac{1}{8} L_v + (F_{s,c,4} + F_{s,k,4}) \cdot \frac{3}{8} L_v = 0 \quad (6.63)$$

where

$m_v$  mass of carriage body  
 $I_v$  pitch inertia of carriage body

The governing equations of the vehicle model are obtained from Equation (6.58) to (6.63). They can also be written in matrix form. We will define the mass matrix  $\mathbf{M}$ , damping matrix  $\mathbf{C}$ , stiffness matrix  $\mathbf{K}$ , displacement vector  $\mathbf{Y}$ , and force vector  $\mathbf{F}$  as follows.

$\mathbf{Y}$  is the displacement vector including the heave motion and rotational motion of the carriage body, and the vertical motion of four levitation frames. It can be written as:

$$\mathbf{Y} = [y_{f,1}, y_{f,2}, y_{f,3}, y_{f,4}, y_v, \theta_v]^T \quad (6.64)$$

In the mass matrix  $\mathbf{M}$ , the elements which represent the masses and inertia of the vehicle model will appear on the diagonal:

$$\mathbf{M} = \begin{bmatrix} m_f & 0 & 0 & 0 & 0 & 0 \\ 0 & m_f & 0 & 0 & 0 & 0 \\ 0 & 0 & m_f & 0 & 0 & 0 \\ 0 & 0 & 0 & m_f & 0 & 0 \\ 0 & 0 & 0 & 0 & m_v & 0 \\ 0 & 0 & 0 & 0 & 0 & I_v \end{bmatrix} \quad (6.65)$$

The damping matrix  $\mathbf{C}$  is derived as:

$$\mathbf{C} = \begin{bmatrix} c_s + c_p & 0 & 0 & 0 & -c_s & \frac{3}{8}L_v c_s \\ 0 & c_s + c_p & 0 & 0 & -c_s & \frac{1}{8}L_v c_s \\ 0 & 0 & c_s + c_p & 0 & -c_s & -\frac{1}{8}L_v c_s \\ 0 & 0 & 0 & c_s + c_p & -c_s & -\frac{3}{8}L_v c_s \\ -c_s & -c_s & -c_s & -c_s & 4c_s & 0 \\ \frac{3}{8}L_v c_s & \frac{1}{8}L_v c_s & -\frac{1}{8}L_v c_s & -\frac{3}{8}L_v c_s & 0 & \frac{5}{16}L_v^2 c_s \end{bmatrix} \quad (6.66)$$

Similarly the stiffness matrix  $\mathbf{K}$  can be derived as:

$$\mathbf{K} = \begin{bmatrix} k_s + k_p & 0 & 0 & 0 & -k_s & \frac{3}{8}L_v k_s \\ 0 & k_s + k_p & 0 & 0 & -k_s & \frac{1}{8}L_v k_s \\ 0 & 0 & k_s + k_p & 0 & -k_s & -\frac{1}{8}L_v k_s \\ 0 & 0 & 0 & k_s + k_p & -k_s & -\frac{3}{8}L_v k_s \\ -k_s & -k_s & -k_s & -k_s & 4k_s & 0 \\ \frac{3}{8}L_v k_s & \frac{1}{8}L_v k_s & -\frac{1}{8}L_v k_s & -\frac{3}{8}L_v k_s & 0 & \frac{5}{16}L_v^2 k_s \end{bmatrix} \quad (6.67)$$

The terms that contain  $y(x_i, t)$  are assembled in the vector  $\mathbf{F}$ :

$$\mathbf{F} = \begin{bmatrix} c_p \frac{dy(x_1, t)}{dt} + k_p y(x_1, t) \\ c_p \frac{dy(x_2, t)}{dt} + k_p y(x_2, t) \\ c_p \frac{dy(x_3, t)}{dt} + k_p y(x_3, t) \\ c_p \frac{dy(x_4, t)}{dt} + k_p y(x_4, t) \\ 0 \\ 0 \end{bmatrix} \quad (6.68)$$

The equation of motion of the Transrapid vehicle model moving along the guideway can be written as:

$$\mathbf{M}\ddot{\mathbf{Y}} + \mathbf{C}\dot{\mathbf{Y}} + \mathbf{K}\mathbf{Y} = \mathbf{F} \quad (6.69)$$

The **State-Space Approach** will be used to create this dynamic model in Simulink. When modeling a system using a state-space equation, we first need to define three vectors: the input variables, the output variables and the state variables. The state variables represent value from inside the system, which can change over time. We denote the input variables with  $\mathbf{u}$ , the output variables with  $\mathbf{y}$ , and the state variables with  $\mathbf{x}$ .

The state-space system consists of two equations: an equation for determining the state of the system, and another equation for determining the output of the system.

$$\begin{aligned} \dot{\mathbf{x}} &= \mathbf{A}\mathbf{x} + \mathbf{B}\mathbf{u} \\ \mathbf{y} &= \mathbf{C}\mathbf{x} + \mathbf{D}\mathbf{u} \end{aligned} \quad (6.70)$$

Matrix  $\mathbf{A}$  is the system matrix which relates how the current state affects the state change  $dx/dt$ . Matrix  $\mathbf{B}$  is the control matrix which determines how the system input affects the state change directly. Matrix  $\mathbf{C}$  is the output matrix which determines the relationship between the system state and system output. Matrix  $\mathbf{D}$  is the feed-forward matrix and allows the system input to affect the system output directly. Note there is no feed-forward element in this vehicle model thus the  $\mathbf{D}$  matrix is a zero matrix.

Then Equation (6.69) will be rewritten in the state-space form. The state vector  $\mathbf{x}$  is first introduced as:

$$\mathbf{x} = \begin{bmatrix} \mathbf{Y} \\ \dot{\mathbf{Y}} \end{bmatrix} \quad (6.71)$$

where displacement vector  $\mathbf{Y}$  is defined in Equation (6.64) as  $\mathbf{Y} = [y_{f,1}, y_{f,2}, y_{f,3}, y_{f,4}, y_v, \theta_v]^T$

Substitution of Equation (6.71) in Equation (6.69) gives:

$$\begin{bmatrix} \mathbf{I} & \mathbf{0} \\ \mathbf{0} & \mathbf{M} \end{bmatrix} [\dot{\mathbf{x}}] + \begin{bmatrix} \mathbf{0} & -\mathbf{I} \\ \mathbf{K} & \mathbf{C} \end{bmatrix} [\mathbf{x}] = \begin{bmatrix} \mathbf{0} \\ \mathbf{F} \end{bmatrix} \quad (6.72)$$

Rewriting Equation (6.72) gives:

$$[\dot{\mathbf{x}}] = \begin{bmatrix} \mathbf{0} & \mathbf{I} \\ -\mathbf{M}^{-1}\mathbf{K} & -\mathbf{M}^{-1}\mathbf{C} \end{bmatrix} [\mathbf{x}] + \begin{bmatrix} \mathbf{I} & \mathbf{0} \\ \mathbf{0} & \mathbf{M}^{-1} \end{bmatrix} \begin{bmatrix} \mathbf{0} \\ \mathbf{F} \end{bmatrix} \quad (6.73)$$

The output vector  $\mathbf{y}$  consists of the same element as the state vector  $\mathbf{x}$ :

$$[\mathbf{y}] = [\mathbf{x}] \quad (6.74)$$

Equation (6.73) and (6.74) are the state-space equations of the vehicle model. To get the identical forms with Equation (6.70), they can be rewritten as:

$$\begin{aligned} [\dot{\mathbf{x}}] &= \begin{bmatrix} \mathbf{0} & \mathbf{I} \\ -\mathbf{M}^{-1}\mathbf{K} & -\mathbf{M}^{-1}\mathbf{C} \end{bmatrix} [\mathbf{x}] + \begin{bmatrix} \mathbf{0} \\ \mathbf{M}^{-1} \end{bmatrix} [\mathbf{F}] \\ [\mathbf{y}] &= \begin{bmatrix} \mathbf{I} & \mathbf{0} \\ \mathbf{0} & \mathbf{I} \end{bmatrix} [\mathbf{x}] + \begin{bmatrix} \mathbf{0} \\ \mathbf{0} \end{bmatrix} [\mathbf{F}] \end{aligned} \quad (6.75)$$

Now the four matrix coefficients for state-space equation are obtained:

$$\begin{aligned} \mathbf{A} &= \begin{bmatrix} \mathbf{0} & \mathbf{I} \\ -\mathbf{M}^{-1}\mathbf{K} & -\mathbf{M}^{-1}\mathbf{C} \end{bmatrix} & (12 \times 12) \\ \mathbf{B} &= \begin{bmatrix} \mathbf{0} \\ \mathbf{M}^{-1} \end{bmatrix} & (12 \times 6) \\ \mathbf{C} &= \begin{bmatrix} \mathbf{I} & \mathbf{0} \\ \mathbf{0} & \mathbf{I} \end{bmatrix} & (12 \times 12) \\ \mathbf{D} &= \begin{bmatrix} \mathbf{0} \\ \mathbf{0} \end{bmatrix} & (12 \times 6) \end{aligned} \quad (6.76)$$

The input variables  $\mathbf{u}$  is:

$$\mathbf{u} = [\mathbf{F}] \quad (6.77)$$

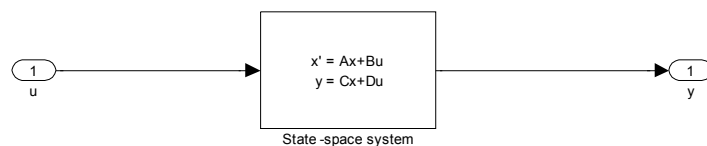


Figure 6.55 Vehicle model, State-space system

Having obtained the vehicle model in state-space approach, we will create the guideway model in the same way as previous dynamic interaction models. The guideway model will provide the input vector  $\mathbf{u}$  to the vehicle model and use its output vector  $\mathbf{y}$  as the input.

In this case the equation of motion of the guideway in terms of the modal amplitude (6.11) is written as:

$$\frac{d^2 A_k(t)}{dt^2} + 2\zeta_k \omega_k \frac{dA_k(t)}{dt} + \omega_k^2 A_k(t) = \frac{\sqrt{2}}{mL} \sum_{i=1}^4 \left( \left( m_f + \frac{1}{4} m_v \right) g + F_{p,k,i} + F_{p,c,i} \right) \sin\left( \frac{k\pi x_i}{L} \right) \quad (6.78)$$

where

$m_v$	mass of carriage body
$m_f$	mass per levitation frame
$F_{p,k,i}$	$i$ -th primary spring force
$F_{p,c,i}$	$i$ -th primary damping force

The location of  $i$ -th force,  $x_i$ , can be calculated as:

$$x_i = vt_i = v \left[ t - (i-1) \frac{L_v}{4v} \right] \quad (6.79)$$

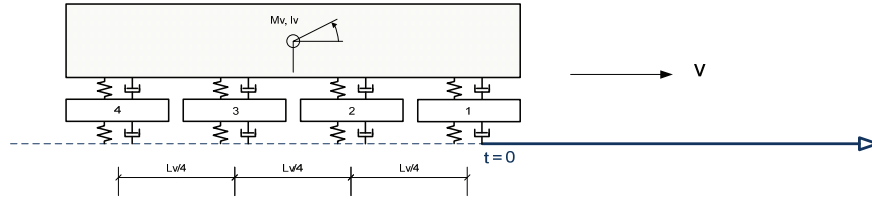


Figure 6.56 Dynamic interaction model

Substitution of Equation (6.79) in Equation (6.78) gives:

$$\frac{d^2 A_k(t)}{dt^2} + 2\zeta_k \omega_k \frac{dA_k(t)}{dt} + \omega_k^2 A_k(t) = \frac{\sqrt{2}}{mL} \sum_{i=1}^4 \left( \left( m_f + \frac{1}{4} m_v \right) g + F_{p,k,i} + F_{p,c,i} \right) \sin\left( \frac{k\pi v}{L} \left[ t - (i-1) \frac{L_v}{4v} \right] \right) \quad (6.80)$$

where

$L_v$	length of maglev vehicle
$L$	length of simply supported guideway

The displacement of the guideway can be derived from Equation (6.5) and (6.6):

$$y(x, t) = \sum_{k=1}^{\infty} A_k(t) \phi_k(x) = \sum_{k=1}^{\infty} A_k(t) \sqrt{2} \sin\left( \frac{k\pi vt}{L} \right) \quad (6.81)$$

## 6 Vehicle/Guideway Interaction Analysis

Based on Equation (6.80) and (6.81) the guideway model is created in Simulink when only first mode of the guideway is considered:

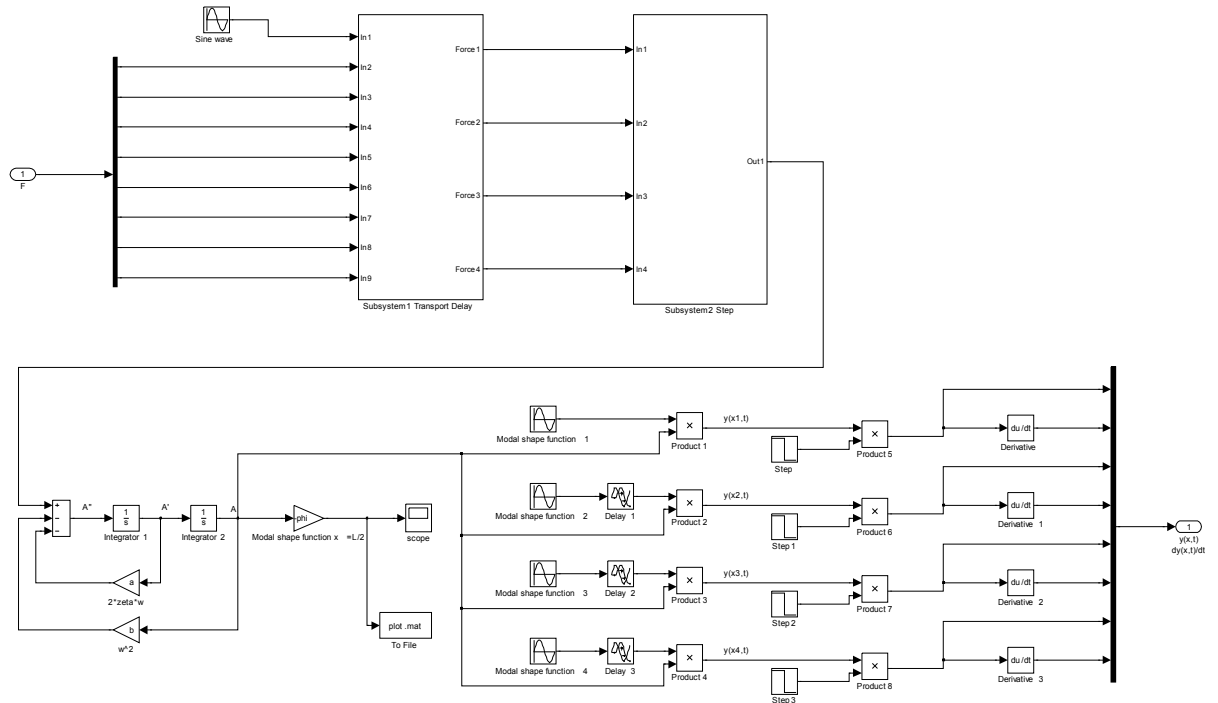


Figure 6.57 Guideway Model

The first subsystem in the guideway model consists of Transport Delay blocks to delay the signal:

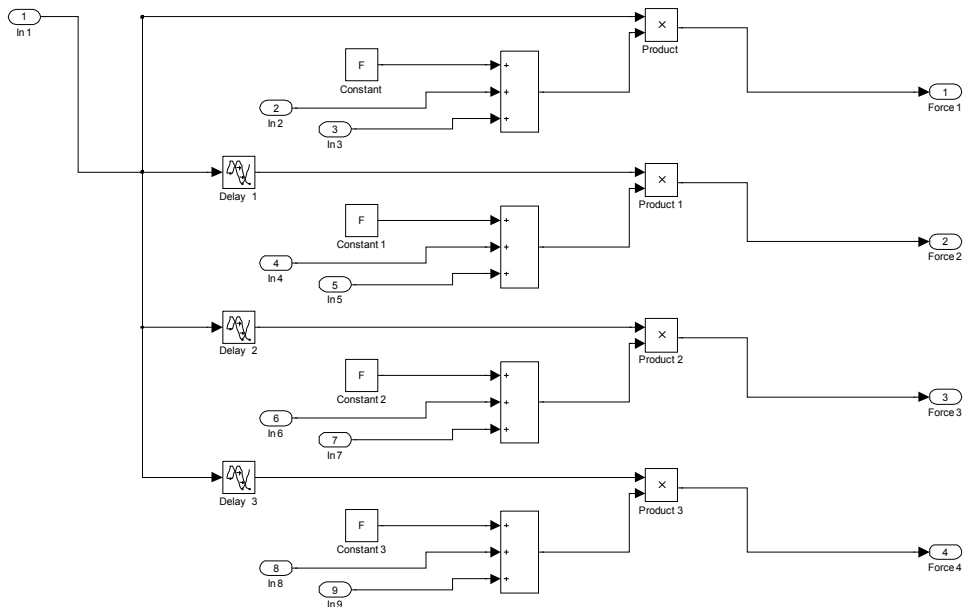


Figure 6.58 Subsystem-1

The second subsystem in the guideway model is made up of the Step blocks. The time step can be calculated as:

$$T_{time,step} = \frac{L}{v} + T_{delay} = \frac{L}{v} + (i-1) \frac{L_v}{nv} \quad (i = 1, 2, \dots, n) \quad (6.82)$$

where

$T_{time,step}$  time step for  $i$ -th input signal  
 $T_{delay}$  time delay for  $i$ -th input signal  
 $n$  number of levitation frames,  $n = 4$

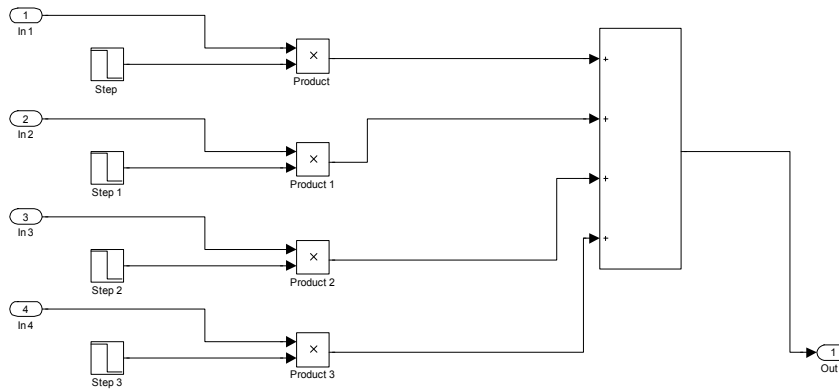


Figure 6.59 Subsystem-2

Having built the vehicle model and the guideway model, we will create a suspension model to let the systems interact with each other. The suspension model is twofold. On one hand it is able to transfer the displacement and velocity of the levitation frame,  $y_{f,i}$  and  $dy_{f,i}/dt$ , to the forces in primary spring and damping. On the other, it is to transfer the guideway displacement and vertical velocity,  $y(x_i,t)$  and  $dy(x_i,t)/dt$ , to the input variable  $\mathbf{u}$  of the state-space system of the vehicle.

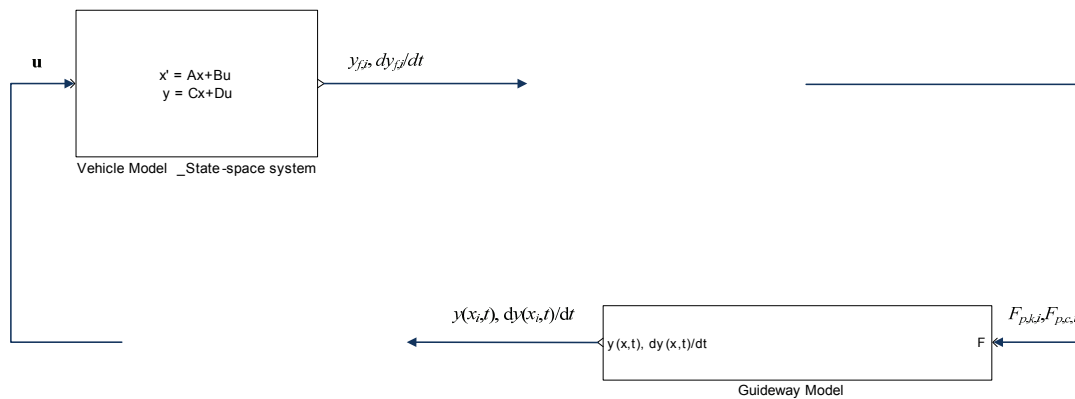
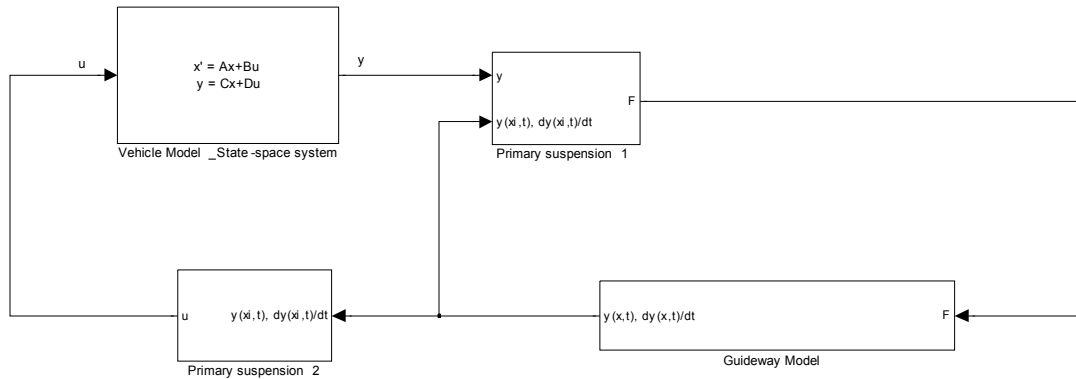


Figure 6.60 Vehicle Model and Guideway Model

## 6 Vehicle/Guideway Interaction Analysis

The complete interaction model and two suspension subsystems are showed in Figure 6.61-6.63:



**Figure 6.61 Vehicle-Suspension-Guideway Interaction Model**

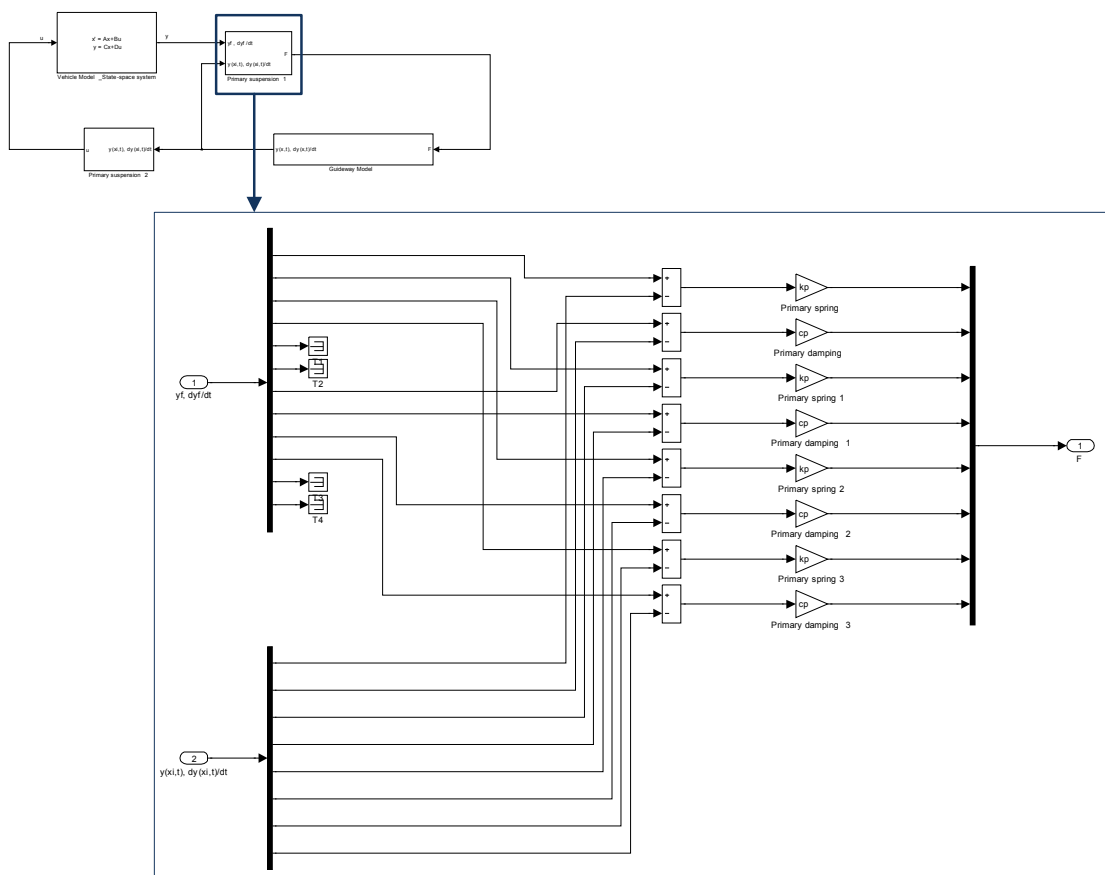


**Figure 6.62 Subsystem-Suspension 1**

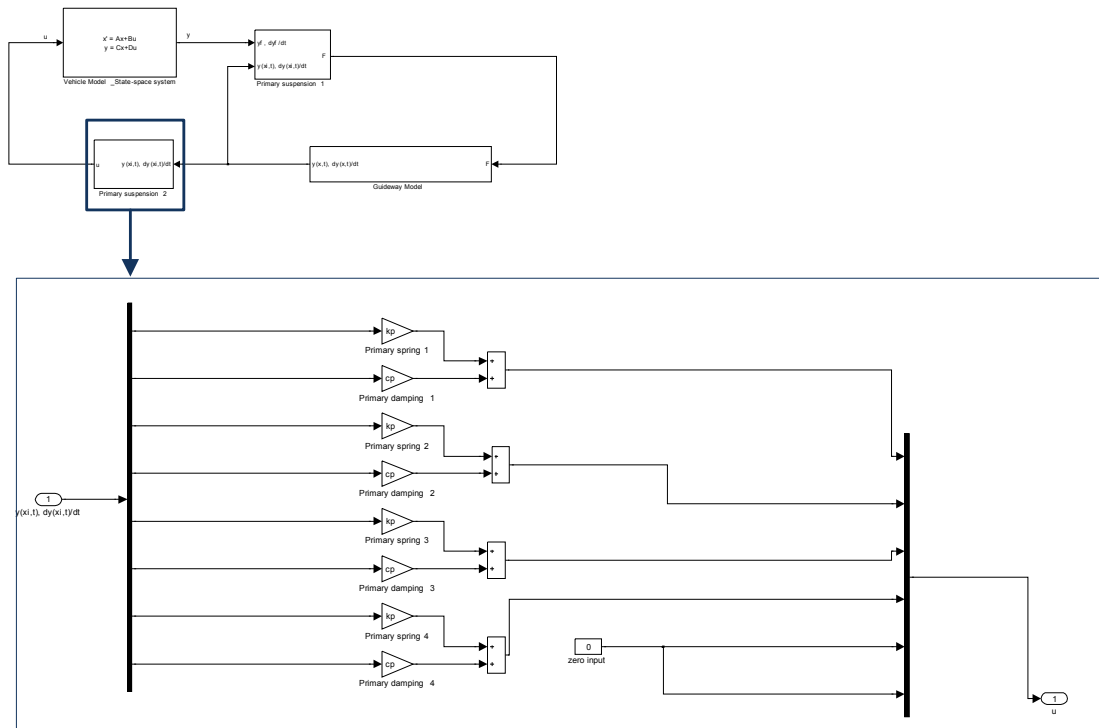


Figure 6.63 Subsystem-Suspension 2

The dynamic model we have built in Figure 6.61 can be used to simulate the process that the maglev vehicle traveling along one simply supported guideway (see Figure 6.64(a)). However, the maglev guideway actually consists of a large number of simply supported girders that will deflect when the vehicle moving on them (see Figure 6.64(b)). The difference between these two cases may be slight on guideway displacement. But when the vertical acceleration of the system is under consideration for passenger ride comfort, the latter model will give more realistic and accurate results.

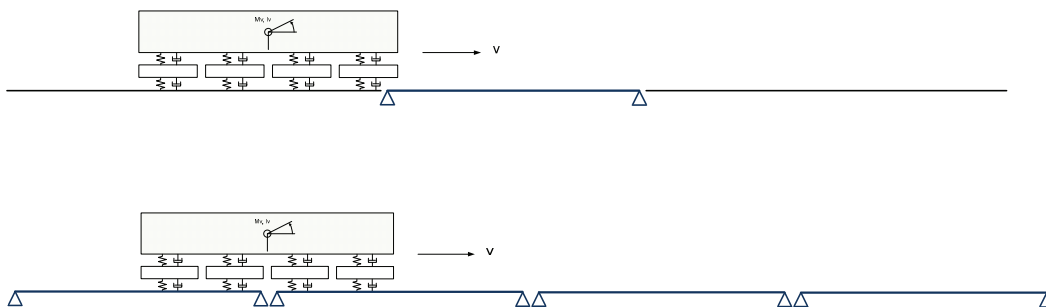


Figure 6.64 (a) Dynamic model with one simply supported guideway  
(b) Dynamic model with multiple guideways

## 6 Vehicle/Guideway Interaction Analysis

Therefore the model can be improved by adding a number of guideway subsystems as show in Figure 6.65. The time delay and time step for the new guideway systems need to be reset properly to simulate the complete process.

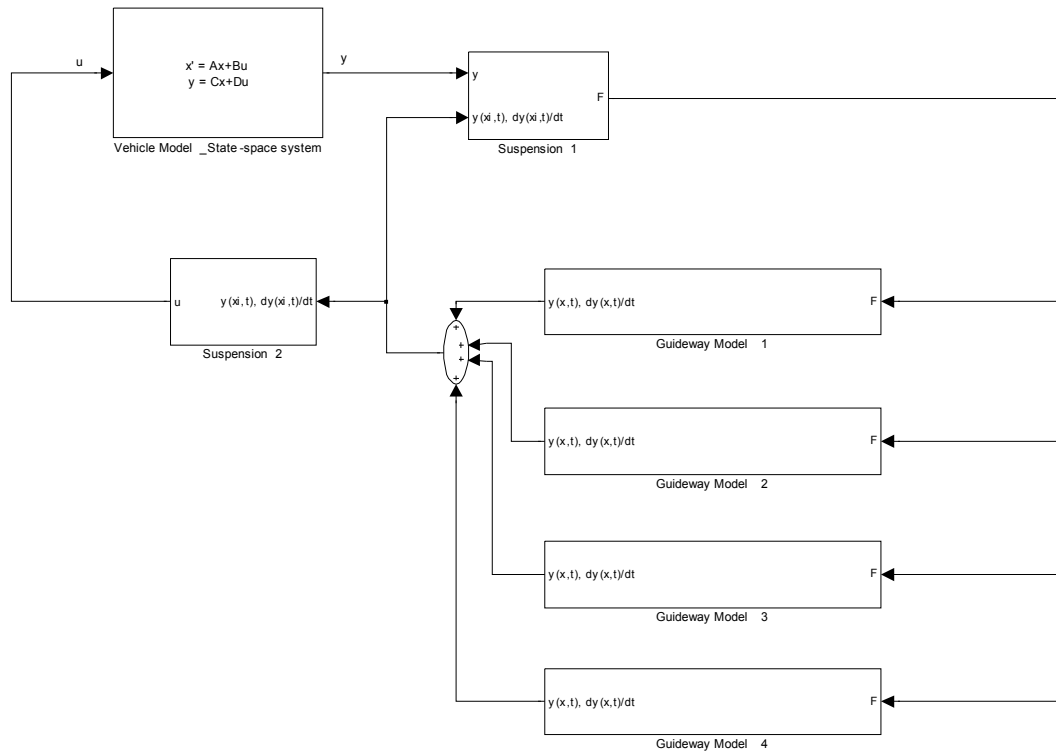


Figure 6.65 Model II-2 with multiple Guideway Subsystems

### 6.8.1 Validation of the model

The static displacement at mid span of the guideway is:

$$u_{static,mid} = 6.27 \times 10^{-3} \text{ m} \quad (6.83)$$

Figure 6.66 shows the simulation result when  $v = 0.1$  m/s:

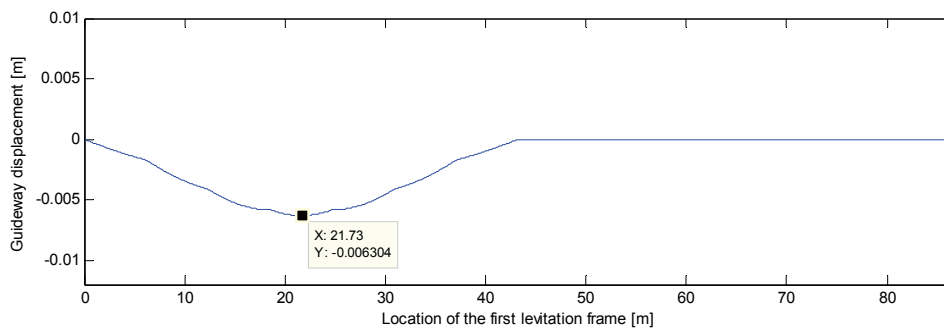


Figure 6.66 Guideway displacement-location of the first moving levitation frame at  $v=0.1$ m/s

### 6.8.2 Dynamic response of guideway

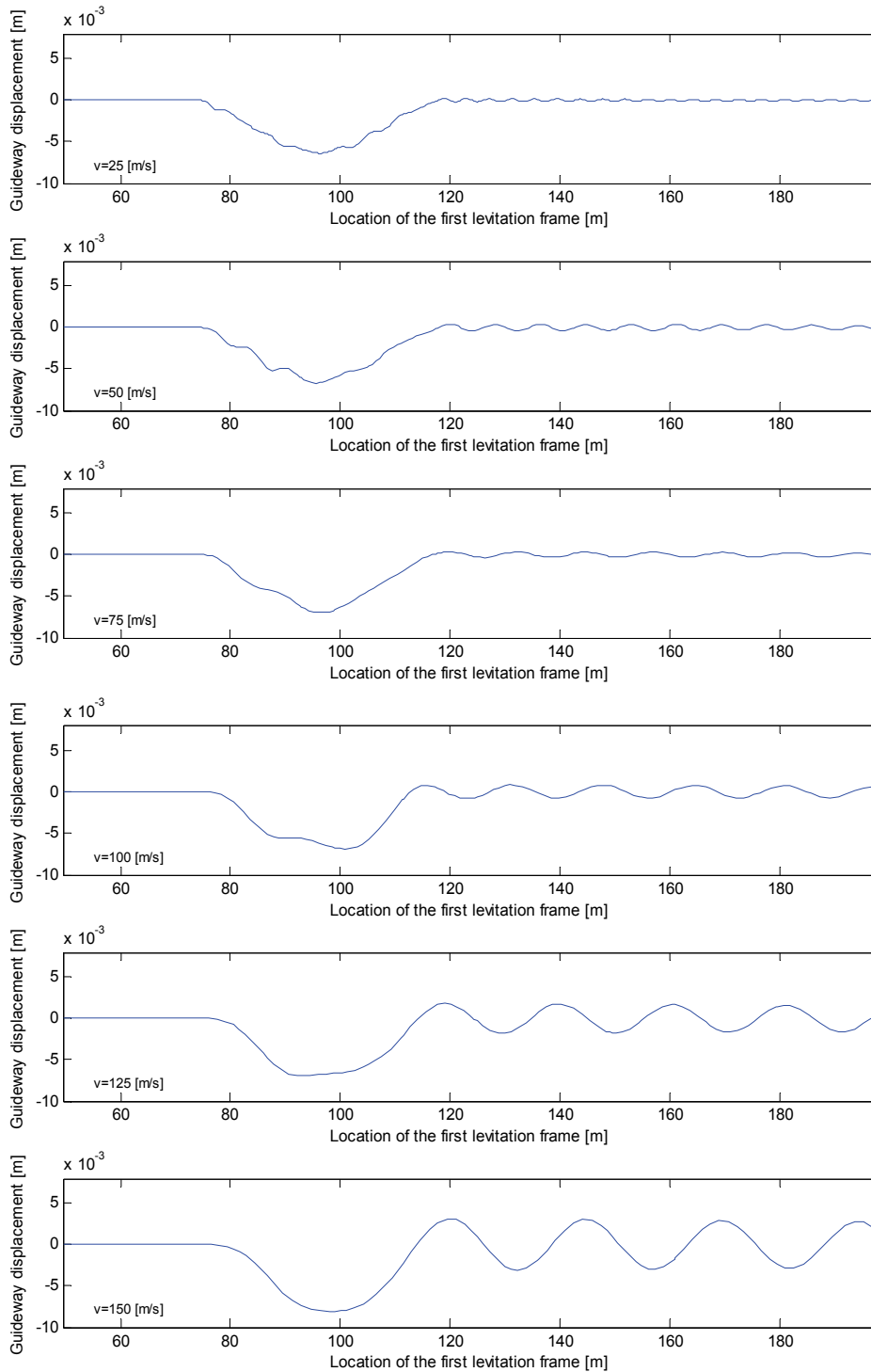
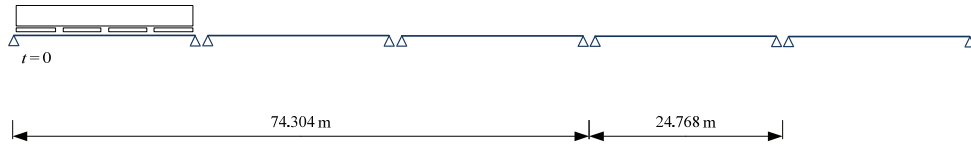


Figure 6.67 Guideway displacement (mid span) as a function of location of the first levitation frame

## 6 Vehicle/Guideway Interaction Analysis



**Figure 6.68 Simply supported guideway model**

A number of simulations are performed to study the influence of traveling velocity on guideway displacement as shown in Figure 6.67 ( $\zeta_k = 0.006$ ). Based on these we can calculate the dynamic factor  $\varphi_{Bg,z}$ . The results are shown in Figure 6.69.

$$\varphi_{Bg,z,\max} = 1.471 \quad (6.84)$$

The maximum dynamic factor is attained when the velocity reaches 200 m/s. Compared with Model I-2 where the maximum dynamic factor is  $\varphi_{Bg,z,\max} = 1.679$  at  $v = 300$  m/s it appears to be of great difference.

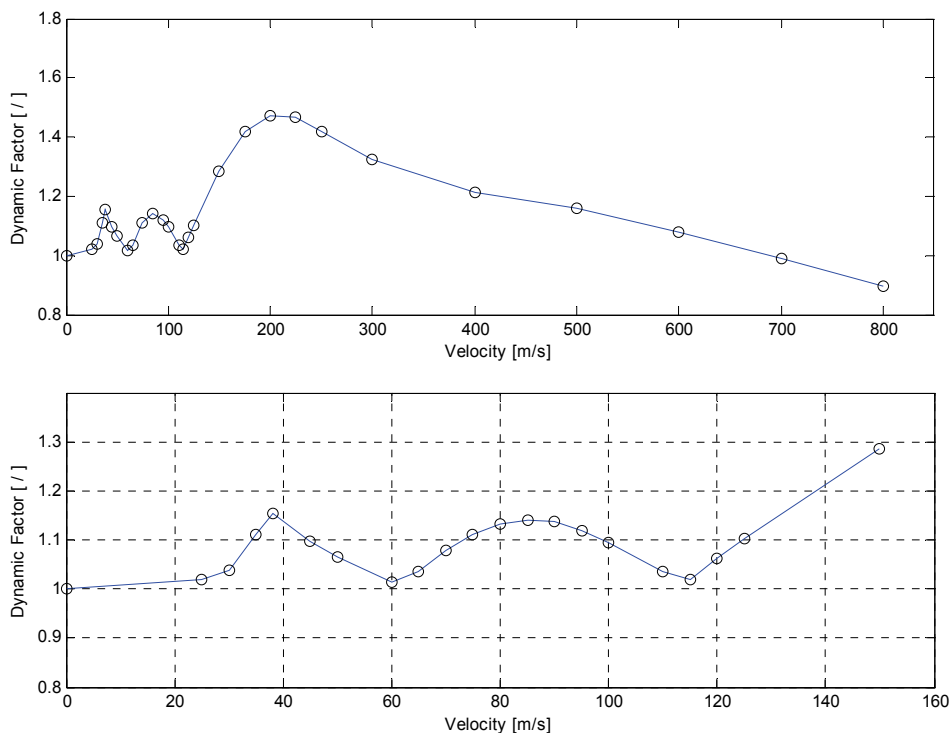


**Figure 6.69 Dynamic factor as a function of velocity**

### 6.8.3 Dynamic response of carriage body

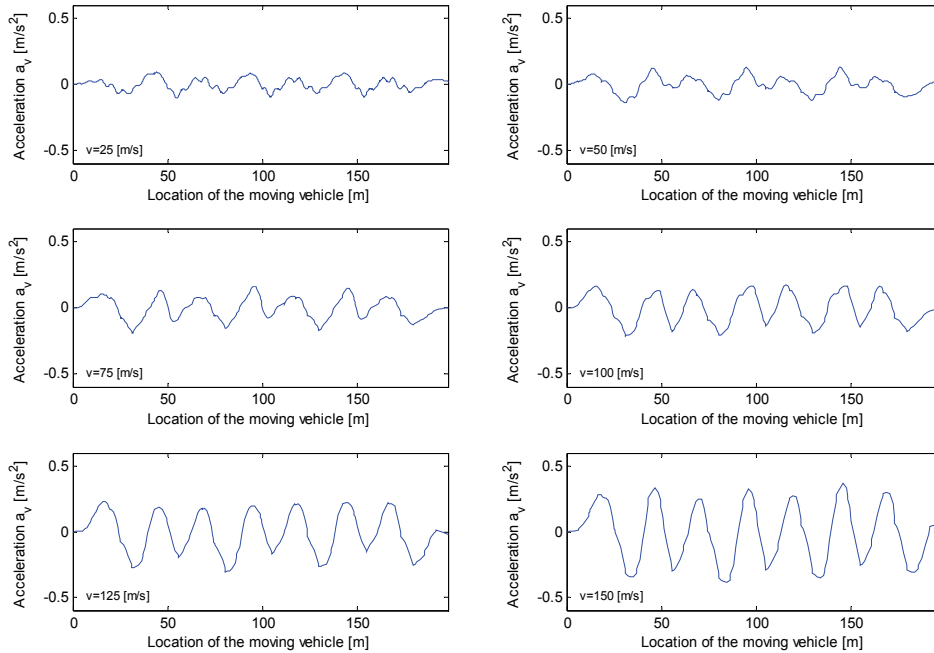


Figure 6.70 Acceleration of carriage body for various velocities

Figure 6.70 shows the vertical acceleration of the carriage body as a function of the location of the moving vehicle. The absolute value of acceleration increases when the velocity varies from 25 m/s to 150 m/s. We will check the acceleration at  $v = 138.889$  m/s, which is the maximum allowed velocity for the Maglev vehicle at current stage.

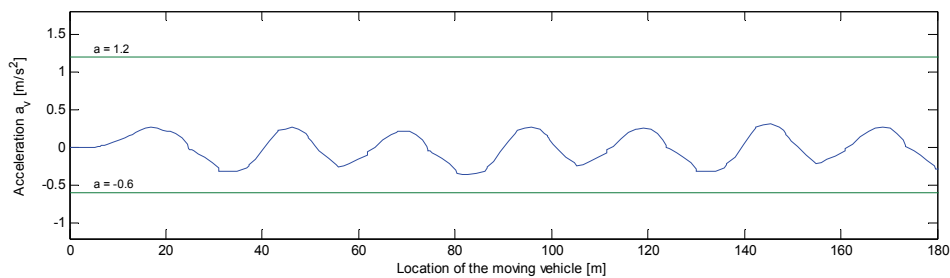
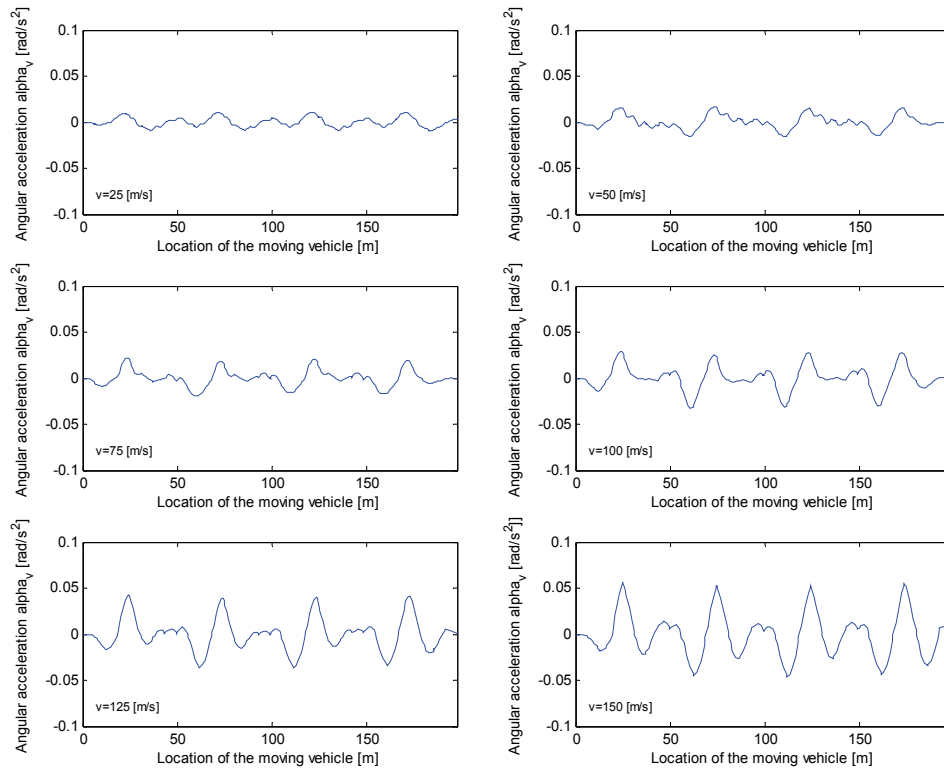


Figure 6.71 Acceleration of carriage body at  $v = 138.889$  m/s

As can be seen in Figure 6.71, the acceleration fluctuates between  $0.3108 \text{ m/s}^2$  and  $-0.3494 \text{ m/s}^2$ . Therefore the requirement for passage ride comfort ( $-0.6 \text{ m/s}^2$ – $1.2 \text{ m/s}^2$ ) in the German design guideline is satisfied.

## 6 Vehicle/Guideway Interaction Analysis



**Figure 6.72 Angular acceleration of carriage body for various velocities**

This model contains the rotational degree of freedom of the carriage body. Simulations are performed to study the angular acceleration of the carriage body at different traveling velocities. The results are shown in Figure 6.72.

When  $v = 138.880$  m/s, the angular acceleration of the carriage body varies between  $0.05066$  rad/s<sup>2</sup> and  $0.04039$  rad/s<sup>2</sup>.



**Figure 6.73 Angular acceleration of carriage body at  $v = 138.889$  m/s**

### 6.8.4 Dynamic response of levitation frame

The vertical acceleration of the levitation frame is also studied. In Figure 6.75 the acceleration of the first levitation frame for various velocities are shown. When  $v = 138.889$  m/s, the first levitation frame will vibrate between  $-9$  m/s<sup>2</sup> and  $9$  m/s<sup>2</sup> and the criteria in Section 8.1.1.7 of *Magnetschnellbahn Ausfahrungsgrundlage Fahrzeug Teil II* is met ( $-15$  m/s<sup>2</sup>– $15$  m/s<sup>2</sup>).

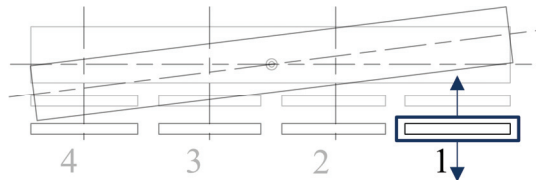


Figure 6.74 Vertical motion of levitation frame 1

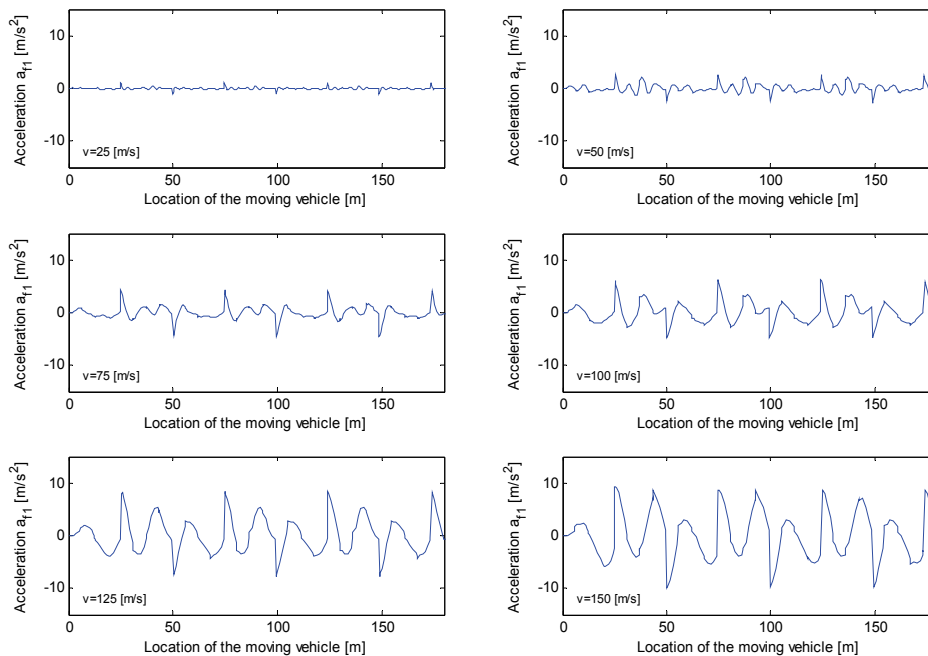


Figure 6.75 Acceleration of levitation frame 1 for various velocities

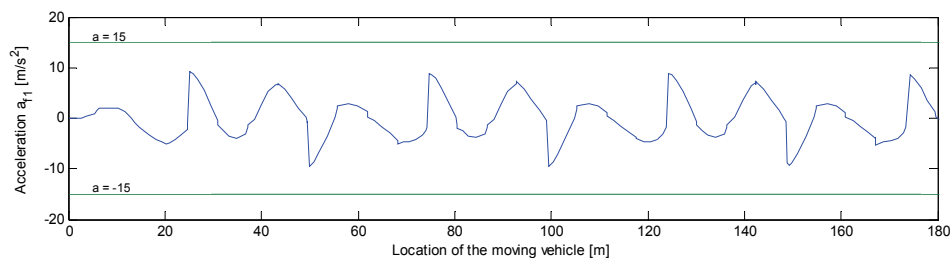
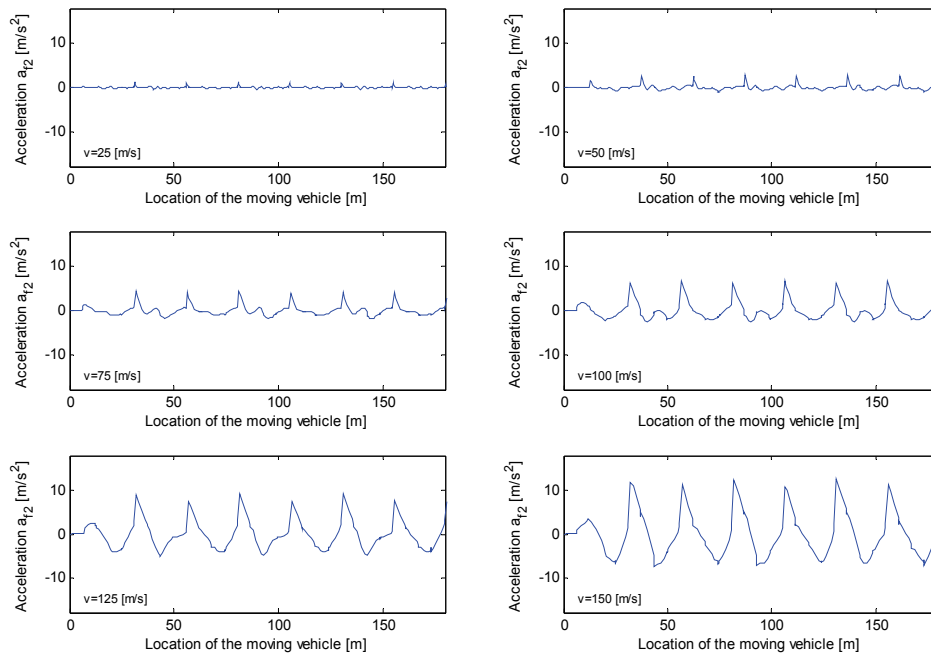


Figure 6.76 Acceleration of levitation frame 1 at  $v = 138.889$  m/s

## 6 Vehicle/Guideway Interaction Analysis



**Figure 6.77 Acceleration of levitation frame 2 for various velocities**

Similarly the simulating results for levitation frame 2 are shown in Figure 6.78. The requirement is also met when  $v = 138.889$  m/s as can be seen in Figure 6.79.

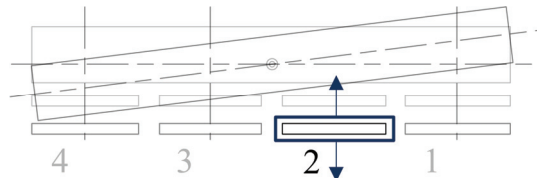


**Figure 6.78 Vertical motion of levitation frame 2**

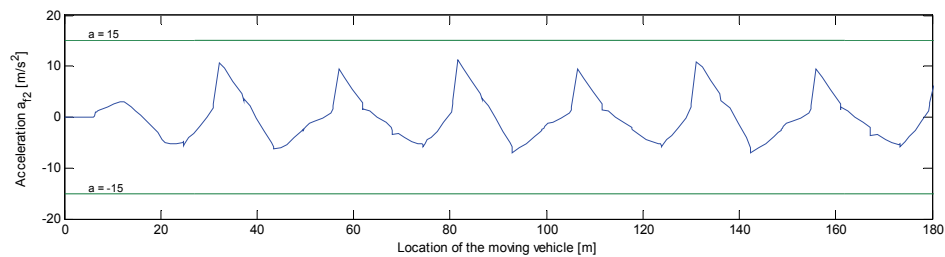


**Figure 6.79 Acceleration of levitation frame 1 at  $v = 138.889$  m/s**

## 6.9 Summary

In this section the five dynamic models we have created in Section 6.4-6.8 will be evaluated. They are intended to answer questions such as: Is it necessary to develop the complex interaction models for the maglev guideway design? Under which conditions can we neglect the dynamic coupling of the vehicle and guideway? What model should be used in different situations? Is the design curve in the Maglev Design Guideline conservative on the dynamic factor?

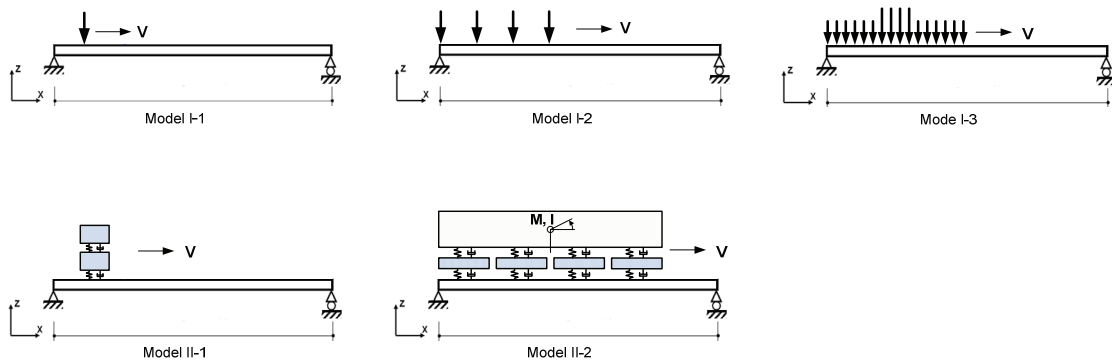


Figure 6.80 Five dynamic vehicle/guideway models

### 6.9.1 Guideway displacement

Figure 6.81 shows the time histories of the guideway displacement when  $v = 138.889$  m/s for different models. Model I-1 and II-1 give much larger displacements than those of the others. A slight difference can be seen between Model I-2, I-3, and II-2.

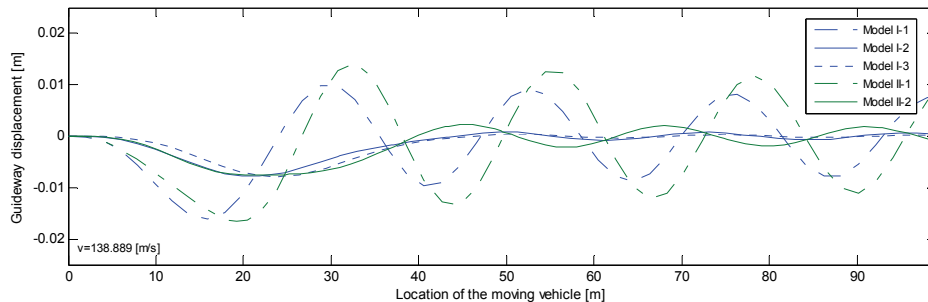
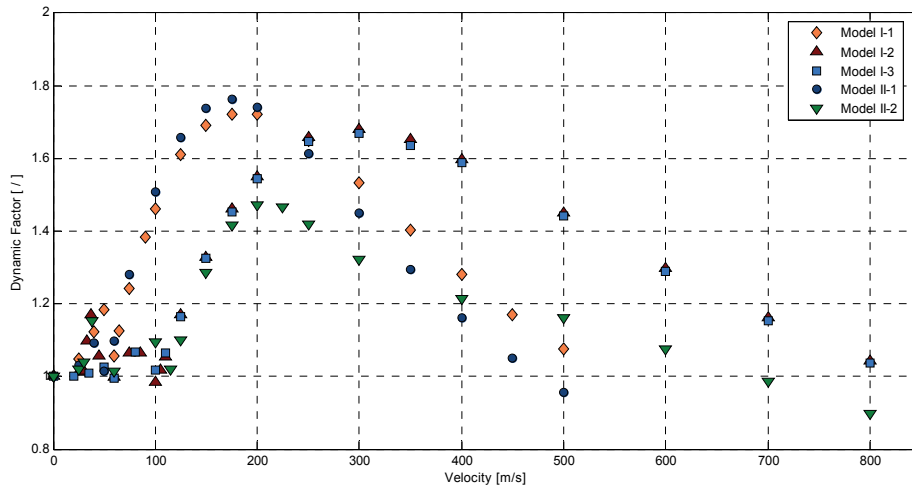


Figure 6.81 Guideway displacement as a function of the location of moving vehicle at  $v = 138.889$  m/s

Based on previous simulating results of all the numerical models, the dynamic factor  $\phi_{Bg,z}$  is plotted vs velocity in Figure 6.82.

## 6 Vehicle/Guideway Interaction Analysis



**Figure 6.82 Dynamic factor vs velocity for different models**

Model I-1 and II-1, where a single moving force or oscillator is applied, produce the highest dynamic factor of all the models at  $v = 175$  m/s. The responses of guideway are similar for these two models before they reach the peak value. After that the dynamic factor from a moving oscillator decreases faster than that of the moving force (see Figure 6.83).

Although easy to build, these two models lead to very large dynamic factors when velocity ranges between 50-200 m/s, which will cause a large amount of construction cost and waste of material. Therefore Model I-1 and Model II-1 are not suitable for a maglev guideway design.

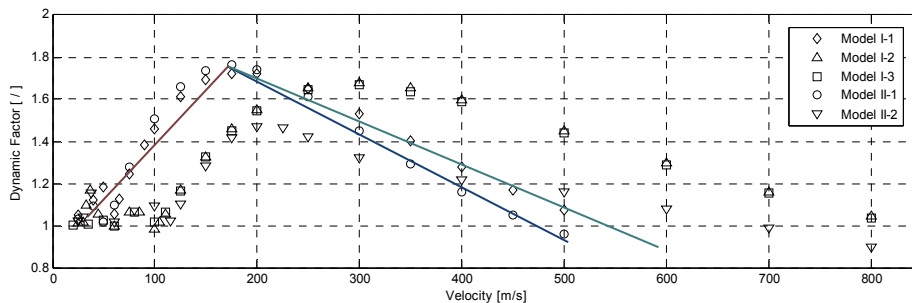


**Figure 6.83 Dynamic factor vs velocity for Model I-1 and Model II-1**

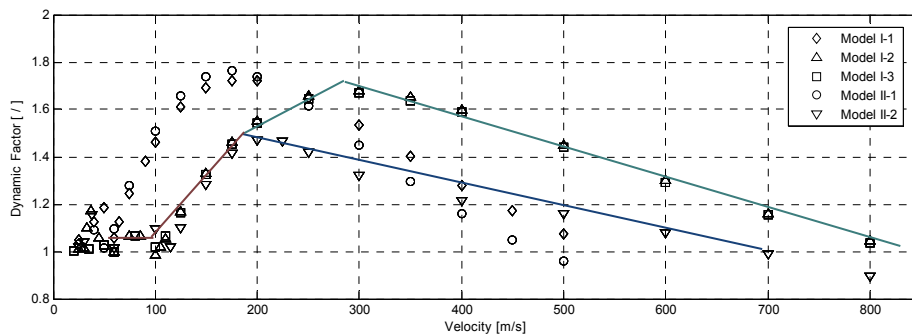


**Figure 6.84 Dynamic factor vs velocity for Model I-2, Model I-3 and Model II-2 [ $v > 50$  m/s]**

Model I-2 and Model I-3 are evaluated as shown in Figure 6.85. When  $v > 50$  m/s, Model I-2 and Model I-3 give almost identical results. Therefore if only the guideway displacement is under consideration, increasing the number of moving forces from four (Model I-2) to sixteen (Model I-3) won't increase the accuracy too much. A model with four moving forces is accurate enough.

When  $v < 50$  m/s, however, a peak value up to 1.2 is obtained at  $v = 38$  m/s for Model I-2 (see Figure 6.85). It is also the case in Model II-2, where four groups of spring and damping forces are modeled. Conversely, Model I-3 with sixteen moving forces gives a relative smooth line without any sharp fluctuation.

To sum up, when a low-speed maglev vehicle is studied (0-50 m/s), using Model I-3 with sixteen forces is more reasonable since it won't give the peak value as Model I-2. When the traveling velocity is larger than 50 m/s, making a complex model with sixteen forces is not necessary and Model I-2 is accurate enough.

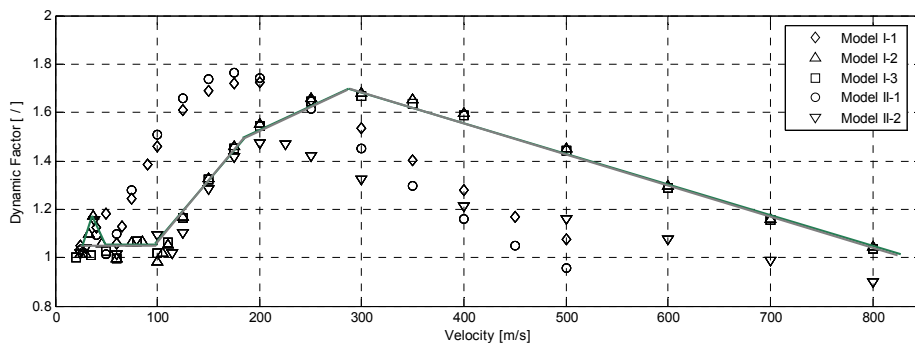


Figure 6.85 Dynamic factor vs velocity for Model I-2 and Model I-3

Figure 6.86 shows the effect of the dynamic coupling of vehicle and guideway on the guideway displacement by comparing Model I-2 and II-2. When  $v$  varies from 0 to 190 m/s they produce almost the same results. Thus, the coupling effect on guideway deformation can be neglected for  $v \leq 190$  m/s. When  $v \geq 190$  m/s, the coupling of vehicle and guideway comes to influence the guideway displacement greatly, where a considerable difference can be seen between these two models.

Therefore if the objective of the modeling is to study the guideway displacement only, it is not necessary to build a complex dynamic interaction model since at current stage the maximum allowed velocity for maglev vehicle is 138.889 m/s (500 km/h), unless this speed limitation is exceeded in the future development.

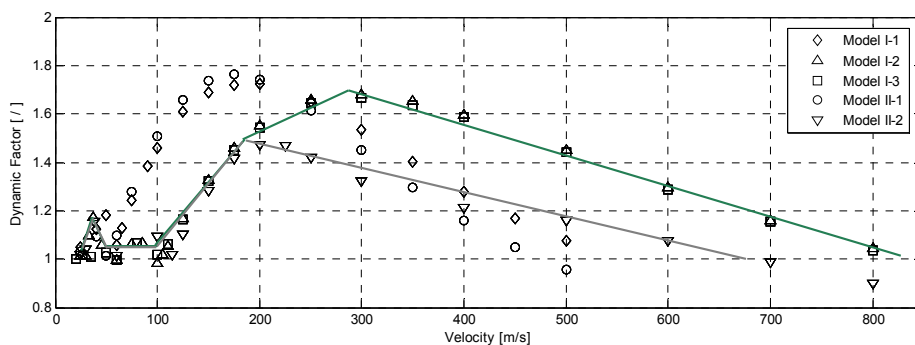


Figure 6.86 Dynamic factor vs velocity for Model I-2 and II-2

### 6.9.2 Dynamic factor in Design Guideline

The dynamic factor for guideway design is also suggested in the German design guideline *Magnetschnellbahn Ausfahrungsgrundlage Fahrweg Teil II Bemessung*. In case of a two-section vehicle and a guideway span length  $L=24.768$  m, the dynamic factor can be calculated as:

$$\varphi_{Bg,z} = \begin{cases} 1.05 & 0 \leq v \leq 33.309 \\ 1.1 & 33.309 \leq v \leq 59.956 \\ 1.2 & 59.956 \leq v \leq 107.065 \\ 1.2 + 0.867(1.4 - k) & 107.065 \leq v \leq 142.753 \end{cases} \quad (6.84)$$

where

$$k \quad \text{factor defined as } k = \frac{L \cdot f_1}{v}$$

Therefore the dynamic factor can be plotted as a function of velocity which varies between 0 and 142.7529 m/s as shown in Figure 6.87.

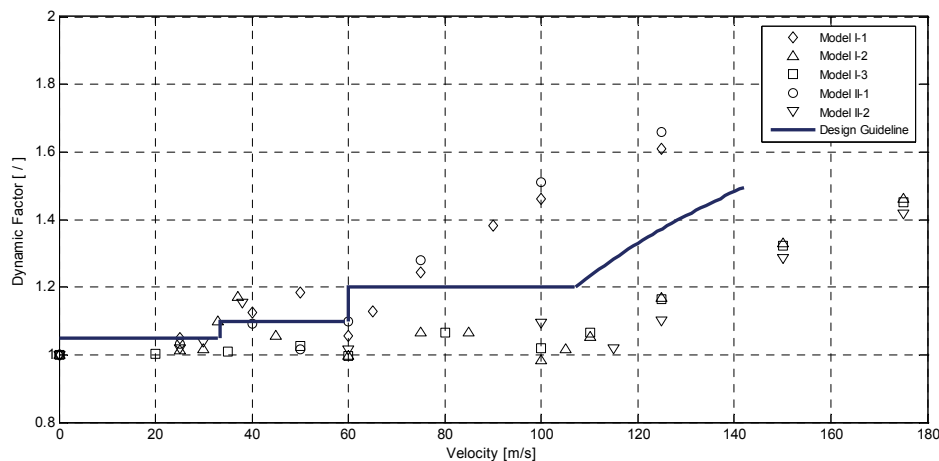


Figure 6.87 Dynamic factor suggested in MSB-AG-Fahrweg Teil II

Figure 6.87 also compares the design curve with the results from numerical models. It appears that the dynamic factors produced by Model I-1 and II-1 are higher than those suggested in the design guideline. As proved in Section 6.9.1, they are not suitable to simulate the maglev system. On the other sides, when compared the design curve with the more accurate models, e.g. Model I-2, I-3 and II-2, the dynamic factor from *Magnetschnellbahn Ausfahrungsgrundlage-Fahrweg* is a little conservative, especially when  $v > 60$  m/s with an approximate increase of 10%.

### 6.9.3 Acceleration of carriage body and levitation frames

Although the coupling model is not necessary for  $v < 190$  m/s when only the guideway displacement is under consideration, it is very important to consider it for the passenger riding comfort. In Figure 6.88 and 6.89 the simulation results of acceleration from Model II-1 and II-2

are compared. Model II-2 produces much smaller accelerations both for carriage body and levitation frames. This proves the importance of an accurate coupled system when the acceleration of the maglev system is studied.

It is noted that the guideway surface roughness, which will influence the vibration of the vehicle greatly, has not been considered in the model. It will be studied in the next chapter.

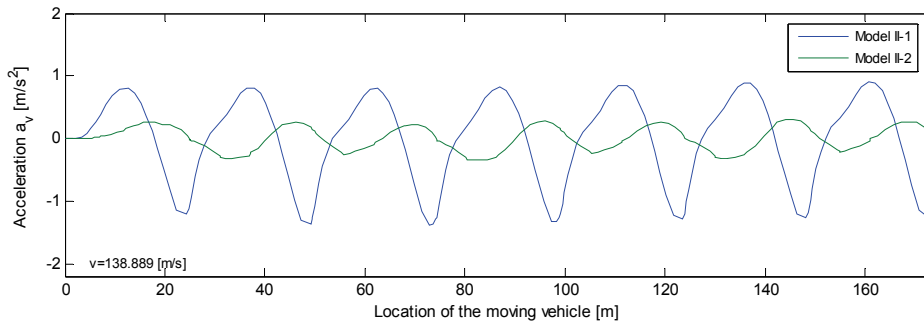


**Figure 6.88 Vertical acceleration of carriage body of Model II-1 and II-2**

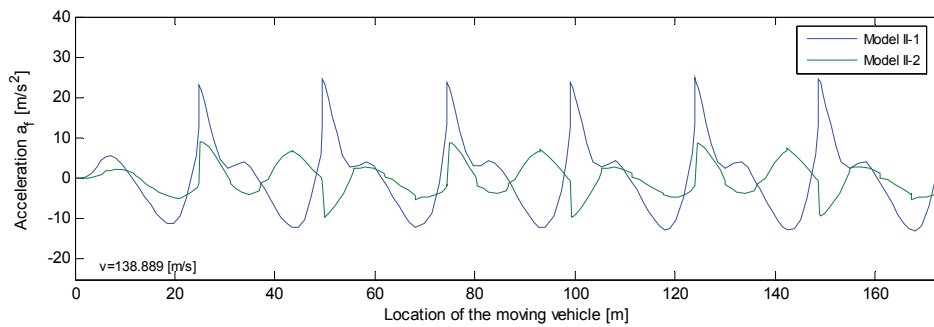


**Figure 6.89 Vertical acceleration of levitation frame of Model II-1 and Model II-2**

# 7

---

## Guideway Surface Roughness Model

## 7.1 General

The roughness of a Maglev guideway may exhibit random characteristics which are important to ride quality. Because the guideway infrastructure and service environment are similar to conventional ground tracks, the surface roughness of guideways can be described approximately by the Power Spectral Density (PSD) of the surface profile (Y. Cai, 1995). The guideway irregularity PSD should have a similar formula as those described railway track or highway surface roughness.

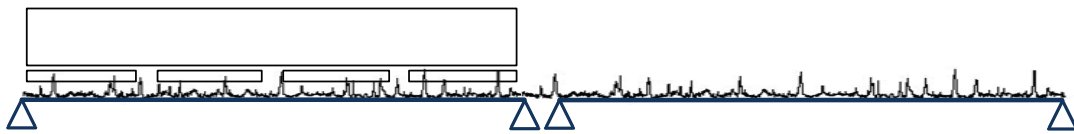


Figure 7.1 The surface roughness of Maglev guideway

Dodds and Robson [1973] studied the road surface roughness and showed that typical road surface may be considered as realization of homogeneous and isotropic Gaussian random process. They developed a new road classification method based on power spectral density. The function they proposed to describe the road surface roughness can be expressed as:

$$S(\phi) = A \left( \frac{\phi}{\phi_0} \right)^{-m} \quad (7.1)$$

where

$S(\phi)$	power spectrum of the surface
$\phi$	wave number in cycle/m
$\phi_0$	discontinuity frequency, $1/2\pi$ cycle/m
$A$	roughness amplitude
$m$	roughness exponent

Based on a wide variety of experimental data, the value of  $m$  ranges from 1.5 for shorter wavelengths to 2.5 for longer wavelengths. In the medium-to-longer wavelengths, the PSD curve may be approximated by a line with  $m=2$  (Y. Cai, 1995).

Due to the fact that it is difficult to find the Maglev guideway irregularity PSD field data from literature, we will use the roughness amplitudes  $A = 1.5 \times 10^{-6}$ , which are applied to aircraft runway, and  $A = 1.5 \times 10^{-7}$ , which are applied to continuous welded rail tracks, respectively.

The surface roughness model is obtained by using the Signal Processing Tools in Simulink. First a Gaussian White Noise signal is generated and then passed through an Infinite Impulse Response (IIR) filter. This surface roughness model is stored as a subsystem and linked to the vehicle/guideway dynamic model which has been created in Chapter 6.

## 7.2 White Noise and IIR Filter

White noise is a random signal with a flat frequency spectrum. The signal's power spectral density has equal power at any center frequency. A typical white noise in space domain is shown in Figure 7.2.

The Signal Processing Sources block of Simulink is used to generate random numbers drawn from a Gaussian pseudorandom distribution. The signal has approximate white noise properties with zero mean and a specified value of variance. The variance is determined by the guideway roughness amplitude  $A$ .

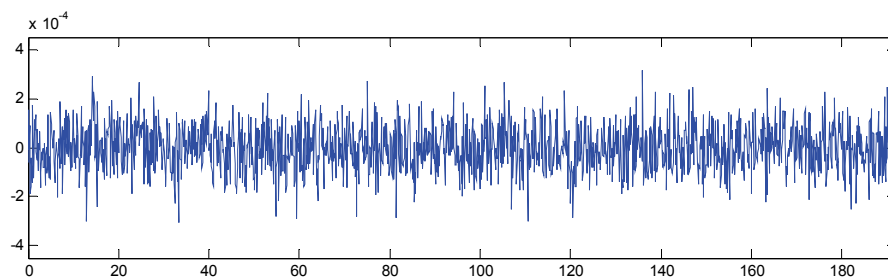


Figure 7.2 White Noise in space domain

The Digital Filter block independently filters each channel of the input signal with a specified IIR filter. We will use IIR-all poles as the transfer function type. The filter structure is a Direct form as shown in Figure 7.3. The filter coefficient contains a Denominator coefficients vector in the form of  $[a_0, a_1, a_2, \dots, a_M]$ . Since a first order recursive filter is applied in this model, the Denominator coefficients vector is  $[1, -1]$ .

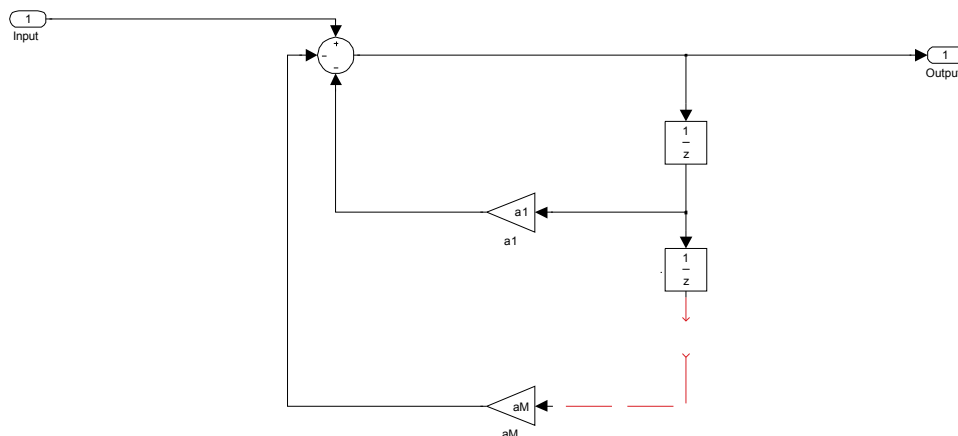


Figure 7.3 IIR(all poles) Direct form Filter

When a random signal with white noise properties is passed through this first order IIR filter, the PSD of the output function gets modified and is related with input PSD through a transfer function. It can be written as:

$$S(\phi)_{output} = |H(\phi)|^2 S(\phi)_{input} \tag{7.2}$$

where

$S(\phi)_{output}$	PSD of the output signal
$S(\phi)_{input}$	PSD of the input signal
$H(\phi)$	Transfer function

The power spectral density of the output function should match with the power spectral density function given in Equation (7.1). The variance required to create the input white noise signal can be calculated by comparing the transfer function with Equation (7.1). The result is expressed as (S. Jerath, 2008):

$$\sigma^2 = \frac{A\lambda}{2} \tag{7.3}$$

where

$\sigma^2$	variance of white noise signal
$\lambda$	length between sample points

### 7.3 Roughness Model I ( $A=1.5 \times 10^{-7}$ )

The roughness amplitude  $A = 1.5 \times 10^{-7}$  for continuous welded rail tracks will be used to create the first Roughness Model for the Maglev guideway. We choose 1536 sample points in a length of 192 m along the simply supported guideway. Then the length between sample points is:

$$\lambda = \frac{192}{1536} = 0.125 \tag{7.4}$$

From Equation (7.3), the input value of the variance for the random source can be calculated as:

$$\sigma^2 = \frac{A\lambda}{2} = \frac{1.5 \times 10^{-7} \times 0.125}{2} = 9.375 \times 10^{-9} \tag{7.5}$$

The Gaussian white noise signal is generated by using the variance  $\sigma^2$ , zero mean, and  $\lambda$  as shown in Figure 7.4.

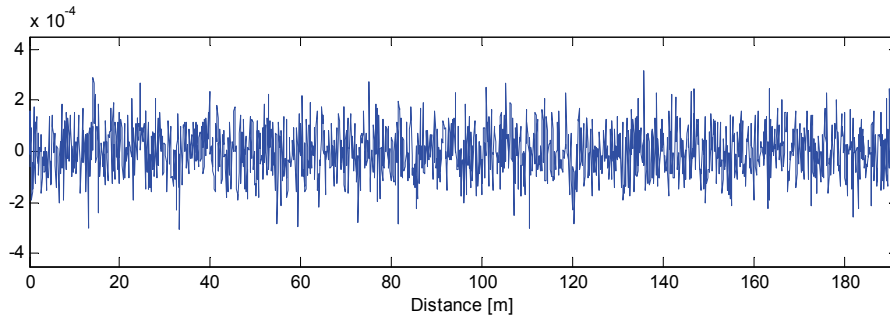


Figure 7.4 White Noise signal when  $A = 1.5 \times 10^{-7}$

## 7 Guideway Surface Roughness Model

The power spectral density of the random signal we have generated is calculated using Welch's averaged modified periodogram method of spectral estimation in MATLAB. The result is plotted in Figure 7.5.

The target PSD of the white noise signal can be calculated as Equation (7.6) and is plotted with green line in Figure 7.5 as well.

$$S_0(\phi) = \sigma^2 \cdot 2\lambda = 2.3437 \times 10^{-9} \quad (7.6)$$

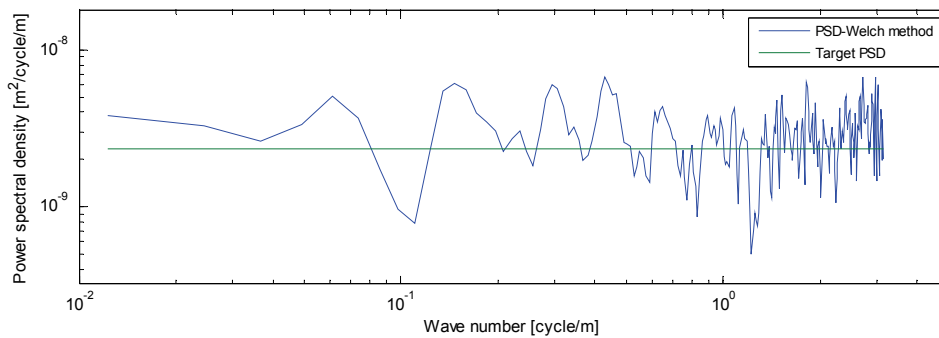


**Figure 7.5 Power Spectral Density of the Gaussian White Noise**

When the random spectrum of Figure 7.4 is passed through the first order recursive filter defined in Section 7.2, output from the filter gives the desired guideway surface profile as shown in Figure 7.6.

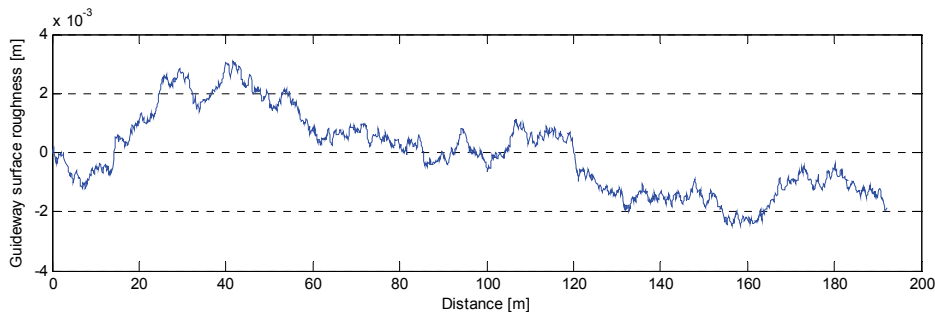


**Figure 7.6 Guideway surface roughness model**

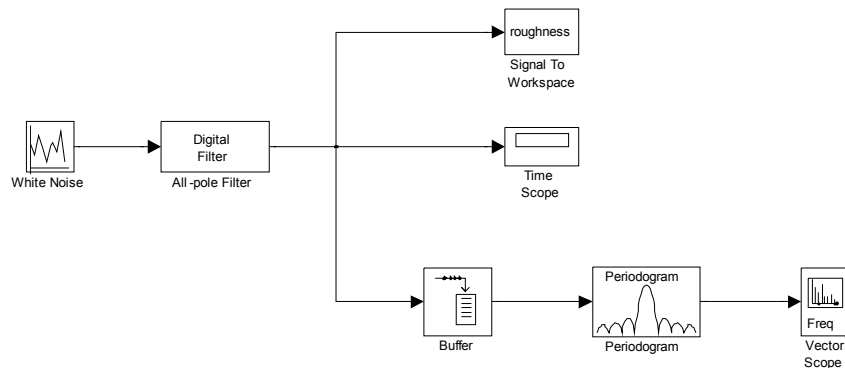


**Figure 7.7 Surface roughness model in Simulink**

The power spectral density of the output spectrum is calculated using Welch’s averaged modified periodogram method and plotted in Figure 7.8.

By taking  $A = 1.5 \times 10^{-7}$  the target PSD can be derived according to Equation (7.1) as:

$$S(\phi) = A \left( \frac{\phi}{\phi_0} \right)^m = 1.5 \times 10^{-7} \left( \frac{1}{2\pi\phi} \right)^2 \tag{7.7}$$

As can be in Figure 7.6, the comparison of the output PSD in Simulink and the target PSD shows a good correlation. So the roughness mode with  $A = 1.5 \times 10^{-7}$  is well built.

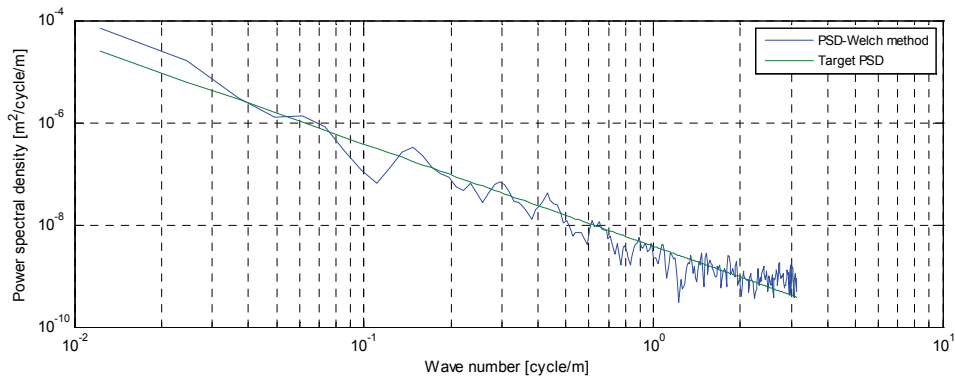


Figure 7.6 Power Spectral Density of the guideway surface roughness

### 7.3.1 Linked with the Vehicle/Guideway Model

The vehicle/guideway Model II-3 which has been created in Chapter 6.8 is used to evaluate the effect of the guideway surface roughness. The Roughness Model is stored as a subsystem and linked with the Guideway Model and the Primary Suspension system as shown in Figure 7.7.

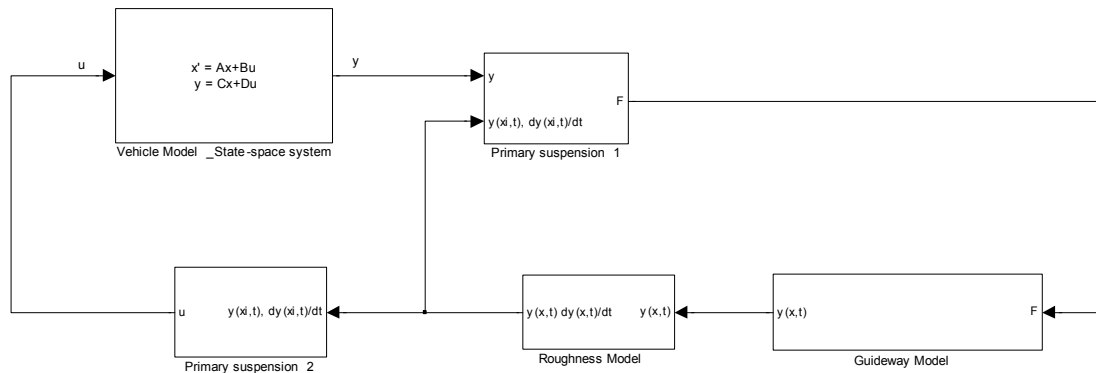


Figure 7.7 Vehicle/Guideway interaction model including surface roughness model

## 7 Guideway Surface Roughness Model

The roughness subsystem for  $i$ -th guideway is shown in Figure 7.9 and 7.10. Note that the roughness model we made in Section 7.3 is in space domain and cannot be used directly. It is first transferred to time domain so that it can interact with other subsystems during the simulation.

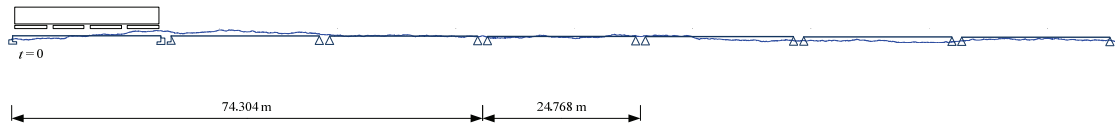


Figure 7.8 Guideway surface roughness

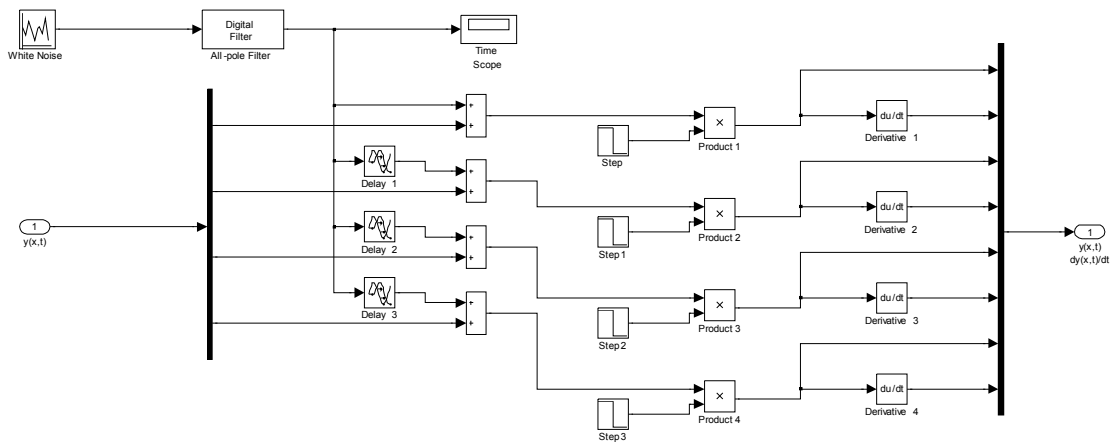


Figure 7.9 Roughness Model for  $i$ -th Guideway Model ( $i=1$ )

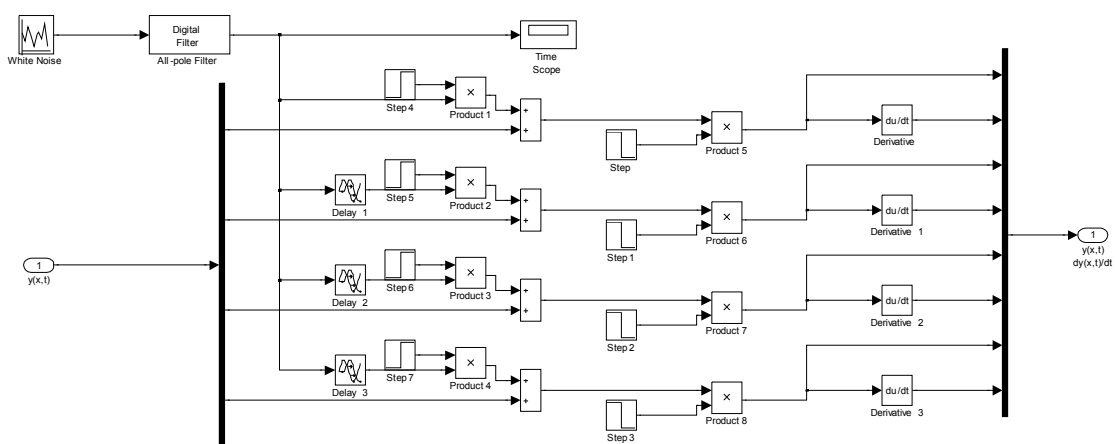


Figure 7.10 Roughness Model for  $i$ -th Guideway model ( $i \geq 2$ )

### 7.3.2 Dynamic response of guideway and vehicle

In order to understand the influence of guideway surface roughness on guideway mid-span displacement and on vehicle acceleration, the time histories of displacement of guideway, the vertical acceleration of carriage body and the angular acceleration of carriage body are compared with the simulation results from a smooth guideway as shown in Figure 7.11-7.13.

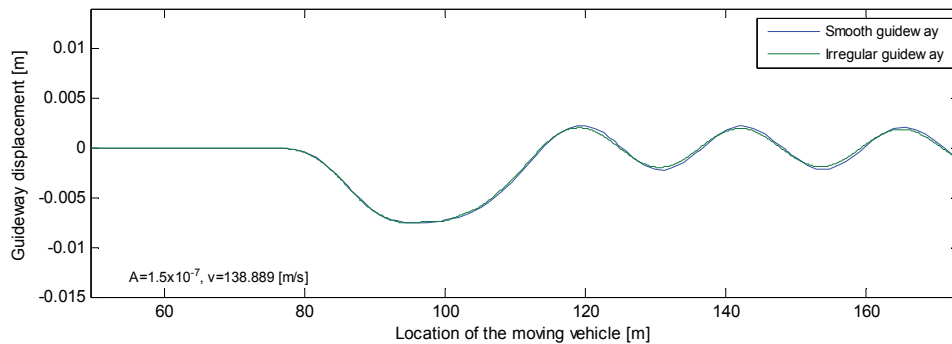


Figure 7.11 Guideway displacement as a function of location of the moving vehicle at  $v = 138.889$  m/s

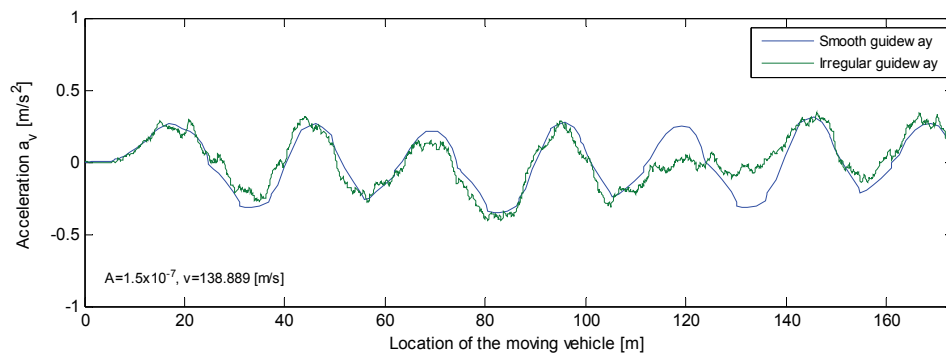


Figure 7.12 Acceleration of carriage body as a function of location of the vehicle at  $v = 138.889$  m/s

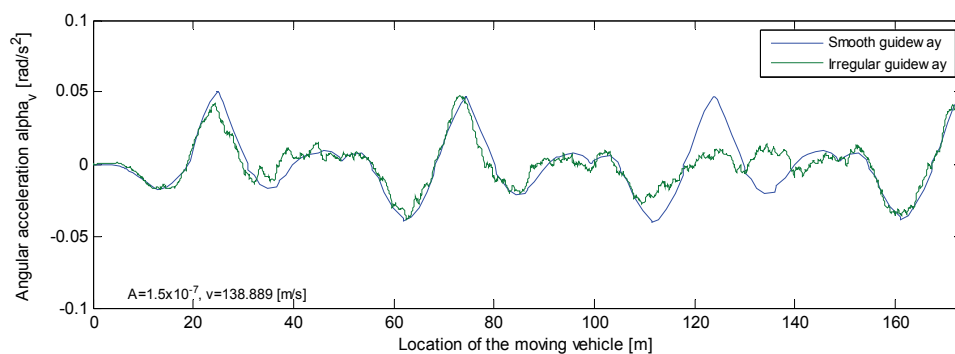
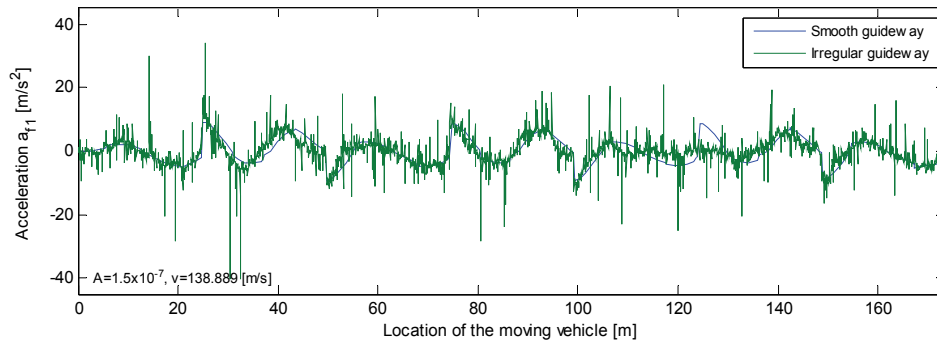


Figure 7.13 Angular acceleration of carriage body as a function of location of the vehicle at  $v = 138.889$  m/s

## 7 Guideway Surface Roughness Model

The vertical acceleration of the first levitation frame is also plotted as functions of the location of the moving vehicle when  $v = 138.889$  m/s in Figure 7.14.



**Figure 7.14 Acceleration of first levitation frame as a function of the location of the vehicle at  $v = 138.889$  m/s**

As can be seen from Figure 7.11–7.14, the guideway mid-span displacement does not distinctly change when the surface roughness model is applied ( $A = 1.5 \times 10^{-7}$ ). Conversely, the vehicle acceleration will be influenced. For the carriage body, the maximum/minimum values are almost kept identical. But for the maximum acceleration of the levitation frame, increase as much as 273% (from  $9.199$  m/s<sup>2</sup> to  $34.310$  m/s<sup>2</sup>) can be obtained.

It is concluded that in the present case ( $A = 1.5 \times 10^{-7}$ ), guideway surface roughness has greater influence on vehicle acceleration than on guideway displacement.

### 7.4 Roughness Model II ( $A=1.5 \times 10^{-6}$ )

The roughness amplitude  $A = 1.5 \times 10^{-6}$  for aircraft runway will be used to create another roughness model for the Maglev guideway. We will use the same sample points and sample length as the first roughness model. Then the length between sample points is:

$$\lambda = \frac{192}{1536} = 0.125 \quad (7.8)$$

From Equation (7.3), the input value of the variance for the random source can be calculated as:

$$\sigma^2 = \frac{A\lambda}{2} = \frac{1.5 \times 10^{-6} \times 0.125}{2} = 9.375 \times 10^{-8} \quad (7.9)$$

The Gaussian white noise signal is generated by using the variance  $\sigma^2$ , zero mean, and  $\lambda$  as shown in Figure 7.15.

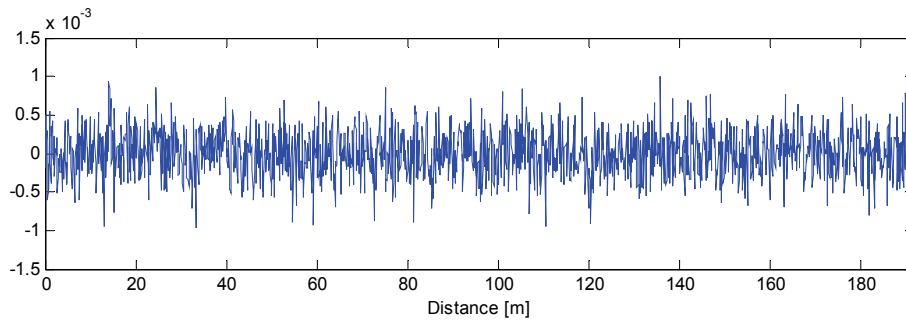


Figure 7.15 White noise signal when  $A = 1.5 \times 10^{-6}$

The power spectral density of this white noise signal is calculated using Welch’s averaged modified periodogram method in MATLAB and is plotted in Figure 7.16.

The target PSD of the white noise signal can be calculated as Equation (7.10) and is plotted with green line in Figure 7.16.

$$S_0(\phi) = \sigma^2 \cdot 2\lambda = 2.3437 \times 10^{-8} \quad (7.10)$$

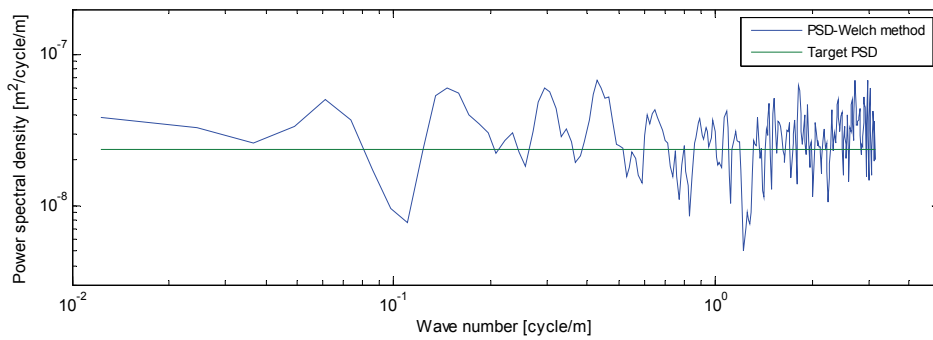


Figure 7.16 Power Spectral Density of the Gaussian White Noise

This random signal is then passes through the IIR filter to obtain the desired guideway surface roughness model as shown in Figure 7.17:

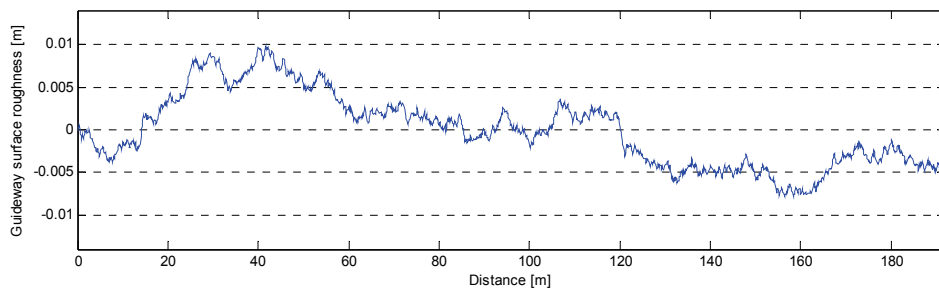
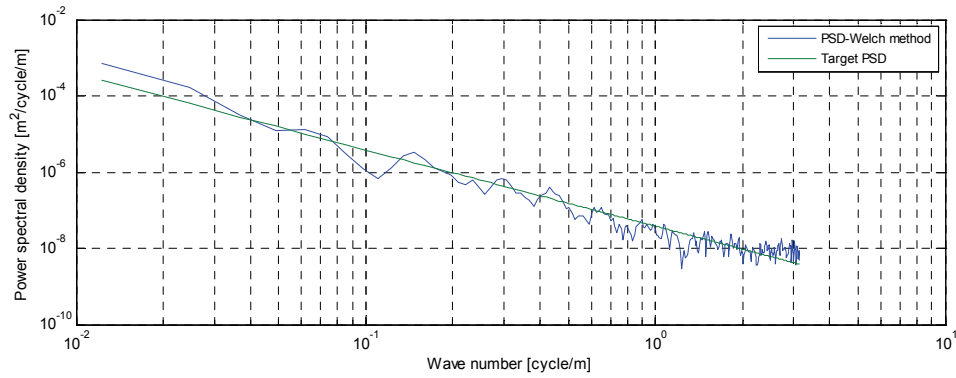


Figure 7.17 Guideway surface roughness model

The power spectral density of the output spectrum is calculated using Welch’s averaged modified periodogram method too. It is plotted in Figure 7.18 as well as the target PSD when  $A = 1.5 \times 10^{-6}$ , which can be calculated as:

## 7 Guideway Surface Roughness Model

$$S(\phi) = A \left( \frac{\phi}{\phi_0} \right)^m = 1.5 \times 10^{-6} \left( \frac{1}{2\pi\phi} \right)^2 \quad (7.11)$$



**Figure 7.18 Power Spectral Density of the guideway surface roughness**

In Figure 7.18 the output PSD in Simulink and the target PSD when  $A = 1.5 \times 10^{-6}$  show a good agreement.

The roughness model is linked to the vehicle/guideway interaction model II-2 in the same way as that in Chapter 7.3. The simulation results for guideway mid-span displacement at various velocities are plotted in Figure 7.19 and 7.20.

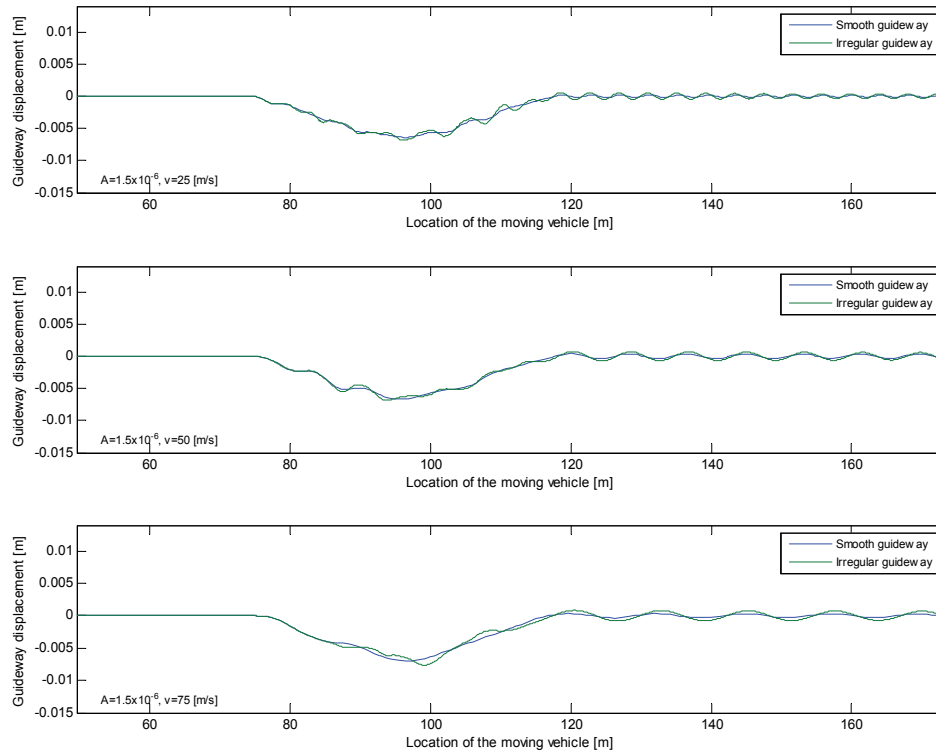


**Figure 7.19 Guideway displacement as a function of location of the vehicle at  $v = 25$  m/s, 50 m/s and 75 m/s**

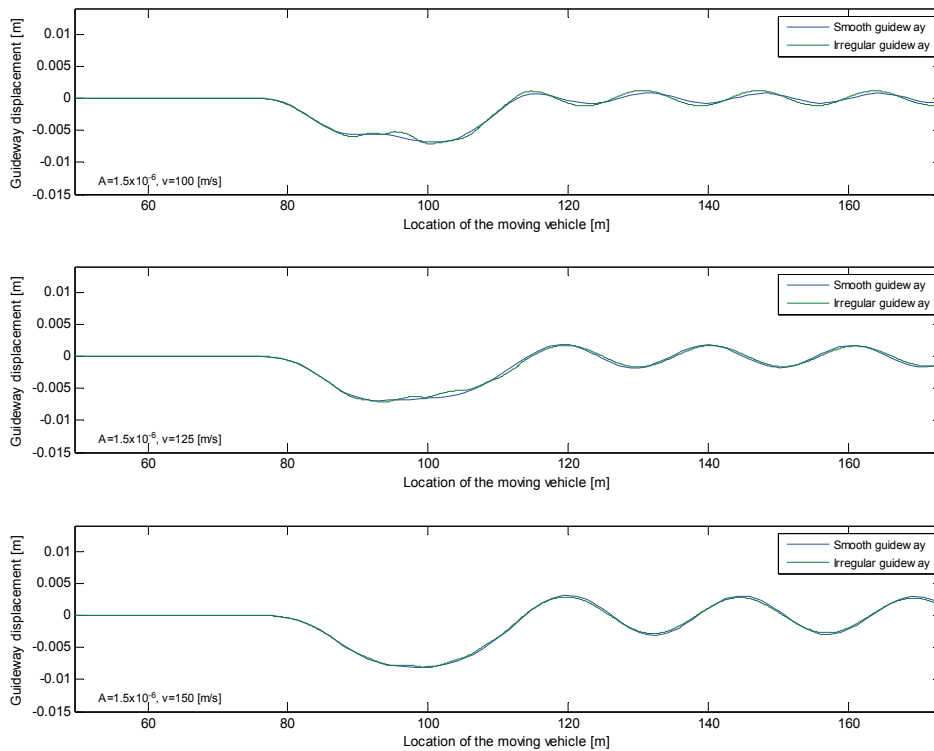


**Figure 7.20** Guideway displacement as a function of location of the vehicle at  $v = 100$  m/s, 125 m/s and 150 m/s

Velocity [m/s]	25	50	75	100	125	150
Displacement Irregular Guideway [mm]	6.839	6.855	7.613	7.124	7.153	8.144
Displacement Smooth Guideway [mm]	6.392	6.679	6.966	6.864	6.907	8.057
Increase [%]	6.99	2.64	9.29	3.79	3.56	1.08

**Table 7.1** Comparison of guideway displacement between irregular guideway and smooth guideway

The acceleration and angular acceleration of the carriage body and the acceleration of the first levitation frame at the maximum allowed velocity  $v = 138.889$  m/s are shown in Figure 7.21-7.23.

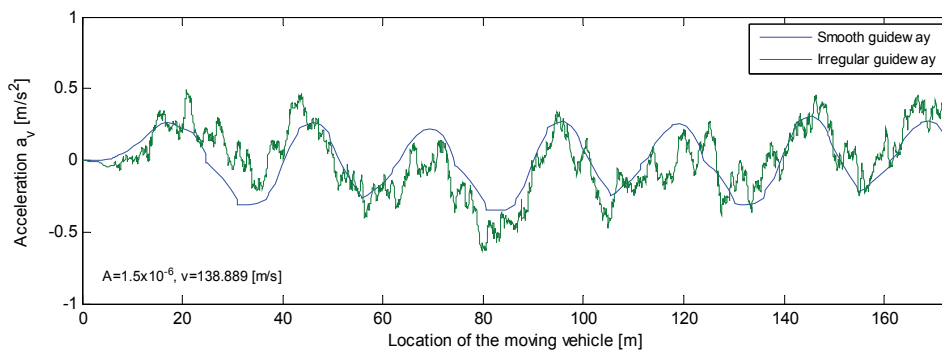


**Figure 7.21** Acceleration of carriage body as a function of location of the vehicle at  $v = 138.889$  m/s

## 7 Guideway Surface Roughness Model

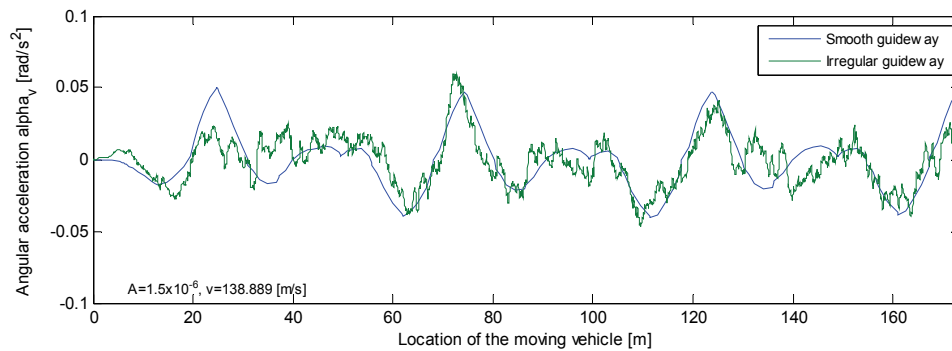


**Figure 7.22 Angular acceleration of carriage body as a function of location of the moving vehicle at  $v = 138.889$  m/s**

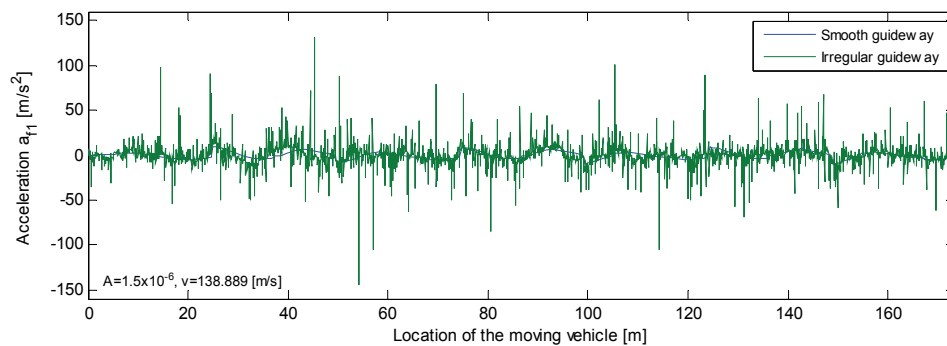


**Figure 7.23 Acceleration of the first levitation frame as a function of location of the moving vehicle at  $v = 138.889$  m/s**

As seen from the simulation results, when a roughness amplitude  $A = 1.5 \times 10^{-6}$  is chosen, the guideway surface roughness will make influence on the guideway mid-span displacement. Table 7.1 lists the increases of guideway mid-span displacement at various velocities. A maximum increase as much as 9.29% is reached when  $v = 75$  m/s (from 6.966 mm to 7.613 mm).

Figure 7.21-7.23 show that the acceleration of the vehicle is greatly influenced by this surface roughness model. The maximum vertical acceleration of the carriage body at 500 km/h increases by 80.14% from  $0.265 \text{ m/s}^2$  to  $0.494 \text{ m/s}^2$ , while the maximum angular acceleration increases by 28.17% from  $0.047 \text{ rad/s}^2$  to  $0.060 \text{ rad/s}^2$ .



# 8

---

## Finite Element Model

## 8.1 General

In this Chapter a finite element model of a simply supported guideway is created with the finite element software Midas/Civil. The main purpose of conducting a FE analysis is to verify the numerical models described in Chapter 6, and to discuss the problems associated with modeling Maglev guideway in Midas/Civil.

Neither the multiple degree-of-freedom vehicle models nor the guideway surface roughness can be modeled directly due to the limitation of element type in Midas. Therefore only the first three models in Chapter 6 are to be created, with single or multiple moving forces on beam element. Time-history analysis is performed and the dynamic response is compared with the results of previous numerical simulations.

## 8.2 Modeling

The simply supported concrete guideway is designed mainly based on the first generation of elevated concrete guideway at Test Facility Emsland. It has a standard length of 24.768 m and a height of 1.827 m. The cross section contains a box girder with cantilever arm and circular bottom chord (see Figure 8.1). The sloping sides and rounded bottom are aesthetically pleasing and serve a minimal purpose in reducing wind loadings. On the other, these features possibly add to the complexity and cost.

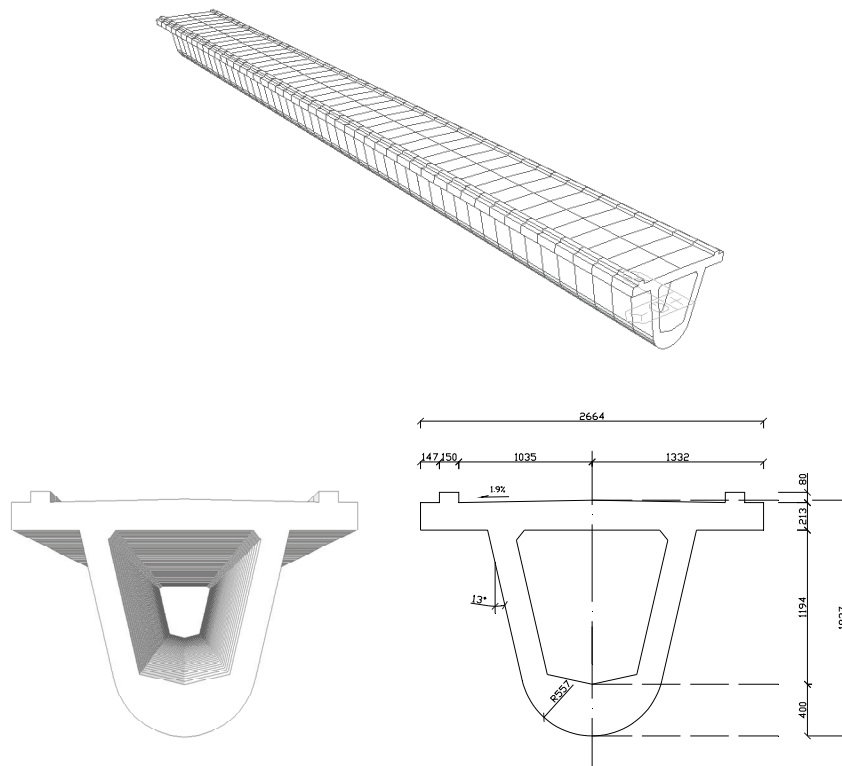
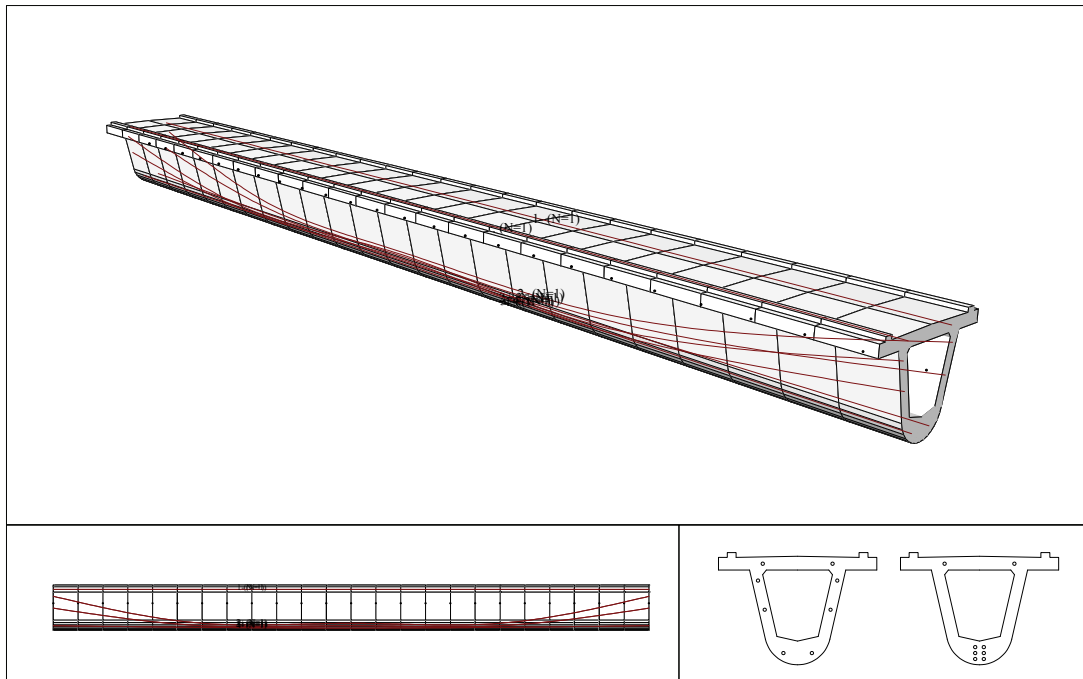


Figure 8.1 Maglev guideway model in Midas

## 8 Finite Element Model

The hollow space can be obtained by extractable inner formwork and the diaphragms are cast subsequently. The diaphragms are not considered in the FE model.

The cross section is generated by Sectional Property Calculator (SPC) in Midas which enable user to freely represent a cross sectional shape. The section properties and parameters are listed in Table 6.1 and they have already been used in the numerical models in Chapter 6.



**Figure 8.2 Post-tensioned bar in guideway**

A combination of straight and parabolically draped Dywidag post-tensioned bars is used to reinforce the girder as shown in Figure 8.2. The properties of the standard Dywidag bars are listed in Figure 8.3. The 32-mm-diameter high-strength bars are straightly post tensioned in top flange, and the 36-mm-diameter high-strength bars are parabolically draped in the web.

Nominal Bar Diameter (in.)/(mm)	Ultimate Stress $f_{pu}$ (ksi)/(Mpa)	Cross Section Area $A_{ps}$ (in. <sup>2</sup> )/(mm <sup>2</sup> )	Ultimate Strength $f_{pu} A_{ps}$ (kips)/(KN)	Prestressing Force—kips KN			Weight (lbs./ft.) (kg/m)	Minimum* Elastic Bending Radius (ft.)/(m)
				0.8/ $f_{pu} A_{ps}$	0.7/ $f_{pu} A_{ps}$	0.6/ $f_{pu} A_{ps}$		
1 in. 26 mm	150 1030	0.85 548	127.5 567	102.0 454	89.3 397	76.5 340	3.01 4.48	52 15.9
1 in. 26 mm	160** 1100	0.85 548	136.0 605	108.8 485	95.2 423	81.6 363	3.01 4.48	49 14.9
1 1/4 in. 32 mm	150 1030	1.25 806	187.5 834	150.0 662	131.3 584	112.5 500	4.39 6.54	64 19.5
1 1/4 in. 32 mm	160** 1100	1.25 806	200.0 890	160.0 707	140.0 623	120.0 534	4.39 6.54	60 18.3
1 in. 36 mm	150 1030	1.58 1018	237.0 1055	189.6 839	165.9 738	142.2 633	5.56 8.28	72 22.0
1 in. 36 mm	160** 1100	1.58 1018	252.8 1125	202.3 899	177.0 787	151.7 675	5.56 8.28	67 20.4
1 in. 46 mm	150 1030	2.62 1690	400 1779	320 1423	280 1245	240 1068	9.23 13.74	92 28.0

\*Prebent bars are required for radii less than the minimum elastic radius.  
\*\*Grade 160 bar is available only on special order.

**Figure 8.3 Standard Dywidag bar, [www.dywidag-systems.com](http://www.dywidag-systems.com)**

Lever studied different types of FE models for guideway and concluded that the beam-element model is as accurate as the solid-element model for a dynamic interaction analysis at high speed (J.H. Lever, 1998). Therefore the beam element is used to create the guideway model.

The FE mesh must be of such refinement that its solution will correctly reproduce those characteristic mode shapes of the guideway which are likely to be excited by the traversing vehicle. Richardson and Wormely (1974) indicate that for guideway with  $k$  equal spans, the number of modes important for accurate displacement calculation will be equal to  $k$  and that for bending moment and stress can be greater than  $3k$ . Thus, for a single-span guideway, the mesh should be sufficiently refined to accurately represent the first 3 bending modes. Based on these the minimal mesh to represent the simply supported guideway for mode 3 is six elements.

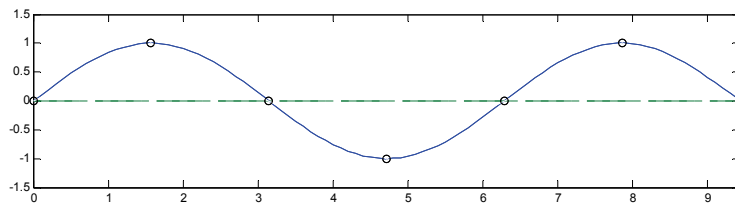


Figure 8.4 Minimal mesh to represent Mode 3

To increase the accuracy of the dynamic result, the beam is subdivided into 48 elements as Figure 8.5. Conducting an eigenvalue analysis is a prerequisite for the time history analysis in Midas. The first six mode shapes are shown in Figure 8.6.



Figure 8.5 Mesh of guideway model

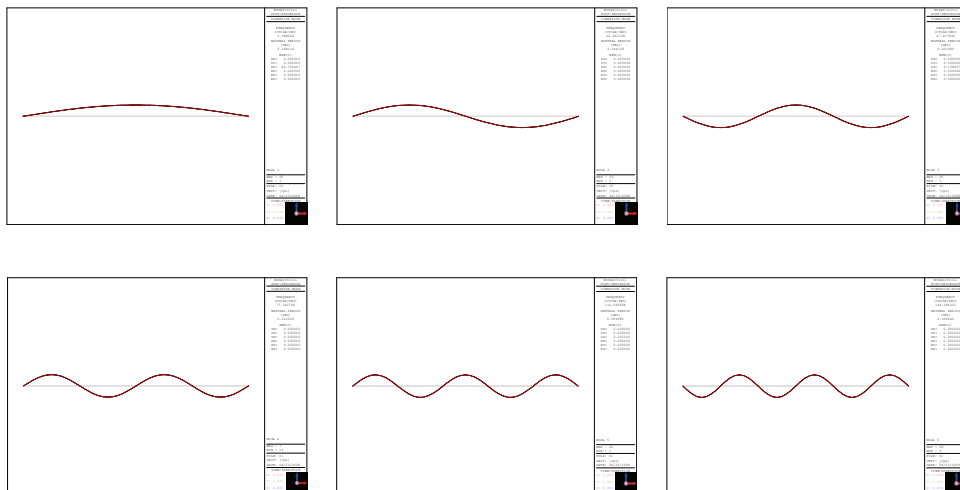


Figure 8.6 First six mode shapes in global z direction

### 8.3 FE Model 1

Like the first Simulink model in Chapter 6, the FE Model 1 contains a single force moving at constant velocity along the beam element. The dynamic load is applied by using a time forcing function  $F(t)$  as Figure 8.8.

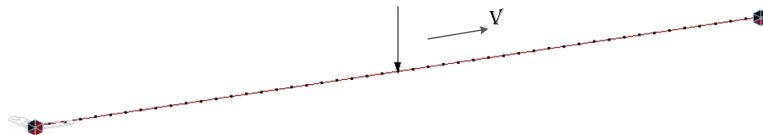


Figure 8.7 Finite Element Model 1

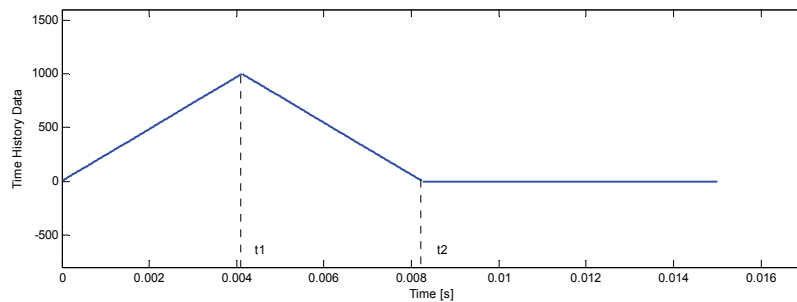


Figure 8.8 Time forcing function

The time steps  $t_1$  and  $t_2$  depend on the length of guideway, number of element and the traversing velocity of the vehicle, which can be calculated as:

$$t_1 = \frac{L}{mv} = 0.0041s, \quad t_2 = \frac{2L}{mv} = 0.0082s \quad (8.1)$$

where

- $m$  number of elements
- $v$  traversing velocity of the vehicle
- $L$  length of the guideway

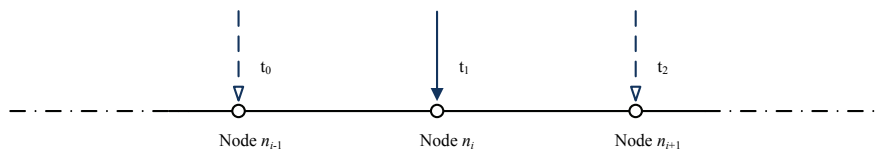
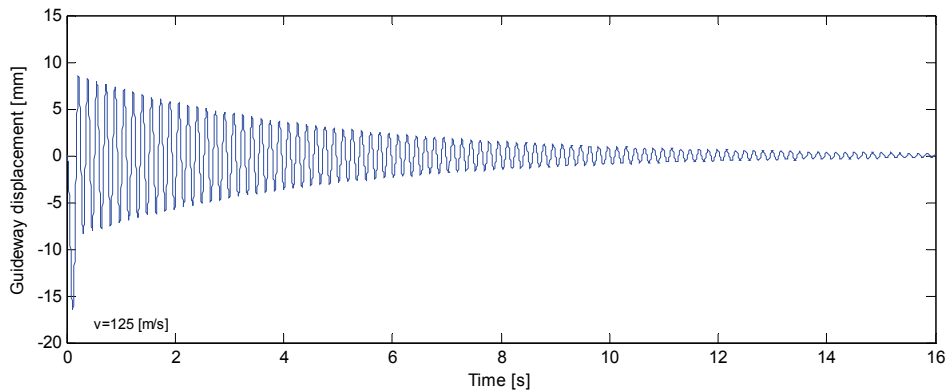


Figure 8.9 Moving force on beam element

The arrival time for  $i$ -th node can be calculated as:

$$t_i = 0 \quad (i=1), \quad t_i = t_{i-1} + \frac{L}{mv} \quad (i \geq 2) \quad (8.2)$$



**Figure 8.10 Time history of guideway mid-span displacement from FE Model 1**

Figure 8.10 shows the result from a time history analysis in Midas at  $v = 125$  m/s. The time histories of guideway displacement are then compared with the results from the numerical simulation as Figure 8.11.

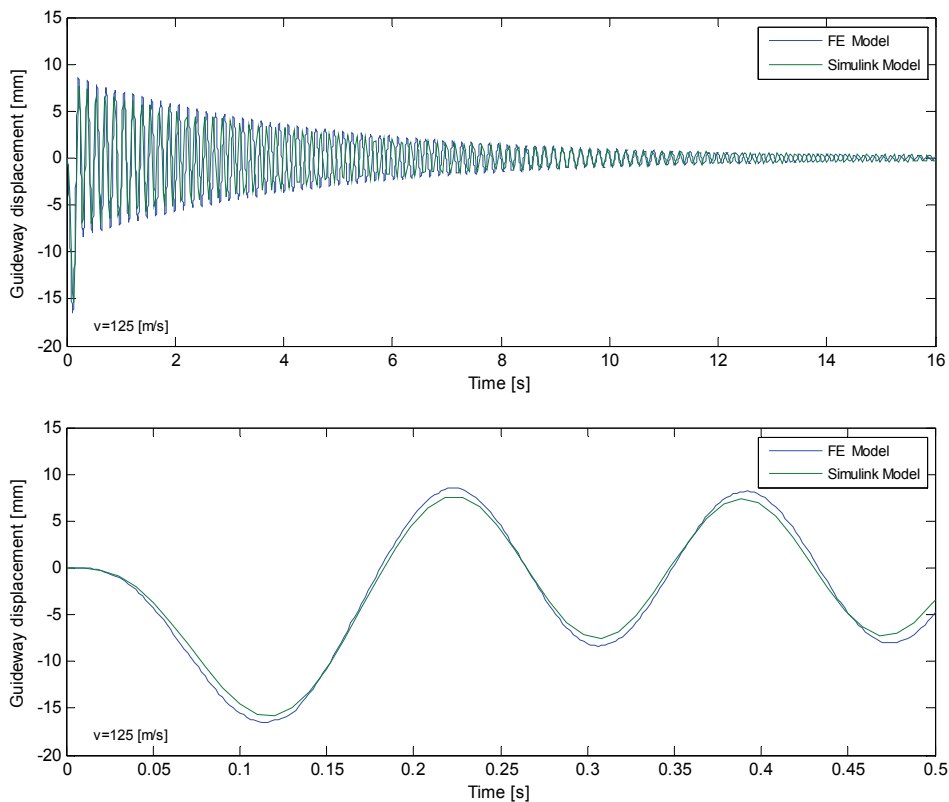


**Figure 8.11 Comparison of FE model and numerical model for  $t=16$ s and  $t=2$ s**

The maximum mid-span displacement from FE model is 16.50 mm at 0.116 s, while the maximum values from numerical simulation is 15.75 mm at 0.120 s. We attribute the small differences in guideway displacement between the plots to the assumption that only first mode is dominant and thus higher modes are neglected in the numerical model.

## 8.4 FE Model 2

In the second model four moving forces are applied on the beam model. The same time forcing function  $F(t)$  and time step as in Section 8.3 are used in this model.

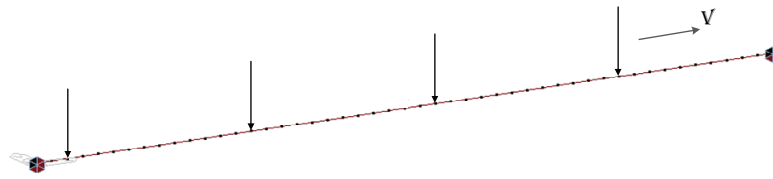


**Figure 8.12 Finite Element Model 2**

The arrival time for  $i$ -th node under  $k$ -th force is written as:

$$\begin{aligned} t_{i,k} &= (k-1) \frac{L}{nv} \quad (i=1) \\ t_{i,k} &= t_{i-1,k} + \frac{L}{mv} \quad (i \geq 2) \end{aligned} \quad (8.3)$$

where

$t_{i,k}$	arrival time for $i$ -th node under $k$ -th force
$m$	number of elements
$n$	number of forces

Based on Equation (8.1) and (8.3), the load file can be prepared for a time history analysis in Midas. Figure 8.13 shows the time history of guideway mid-span displacement at  $v = 125$  m/s using FE Model 2.

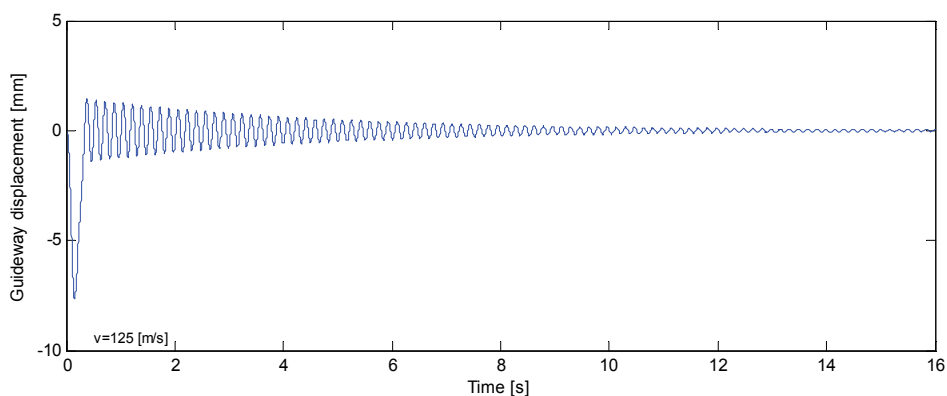


**Figure 8.13 Time history of guideway mid-span displacement From FE Model 2**

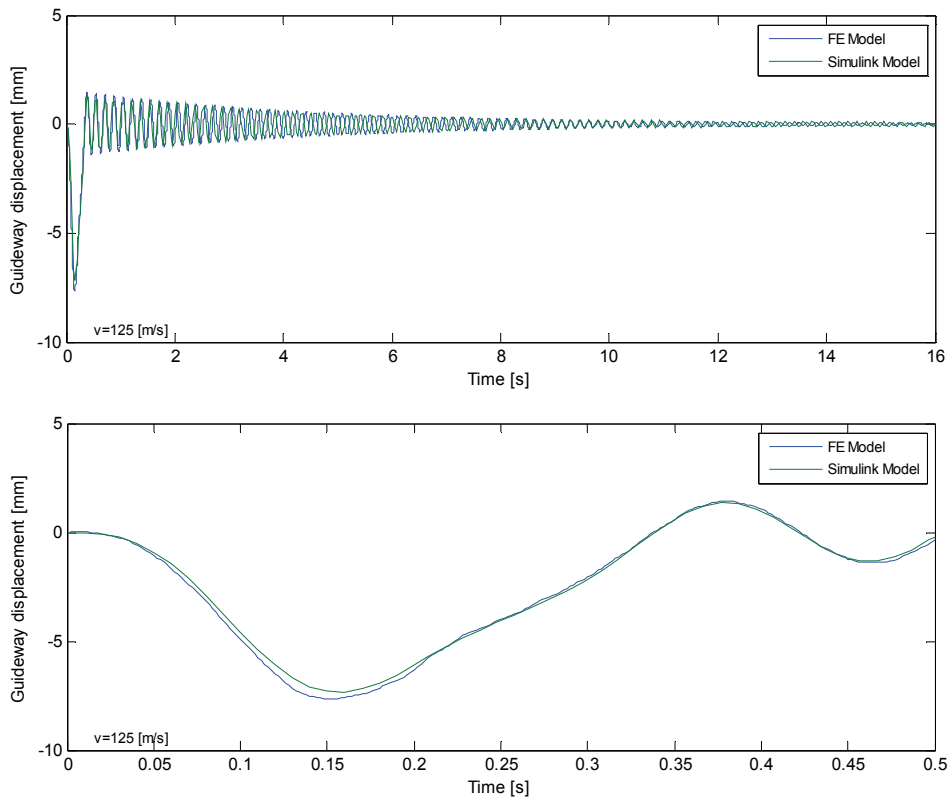


**Figure 8.14 Comparison of FE model and numerical model for  $t=16s$  and  $t=2s$**

The FE model and numerical model are compared in Figure 8.14. The FE-model curve shows a larger maximum guideway displacement with 7.67 mm at 0.154 s, while the simulation result has a maximum value of 7.33 mm at 0.160 s.

### 8.5 FE Model 3

FE Model 3 consists of sixteen forces moving at a constant velocity. The magnitude of each force is determined based on the distribution of electromagnetic force between the levitation magnet and the stator packs (see Section 6.6).

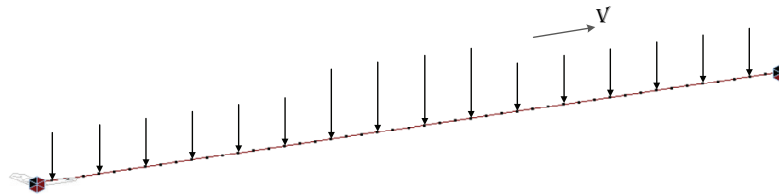


**Figure 8.15 Finite Element Model 3**

## 8 Finite Element Model

The time forcing function in Figure 8.8 is used and the load data is prepared according to Equation (8.1) and (8.3). The result is plotted in Figure 8.16.

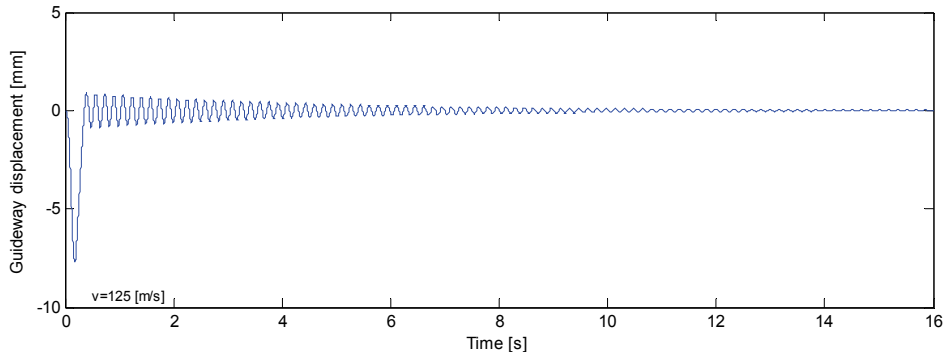


**Figure 8.16 Time history of guideway mid-span displacement From FE Model 3**

Figure 8.17 compares the results of FE model and Simulink model. Midas gives a maximum guideway displacement of 7.69 mm at 0.182 s and for Simulink the value is 7.347 mm at 0.180 s.

The comparisons of finite element analysis and numerical simulation for all the three models show a good agreement on the time history of guideway displacement under a moving load. The maximum value from a finite element model by Midas/Civil is always slightly larger than that of a numerical model by Matlab/Simulink. This is attributed to the approximation that only first mode is calculated in the numerical model.

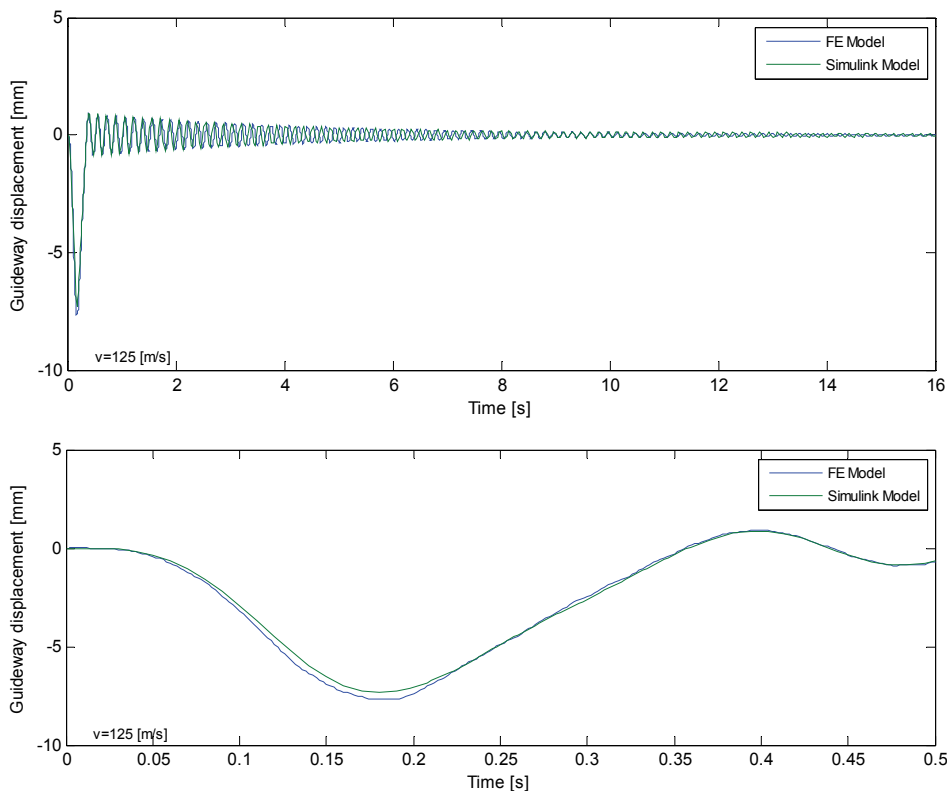


**Figure 8.17 Comparison of FE model and numerical model for  $t=16s$  and  $t=2s$**

## 8.6 Two-section Vehicle Model

Except for the single-section vehicle models, a FE model including 32 forces to represent a two-section vehicle is also created in Midas. The time history analysis is performed and the result is plotted in Figure 8.19.

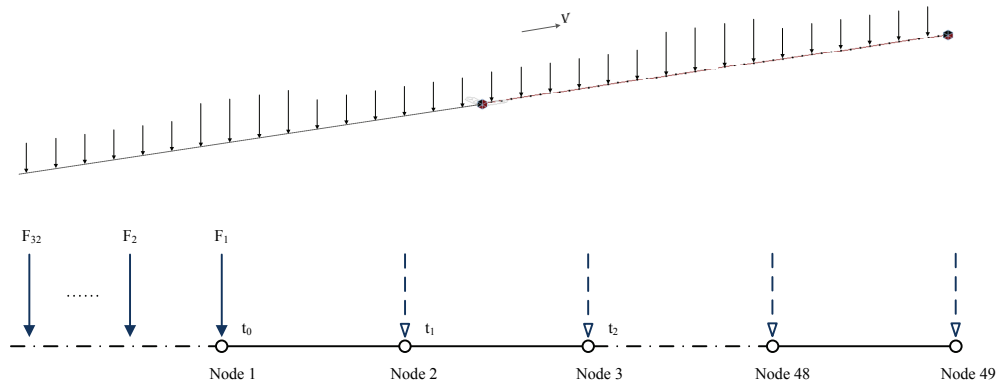


Figure 8.18 Two-section vehicle model

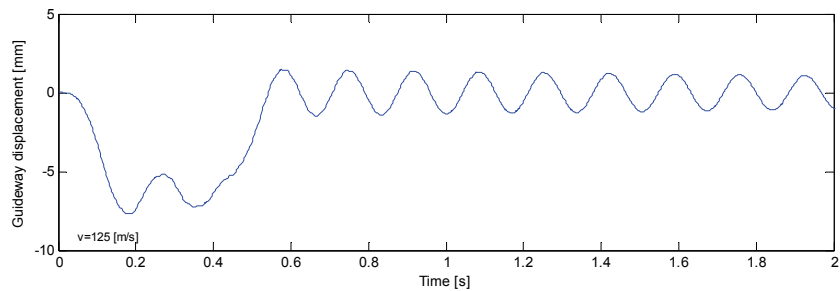


Figure 8.19 Time history of guideway mid-span displacement from a Two-section vehicle Model

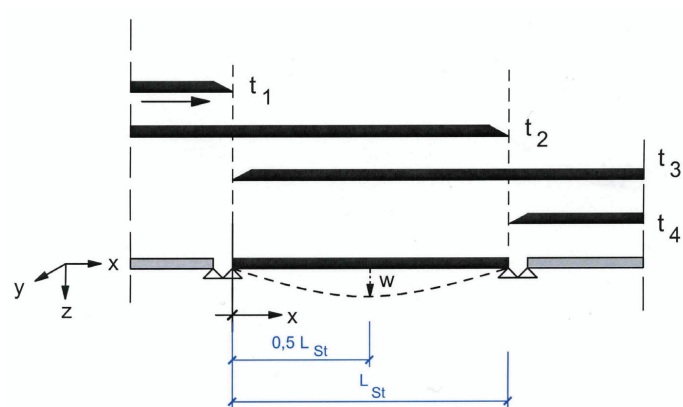


Figure 8.20 Two-section vehicle traversing on single-span guideway, MSB-AG-Fahrweg Teil II, 2007

Figure 8.21 compares the time history of guideway displacements from a two-section vehicle model and from a single-section vehicle model. The curves appear to be identical before reaching the maximum displacements, after which the two-section vehicle model will cause a stronger vibration of the guideway.

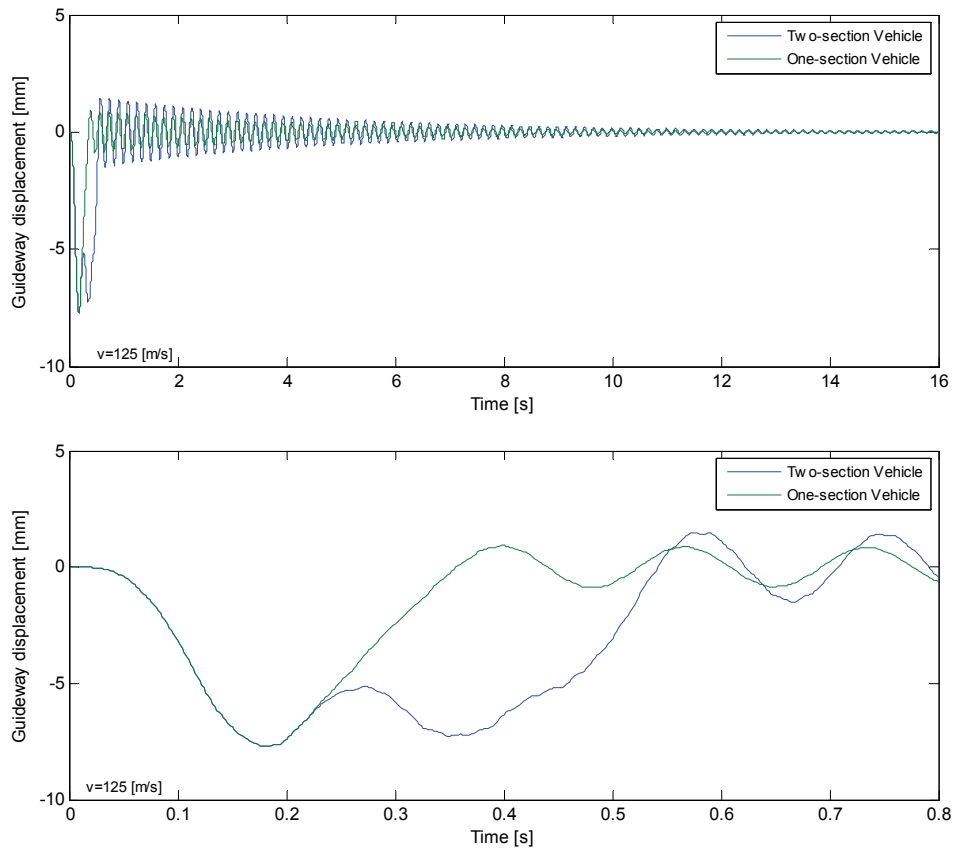


Figure 8.21 Comparison of Two-section vehicle model and single-section vehicle model for  $t=0.8s$



# 9

---

## Conclusions and Recommendations

## 9.1 Conclusions

- The numerical method developed in this report is flexible and efficient. The span length of the guideway is one of the input parameters and can be adjusted conveniently. The carriage body, the levitation frame, the surface roughness and the guideway model are packaged into subsystems which can be easily changed. The governing equation and boundary conditions can also be replaced so as to evaluate a wide range of guideway designs for various supporting schemes and operating conditions.
- The numerical models with single moving force (Model I-1) or single moving oscillator (Model II-1) produce the highest dynamic factor  $\phi_{Bg,z} = 1.72$  at  $v = 175$  m/s. After the peak value the dynamic factor from the oscillator model decrease faster than that of the force model. These two models can be built quickly but will lead to a large dynamic response when the traversing velocity ranges between 50 and 200 m/s. Therefore they are not suitable to study both the guideway dynamic displacement and the acceleration of the vehicle.
- When  $v > 50$  m/s, the numerical model with four moving forces (Model I-2) and sixteen forces (Model I-3) give almost identical result on dynamic factor for various velocities. Therefore increasing the number of moving forces won't increase the accuracy of the results too much.
- When  $v < 50$  m/s, the dynamic factor from Model I-2 shows an obvious fluctuation where a maximum value of 1.20 is reached at  $v = 38$  m/s, while in Model I-3 a smoother curve is obtained. Thus, for low speed maglev vehicle, increasing the number of moving force in the numerical model from four to sixteen is helpful to get more realistic results.
- The influence of guideway damping on the guideway mid-span displacement can be neglected when it varies between 0 and 1.6% for a single-section vehicle model.
- The effect of the vehicle/guideway dynamic interaction on guideway displacement can be neglected if the traversing velocity is less than 190 m/s. When  $v > 190$  m/s, the coupling effect will influence the guideway displacement considerably.
- The effect of the vehicle/guideway dynamic interaction on accelerations of maglev vehicle cannot be neglected. A well-designed complex coupling system (Model II-2) will produce much more accurate results than that of a simple coupling model (Model II-1).
- The design curve for dynamic factor in the German design guideline is conservative when compared with the numeric models with an approximate increase of 10%.
- The influence of guideway surface irregularity on guideway displacement can be neglected when  $A = 1.5 \times 10^{-7}$ . When the roughness amplitude for aircraft runway,  $A = 1.5 \times 10^{-6}$ , is applied, a maximum increase of 9.29% on guideway displacement can be reached.
- The influence of guideway surface irregularity on vehicle acceleration cannot be neglected in both cases ( $A = 1.5 \times 10^{-7}$  and  $A = 1.5 \times 10^{-6}$ ).

- The results of the finite element modes in Midas/Civil show a good agreement with the result of numerical model in Matlab/Simulink. The small differences between these two approaches are attributed to the assumption that only first mode is considered in the numerical model.
- A two-section vehicle model in Midas/Civil gives the same maximum guideway mid-span displacement as the single-section model. Nevertheless, a stronger vibration of the guideway will be activated by the two-section model after reaching the peak value.
- Midas/Civil is capable to perform dynamic analysis to study the guideway characteristics under high-speed loadings. However, in case that a complex model is desired, e.g. a multiple degree-of-freedom vehicle model, the guideway irregularity model, and an active control system, the numerical model will be a better choice.

### 9.2 Recommendations

- The numerical model developed in this report contains a maglev vehicle model, a passive suspension model, a guideway model and a guideway surface roughness model. An active control system of the current and air gap is not considered. It is expected a subsystem including the active control algorithm is added to the numerical model in Simulink. In that way the numerical model can be made more realistic and accurate.
- Two assumptions have been made for the numerical models: First, the vibration of the guideway in vertical direction is not coupled with the vibration in other directions. Second, when using the modal analysis method, it is assumed that the first mode is dominant and any other higher modes are neglected. A further study can be perform to consider the transverse vibration and the effects of higher modes.
- Due to lack of the test data, the roughness amplitudes used in the guideway irregularity model are from continuous welded rail tracks and aircraft runway. The maglev guideway under high speed vehicle should have a similar form as those but slightly different characteristic. A more accurate guideway surface roughness model which is especially for Transrapid guideway is expected.
- Although a FE two-section vehicle model has been created in Midas/Civil, all the numerical models in Matlab/Simulink are coded to represent a single-section vehicle model. A further study can be made to evaluate the influence of multiple-section vehicle on the guideway displacement and vehicle acceleration.
- In this report it is mainly focused on the simply supported guideway. Different supporting schemes are necessary to be discussed in order to find the most optimal solution, e.g. the continuous girder and the integral concept.



## References

- [1] Antlauf, W., *A new guideway for Transrapid – The Munich girder*, The 19<sup>th</sup> International Conference on Magnetically Levitated Systems and Linear Drives, 2006
- [2] Bachmann, H., *MSB-Track-2010, a new guideway for the Transrapid*, The 19<sup>th</sup> International Conference on Magnetically Levitated Systems and Linear Drives, 2006
- [3] Bachmann, H., *MSB-Fahrweg-2010: Der für alle Falle*, 7<sup>th</sup> Dresdner Fachtagung Transrapid, 2007
- [4] Breen, H., *Tall storeys: active control of wind impact on high-rise buildings*, Master of Science report, Delft University of Technology, 2007
- [5] Cai, Y., Chen, S.S., Rote, D.M., and Coffey, H.T., *Vehicle-guideway interaction for high speed vehicles on a flexible guideway*, Journal of Sound and Vibration, 175(5), 625-646, 1994
- [6] Cai, Y. and Chen, S.S., *A review of dynamic characteristics of magnetically levitated vehicle system*, US Energy Technology Division, 1995
- [7] Dai, H., *Dynamic behavior of maglev vehicle/guideway system with control*, PhD thesis, Case Western Reserve University, 2005
- [8] Eisenbahn-Bundesamt, *Magnetschnellbahn Ausführungsgrundlage, Fahrweg Teil I–VI*, 2007
- [9] Eisenbahn-Bundesamt, *Magnetschnellbahn Ausführungsgrundlage, Fahrzeug Teil I–V*, 2007
- [10] Falkner, H., *Guideway for a high-speed magnetic levitation train system*, 2<sup>nd</sup> International Oleg Kerensky Memorial Conference, 1990
- [11] Falkner, H., *Transrapid - A high speed magnetically levitated train system*, 16<sup>th</sup> IABSE, 2000
- [12] Feix, J., *The hybrid Transrapid guideway Development in Germany - First use in China*, 19<sup>th</sup> ISBSE, 2003
- [13] Grossert, E., *Actual development in guideway constructions at the example of the Transrapid Munich Project*, The 18<sup>th</sup> International Conference on Magnetically Levitated Systems and Linear Drives, 2004
- [14] Jerath, S. and Gurav, S., *Road surface roughness generation by power spectral density in bridge design*, ASCE Structural Congress, 2008
- [15] Lever, J.H., *Technical assessment of maglev system concepts*, US Army Corps of Engineers, 1998
- [16] Li, G., *Stability and vibration of bridges*, China railway publishing house, 1992
- [17] Mangerig, I., Zapfe, C., Zapfe, O., Lichte, U. and Retze, U., *Studie über einen temperaturoptimierten Einfeld-Fahrwegträger für die Magnetschwebbahn Transrapid. Forschungsauftrag im Auftrag des Bundesministeriums für Verkehr-, Bau und Wohnungswesen*, München, 2002.
- [18] Schwindt, G., *Darstellung der Transrapid Fahrwegtypen und der Rolle der TRI als Systemingenieur für den Fahrweg*, 5<sup>th</sup> Dresdner Tagung, 2005
- [19] Schwindt, G., *The guideway*, The 19<sup>th</sup> International Conference on Magnetically Levitated Systems and Linear Drives, 2006
- [20] Shi, J., Wei, Q. and Zhao Y., *Analysis of dynamic response of the high-speed EMS maglev vehicle-guideway coupling system with random irregularity*, Vehicle system dynamics, Vol.45, No.12 pp.1077-1095, 2007

- [21] Tum, L., Huhn, G. and Harbeke, C., *Design and development of the Transrapid TR09*, The 19<sup>th</sup> International Conference on Magnetically Levitated Systems and Linear Drives, 2006
- [22] Wu, X. and Huang, J., *Guideway structure, Maglev Demonstration Line*, Shanghai, 2004
- [23] Zhao, C. and Zhai, W., *Maglev vehicle/guideway vertical random response and ride quality*, Vehicle system dynamics, Vol.38, No.3 pp.185-210, 2002

# Appendices

- A Matlab code
- B Midas/Civil input file



## A Matlab code

### Matlab code, numerical Model II-1

```

%{
Dynamic Interaction Model II-1
2 DOF Moving oscillator on simply supported guideway
%}
%
v=125;           % [m/s]           Velocity of maglev vehicle
L=24.768;       % [m]             Length of guideway
t=L/v;          % [s]             Traversing time
%
mv=29200;       % [kg]           Carriage body mass
mf=32000;       % [kg]           Levitation frame mass
g=9.806;        % [m/s^2]        Gravitational acceleration
F=(mv+mf)*g;   % [N]            Total force caused by carriage
body and levitation frame
%
A=1.44565;     % [m^2]          Area of cross section
E=35.684e9;    % [N/m^2]        Young's modulus
I=0.543244;    % [m^4]          Moment of inertia
W=23540;       % [N/m^3]        Weight of guideway
m=W/9.806*A;   % [kg/m]         Guideway mass per unit length
%
zeta=0.016;    % []             Damping ratio
k=1;           % []             Mode number
w1=(pi/L)^2*sqrt(E*I/m); % [rad/s]       First mode natural frequency
phi=sqrt(2)*sin(k*pi/2); % []             Modal shape function kth mode
%
% Primary and secondary suspension
kp=1.18e8;     % [N/s]          Total primary stiffness
cp=2.15e6;     % [Ns/m]         Total primary damping
ks=6.812e5;    % [N/s]          Total secondary stiffness
cs=8.46e4;     % [Ns/m]         Total primary damping
%
% Parameters for numerical simulation
a=2*zeta*w1;
b=w1^2;
c=sqrt(2)/(m*L);
d=k*pi*v/L;
%
% Static displacement at mid span
Static_disp=1/48*(F*L^3)/(E*I);
%
% plot the displacement vs time at middle of guideway
load plot
plot(displacement(1,:)*v,displacement(2,:),axis([0 5*L -24e-3 20e-3]);grid;
xlabel('Location of the moving force [m]');
ylabel('Guideway displacement [m]');

```

### Matlab code, numerical Model II-2 with guideway surface roughness

```

%{
Dynamic Interaction Model II-2
6 DOF Moving vehicle on simply supported guideway
%}
%

```

## Dynamic Simulation of the Maglev Guideway Design

```

%
v=138.889;           % [m/s]           Velocity of maglev vehicle
L=24.768;            % [m]             Length of guideway
t=L/v;               % [s]             Traversing time
%
dof=6;               % [/]             Degree of freedom
Lv=24.768;           % [m]             Length of maglev vehicle
mv=29200;             % [kg]            Carriage body mass
Iv=1.75e6;            % [kgm2]          Pitch inertia of carriage body
%
n=4;                  % [/]             Number of levitation frames
mf=32000/n;           % [kg]            Levitation frame mass
g=9.806;              % [m/s2]          Gravitational acceleration
F=(mv/n+mf)*g;       % [N]             Static force at each levitation
%
A=1.44565;           % [m2]            Area of cross section
E=35.684e9;           % [N/m2]          Young's modulus
I=0.543244;           % [m4]            Moment of inertia
W=23540;              % [N/m3]          Weight of guideway
m=W/9.806*A;          % [kg/m]          Guideway mass per unit length
%
zeta=0.006;           % [/]             Damping ratio
k=1;                  % [/]             Mode number
wl=(pi/L)^2*sqrt(E*I/m); % [rad/s]         First mode natural frequency
phi=sqrt(2)*sin(k*pi/2); % [/]             Modal shape function_kth mode
%
% Primary and secondary suspension
kp=1.18e8/n;           % [N/s]            Primary stiffness
cp=2.15e6/n;           % [Ns/m]           Primary damping
ks=6.812e5/n;           % [N/s]            Secondary stiffness
cs=8.46e4/n;           % [Ns/m]           Secondary damping
%
% Define parameters for roughness model
Ls=192;                 % [m]              Guideway sample length
A=1.5e-6;                % [m3/cycle]       Roughness coefficient
%
nsp=1536;                % [/]              Number of sample points
lambda=Ls/nsp;           % [m]              Sample length
ts=lambda/v;             % [s]              Sample time
var=A*lambda/2;          % [/]              Variance of white noise
S0=2*var*ts;             % [m2/Hz]          PSD of white noise in time domain
%
% Define Mass Matrix
M=zeros(dof, dof);
for i=1:l:dof-2;
    M(i, i)=mf;
end
M(5, 5)=mv;
M(6, 6)=Iv;
%
% Define Damping Matrix
C=zeros(dof, dof);
for i=1:l:dof-2;
    C(i, i)=cs+cp;
    C(i,dof-1)=-cs;
    C(dof-1,i)=-cs;
    C(i, dof)=3/8*Lv*cs-(i-1)*2/8*Lv*cs;
    C(dof, i)=3/8*Lv*cs-(i-1)*2/8*Lv*cs;
end
C(dof-1, dof-1)=4*cs;
C(dof, dof)=5/16*Lv^2*cs;
%

```

## Appendix A Matlab Code

```
% Stiffness Matrix
K=zeros(dof, dof);
for i=1:1:dof-2;
    K(i, i)=ks+kp;
    K(i,dof-1)=-ks;
    K(dof-1,i)=-ks;
    K(i, dof)=3/8*Lv*ks-(i-1)*2/8*Lv*ks;
    K(dof, i)=3/8*Lv*ks-(i-1)*2/8*Lv*ks;
end
K(dof-1, dof-1)=4*ks;
K(dof, dof)=5/16*Lv^2*ks;
%
%{
Define the matrix coefficients for State-Space Approach
    x'=A0*x + B0*u
    y= C0*x + D0*u
A0 (12*12); B0 (12*6); C0 (12*12); D0 (12*6);
%}
A0_11=zeros(6);
A0_12=eye(6);
A0_21=-inv(M)*K;
A0_22=-inv(M)*C;
A0=[A0_11, A0_12
    A0_21, A0_22];
%
B0_11=zeros(6);
B0_21=inv(M);
B0=[B0_11
    B0_21];
%
C0=eye(12);
%
D0=zeros(12,6);
%
% Parameters for simulation
a=2*zeta*w1;
b=w1^2;
c=sqrt(2)/(m*L);
d=k*pi*v/L;
%
%
% plot the guideway mid-span displacement v.s. location of moving vehicle
load plot
plot(displacement(1,:)*v,displacement(2,:)),axis([0 4*L -24e-3 20e-3]);grid;
xlabel('Location of the first levitation frame [m]');
ylabel('Guideway displacement [m]');
```

Matlab code, calculate the PSD of the white noise and compare it with the target PSD

```
%{
White noise model
First order IIR filter
Spatial frequency
%}
%
%
Ls=192;           % [m]           Guideway sample length
A=1.5e-6;        % [m3/cycle]       Roughness coefficient
%
nsp=1536;        % [/]           Number of sample points
lambda=Ls/nsp;  % [m]           Sample length
%
var=A*lambda/2;  % [/]           Variance of white noise
S0=A*lambda^2    % [m2/cycle/m]   Target PSD of the white noise
%
[Pxx,w]=pwelch(wn); % Estimate the Power Spectral Density Pxx of
                    % the input signal using Welch's averaged
                    % modified periodogram method
%
loglog(w,Pxx, w,0*w+S0),axis([0.01 5 3e-9 2e-7]);
legend('PSD-Welch method','Target PSD');
xlabel('Wave number [cycle/m]');
ylabel('Power spectral density [m^2/cycle/m]');
```

Matlab code, calculate the PSD of the surface roughness and compare it with the target PSD

```
%{
Surface roughness model
First order IIR filter
Spatial frequency
%}
%
%
Lv=24.768;       % [m]           Length of maglev vehicle
v=125;           % [m/s]         Velocity of maglev vehicle
Ls=192;          % [m]           Guideway sample length
A=1.5e-6;        % [m3/cycle]    Roughness coefficient
%
nsp=1536;        % [/]           Number of sample points
lambda=Ls/nsp;  % [m]           Sample length
var=A*lambda/2;  % [/]           Variance of white noise
S0=A*(lambda)^2 % [m2/cycle/m] PSD of the white noise
%
[Pxx,w]=pwelch(roughness); % Estimate the power spectral density Pxx of
                    % the input signal using Welch's averaged
                    % modified periodogram method
S=A./((2*pi.*w).^2); % Target roughness PSD model
%
loglog(w,Pxx, w,S); grid;
legend('PSD-Welch method','Target PSD');
xlabel('Wave number [cycle/m]');
ylabel('Power spectral density [m^2/cycle/m]');
```

## B Midas/Civil Input File

### Midas/Civil Input File, FE Model 2

Midas/Civil		FE Model 2					
Lv = 24.768 m	v = 125 m/s	mv = 29200 kg	mf = 32000 kg	n=4			
L = 24.768m	m = 48	D = 0.6%					
$t_1 = L / m / v$	$t_2 = t_1$	$F = (mv+mf)g / n$	$t_{delay} = Lv / n / v$				
1	2	Moving Load_1	Force	unit force	Z	0	-150.0318
	3	Moving Load_1	Force	unit force	Z	0.004128	-150.0318
	4	Moving Load_1	Force	unit force	Z	0.008256	-150.0318
	5	Moving Load_1	Force	unit force	Z	0.012384	-150.0318
	6	Moving Load_1	Force	unit force	Z	0.016512	-150.0318
	7	Moving Load_1	Force	unit force	Z	0.02064	-150.0318
	8	Moving Load_1	Force	unit force	Z	0.024768	-150.0318
	9	Moving Load_1	Force	unit force	Z	0.028896	-150.0318
	10	Moving Load_1	Force	unit force	Z	0.033024	-150.0318
	11	Moving Load_1	Force	unit force	Z	0.037152	-150.0318
	12	Moving Load_1	Force	unit force	Z	0.04128	-150.0318
	13	Moving Load_1	Force	unit force	Z	0.045408	-150.0318
	14	Moving Load_1	Force	unit force	Z	0.049536	-150.0318
	15	Moving Load_1	Force	unit force	Z	0.053664	-150.0318
	16	Moving Load_1	Force	unit force	Z	0.057792	-150.0318
	17	Moving Load_1	Force	unit force	Z	0.06192	-150.0318
	18	Moving Load_1	Force	unit force	Z	0.066048	-150.0318
	19	Moving Load_1	Force	unit force	Z	0.070176	-150.0318
	20	Moving Load_1	Force	unit force	Z	0.074304	-150.0318
	21	Moving Load_1	Force	unit force	Z	0.078432	-150.0318
	22	Moving Load_1	Force	unit force	Z	0.08256	-150.0318
	23	Moving Load_1	Force	unit force	Z	0.086688	-150.0318
	24	Moving Load_1	Force	unit force	Z	0.090816	-150.0318
	25	Moving Load_1	Force	unit force	Z	0.094944	-150.0318
	26	Moving Load_1	Force	unit force	Z	0.099072	-150.0318
	27	Moving Load_1	Force	unit force	Z	0.1032	-150.0318
	28	Moving Load_1	Force	unit force	Z	0.107328	-150.0318
	29	Moving Load_1	Force	unit force	Z	0.111456	-150.0318
	30	Moving Load_1	Force	unit force	Z	0.115584	-150.0318
	31	Moving Load_1	Force	unit force	Z	0.119712	-150.0318
	32	Moving Load_1	Force	unit force	Z	0.12384	-150.0318
	33	Moving Load_1	Force	unit force	Z	0.127968	-150.0318
	34	Moving Load_1	Force	unit force	Z	0.132096	-150.0318

## Dynamic Simulation of the Maglev Guideway Design

35	Moving Load_1	Force	unit force	Z	0.136224	-150.0318
36	Moving Load_1	Force	unit force	Z	0.140352	-150.0318
37	Moving Load_1	Force	unit force	Z	0.14448	-150.0318
38	Moving Load_1	Force	unit force	Z	0.148608	-150.0318
39	Moving Load_1	Force	unit force	Z	0.152736	-150.0318
40	Moving Load_1	Force	unit force	Z	0.156864	-150.0318
41	Moving Load_1	Force	unit force	Z	0.160992	-150.0318
42	Moving Load_1	Force	unit force	Z	0.16512	-150.0318
43	Moving Load_1	Force	unit force	Z	0.169248	-150.0318
44	Moving Load_1	Force	unit force	Z	0.173376	-150.0318
45	Moving Load_1	Force	unit force	Z	0.177504	-150.0318
46	Moving Load_1	Force	unit force	Z	0.181632	-150.0318
47	Moving Load_1	Force	unit force	Z	0.18576	-150.0318
48	Moving Load_1	Force	unit force	Z	0.189888	-150.0318
2 2	Moving Load_1	Force	unit force	Z	0.049536	-150.0318
3	Moving Load_1	Force	unit force	Z	0.053664	-150.0318
4	Moving Load_1	Force	unit force	Z	0.057792	-150.0318
5	Moving Load_1	Force	unit force	Z	0.06192	-150.0318
6	Moving Load_1	Force	unit force	Z	0.066048	-150.0318
7	Moving Load_1	Force	unit force	Z	0.070176	-150.0318
8	Moving Load_1	Force	unit force	Z	0.074304	-150.0318
9	Moving Load_1	Force	unit force	Z	0.078432	-150.0318
10	Moving Load_1	Force	unit force	Z	0.08256	-150.0318
11	Moving Load_1	Force	unit force	Z	0.086688	-150.0318
12	Moving Load_1	Force	unit force	Z	0.090816	-150.0318
13	Moving Load_1	Force	unit force	Z	0.094944	-150.0318
14	Moving Load_1	Force	unit force	Z	0.099072	-150.0318
15	Moving Load_1	Force	unit force	Z	0.1032	-150.0318
16	Moving Load_1	Force	unit force	Z	0.107328	-150.0318
17	Moving Load_1	Force	unit force	Z	0.111456	-150.0318
18	Moving Load_1	Force	unit force	Z	0.115584	-150.0318
19	Moving Load_1	Force	unit force	Z	0.119712	-150.0318
20	Moving Load_1	Force	unit force	Z	0.12384	-150.0318
21	Moving Load_1	Force	unit force	Z	0.127968	-150.0318
22	Moving Load_1	Force	unit force	Z	0.132096	-150.0318
23	Moving Load_1	Force	unit force	Z	0.136224	-150.0318
24	Moving Load_1	Force	unit force	Z	0.140352	-150.0318
25	Moving Load_1	Force	unit force	Z	0.14448	-150.0318
26	Moving Load_1	Force	unit force	Z	0.148608	-150.0318
27	Moving Load_1	Force	unit force	Z	0.152736	-150.0318
28	Moving Load_1	Force	unit force	Z	0.156864	-150.0318
29	Moving Load_1	Force	unit force	Z	0.160992	-150.0318
30	Moving Load_1	Force	unit force	Z	0.16512	-150.0318

Appendix B Midas/Civil Input File

31	Moving Load_1	Force	unit force	Z	0.169248	-150.0318
32	Moving Load_1	Force	unit force	Z	0.173376	-150.0318
33	Moving Load_1	Force	unit force	Z	0.177504	-150.0318
34	Moving Load_1	Force	unit force	Z	0.181632	-150.0318
35	Moving Load_1	Force	unit force	Z	0.18576	-150.0318
36	Moving Load_1	Force	unit force	Z	0.189888	-150.0318
37	Moving Load_1	Force	unit force	Z	0.194016	-150.0318
38	Moving Load_1	Force	unit force	Z	0.198144	-150.0318
39	Moving Load_1	Force	unit force	Z	0.202272	-150.0318
40	Moving Load_1	Force	unit force	Z	0.2064	-150.0318
41	Moving Load_1	Force	unit force	Z	0.210528	-150.0318
42	Moving Load_1	Force	unit force	Z	0.214656	-150.0318
43	Moving Load_1	Force	unit force	Z	0.218784	-150.0318
44	Moving Load_1	Force	unit force	Z	0.222912	-150.0318
45	Moving Load_1	Force	unit force	Z	0.22704	-150.0318
46	Moving Load_1	Force	unit force	Z	0.231168	-150.0318
47	Moving Load_1	Force	unit force	Z	0.235296	-150.0318
48	Moving Load_1	Force	unit force	Z	0.239424	-150.0318
3 2	Moving Load_1	Force	unit force	Z	0.099072	-150.0318
3	Moving Load_1	Force	unit force	Z	0.1032	-150.0318
4	Moving Load_1	Force	unit force	Z	0.107328	-150.0318
5	Moving Load_1	Force	unit force	Z	0.111456	-150.0318
6	Moving Load_1	Force	unit force	Z	0.115584	-150.0318
7	Moving Load_1	Force	unit force	Z	0.119712	-150.0318
8	Moving Load_1	Force	unit force	Z	0.12384	-150.0318
9	Moving Load_1	Force	unit force	Z	0.127968	-150.0318
10	Moving Load_1	Force	unit force	Z	0.132096	-150.0318
11	Moving Load_1	Force	unit force	Z	0.136224	-150.0318
12	Moving Load_1	Force	unit force	Z	0.140352	-150.0318
13	Moving Load_1	Force	unit force	Z	0.14448	-150.0318
14	Moving Load_1	Force	unit force	Z	0.148608	-150.0318
15	Moving Load_1	Force	unit force	Z	0.152736	-150.0318
16	Moving Load_1	Force	unit force	Z	0.156864	-150.0318
17	Moving Load_1	Force	unit force	Z	0.160992	-150.0318
18	Moving Load_1	Force	unit force	Z	0.16512	-150.0318
19	Moving Load_1	Force	unit force	Z	0.169248	-150.0318
20	Moving Load_1	Force	unit force	Z	0.173376	-150.0318
21	Moving Load_1	Force	unit force	Z	0.177504	-150.0318
22	Moving Load_1	Force	unit force	Z	0.181632	-150.0318
23	Moving Load_1	Force	unit force	Z	0.18576	-150.0318
24	Moving Load_1	Force	unit force	Z	0.189888	-150.0318
25	Moving Load_1	Force	unit force	Z	0.194016	-150.0318
26	Moving Load_1	Force	unit force	Z	0.198144	-150.0318

## Dynamic Simulation of the Maglev Guideway Design

27	Moving Load_1	Force	unit force	Z	0.202272	-150.0318
28	Moving Load_1	Force	unit force	Z	0.2064	-150.0318
29	Moving Load_1	Force	unit force	Z	0.210528	-150.0318
30	Moving Load_1	Force	unit force	Z	0.214656	-150.0318
31	Moving Load_1	Force	unit force	Z	0.218784	-150.0318
32	Moving Load_1	Force	unit force	Z	0.222912	-150.0318
33	Moving Load_1	Force	unit force	Z	0.22704	-150.0318
34	Moving Load_1	Force	unit force	Z	0.231168	-150.0318
35	Moving Load_1	Force	unit force	Z	0.235296	-150.0318
36	Moving Load_1	Force	unit force	Z	0.239424	-150.0318
37	Moving Load_1	Force	unit force	Z	0.243552	-150.0318
38	Moving Load_1	Force	unit force	Z	0.24768	-150.0318
39	Moving Load_1	Force	unit force	Z	0.251808	-150.0318
40	Moving Load_1	Force	unit force	Z	0.255936	-150.0318
41	Moving Load_1	Force	unit force	Z	0.260064	-150.0318
42	Moving Load_1	Force	unit force	Z	0.264192	-150.0318
43	Moving Load_1	Force	unit force	Z	0.26832	-150.0318
44	Moving Load_1	Force	unit force	Z	0.272448	-150.0318
45	Moving Load_1	Force	unit force	Z	0.276576	-150.0318
46	Moving Load_1	Force	unit force	Z	0.280704	-150.0318
47	Moving Load_1	Force	unit force	Z	0.284832	-150.0318
48	Moving Load_1	Force	unit force	Z	0.28896	-150.0318
4 2	Moving Load_1	Force	unit force	Z	0.148608	-150.0318
3	Moving Load_1	Force	unit force	Z	0.152736	-150.0318
4	Moving Load_1	Force	unit force	Z	0.156864	-150.0318
5	Moving Load_1	Force	unit force	Z	0.160992	-150.0318
6	Moving Load_1	Force	unit force	Z	0.16512	-150.0318
7	Moving Load_1	Force	unit force	Z	0.169248	-150.0318
8	Moving Load_1	Force	unit force	Z	0.173376	-150.0318
9	Moving Load_1	Force	unit force	Z	0.177504	-150.0318
10	Moving Load_1	Force	unit force	Z	0.181632	-150.0318
11	Moving Load_1	Force	unit force	Z	0.18576	-150.0318
12	Moving Load_1	Force	unit force	Z	0.189888	-150.0318
13	Moving Load_1	Force	unit force	Z	0.194016	-150.0318
14	Moving Load_1	Force	unit force	Z	0.198144	-150.0318
15	Moving Load_1	Force	unit force	Z	0.202272	-150.0318
16	Moving Load_1	Force	unit force	Z	0.2064	-150.0318
17	Moving Load_1	Force	unit force	Z	0.210528	-150.0318
18	Moving Load_1	Force	unit force	Z	0.214656	-150.0318
19	Moving Load_1	Force	unit force	Z	0.218784	-150.0318
20	Moving Load_1	Force	unit force	Z	0.222912	-150.0318
21	Moving Load_1	Force	unit force	Z	0.22704	-150.0318
22	Moving Load_1	Force	unit force	Z	0.231168	-150.0318

## Appendix B Midas/Civil Input File

23	Moving Load_1	Force	unit force	Z	0.235296	-150.0318
24	Moving Load_1	Force	unit force	Z	0.239424	-150.0318
25	Moving Load_1	Force	unit force	Z	0.243552	-150.0318
26	Moving Load_1	Force	unit force	Z	0.24768	-150.0318
27	Moving Load_1	Force	unit force	Z	0.251808	-150.0318
28	Moving Load_1	Force	unit force	Z	0.255936	-150.0318
29	Moving Load_1	Force	unit force	Z	0.260064	-150.0318
30	Moving Load_1	Force	unit force	Z	0.264192	-150.0318
31	Moving Load_1	Force	unit force	Z	0.26832	-150.0318
32	Moving Load_1	Force	unit force	Z	0.272448	-150.0318
33	Moving Load_1	Force	unit force	Z	0.276576	-150.0318
34	Moving Load_1	Force	unit force	Z	0.280704	-150.0318
35	Moving Load_1	Force	unit force	Z	0.284832	-150.0318
36	Moving Load_1	Force	unit force	Z	0.28896	-150.0318
37	Moving Load_1	Force	unit force	Z	0.293088	-150.0318
38	Moving Load_1	Force	unit force	Z	0.297216	-150.0318
39	Moving Load_1	Force	unit force	Z	0.301344	-150.0318
40	Moving Load_1	Force	unit force	Z	0.305472	-150.0318
41	Moving Load_1	Force	unit force	Z	0.3096	-150.0318
42	Moving Load_1	Force	unit force	Z	0.313728	-150.0318
43	Moving Load_1	Force	unit force	Z	0.317856	-150.0318
44	Moving Load_1	Force	unit force	Z	0.321984	-150.0318
45	Moving Load_1	Force	unit force	Z	0.326112	-150.0318
46	Moving Load_1	Force	unit force	Z	0.33024	-150.0318
47	Moving Load_1	Force	unit force	Z	0.334368	-150.0318
48	Moving Load_1	Force	unit force	Z	0.338496	-150.0318